

Copyright is owned by the Author of the thesis. Permission is given for a copy to be downloaded by an individual for the purpose of research and private study only. The thesis may not be reproduced elsewhere without the permission of the Author.



MASSEY UNIVERSITY  
TE KUNENGA KI PŪREHUROA  
UNIVERSITY OF NEW ZEALAND

MASSEY UNIVERSITY

DOCTORAL THESIS

---

# Capture Probabilities in Pair-wise Collisions of Emulsion Drops – Measurement and Application.

---

*Author:* Sapna Ravindran

*Supervisor:* Prof. Martin WILLIAMS

*Co-supervisors:* Dr. Rob Ward

Dr. Graeme Gillies

*Report submitted in fulfilment of the requirements  
for the Doctoral Degree (PhD Course)  
in the*

Biophysics And Soft Matter Group  
School Of Fundamental Sciences

*Date of Report:* June 2019

*PhD term:* 2015-2019



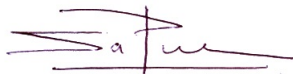


## Declaration of Authorship

I, Sapna Ravindran, declare that this report titled, “Capture Probabilities in Pair-wise Collisions of Emulsion Drops – Measurement and Application.” and the work presented in it are my own. I confirm that:

- This work was done wholly or mainly while in candidature for a research degree at this University.
- Where any part of this thesis has previously been submitted for a degree or any other qualification at this University or any other institution, this has been clearly stated.
- Where I have consulted the published work of others, this is always clearly attributed.
- Where I have quoted from the work of others, the source is always given.
- I have acknowledged all main sources of help.

Signed:

A handwritten signature in dark ink, appearing to read 'Sapna', with a horizontal line underneath.

Date:

Wednesday 18<sup>th</sup> December, 2019



*“Stay Hungry. Stay Foolish”*

- Steve Jobs, *speech delivered at Stanford University* (2005)



*“Dedicated to my Ashtok and Chintu...”*



MASSEY UNIVERSITY

# Abstract

Biophysics And Soft Matter Group

School Of Fundamental Sciences

Doctoral Degree (PhD Course)

## **Capture Probabilities in Pair-wise Collisions of Emulsion Drops – Measurement and Application.**

by Sapna RAVINDRAN

This project seeks to measure and model particle interactions under different environmental conditions with a view to being able to control these interactions. The interactions of emulsion drops will be investigated using an optical tweezer set-up and the results considered in the context of measurements of the zeta potential of the emulsion.

Specifically, how the zeta potential of emulsion drops changes with the physiochemical environment (pH and ionic environment) is captured in a concise mathematical model, the effects of depletion interactions are considered, and a novel experimental procedure is developed to allow hundreds of pairwise stickiness measurements to be taken in an automated fashion.

The major research questions are:



1. Is it possible to address the effects of changes in environmental conditions which are not easily quantifiable with a pragmatic capture probability or pairwise *stickiness* measured at a single particle level?.
2. Can we link these pairwise measurements to induced changes in the surface properties and understand how they yield the rheological behaviour of the system?.

## *Acknowledgements*

I would like to thank my supervisor, Prof Bill Williams and my Co-supervisors Dr. Rob Ward and Dr. Graeme Gillies for their constant support and great guidance. I would also like to express my gratitude to my group mates at IFS for their helps, Mr. Nathan Stanton for his technical support and Dr. Ran Gao for useful discussions. I am grateful to FRDC (Fonterra Research and Development Centre), MMIC (Manawatu Microscopy and Imaging Centre) and Riddet Institute for giving me opportunity to work in their labs. Finally, I would like to thank my husband, Niranjan, family and friends, especially Sanal for all the motivations and help throughout the PhD journey...

This research was supported through the Dairy Primary Growth Partnership programme in Food Structure Design by Fonterra Co-operative Group Ltd. and the New Zealand Ministry for Primary Industries.



# Contents

<b>Declaration of Authorship</b>	<b>iii</b>
<b>Abstract</b>	<b>ix</b>
<b>Acknowledgements</b>	<b>xi</b>
<b>1 Introduction</b>	<b>1</b>
1.1 Colloidal Systems . . . . .	2
1.2 Interaction potentials at the surface . . . . .	2
1.2.1 Electrical double layer . . . . .	3
1.2.2 Van der Waals interaction . . . . .	3
1.2.3 Born repulsion . . . . .	5
1.2.4 Hydration effect . . . . .	5
1.2.5 Steric interaction . . . . .	5
1.2.6 Polymer bridging . . . . .	7
1.2.7 Depletion effect . . . . .	7
1.3 Colloidal aggregation . . . . .	7

1.4	Outline of research project . . . . .	8
1.4.1	Surface properties . . . . .	8
1.4.2	Addition of depletion forces to the system – Application of surface properties . . . . .	10
1.4.3	Stickiness measurements . . . . .	11
1.4.4	Application to shelf life . . . . .	12
1.4.5	Approach . . . . .	13
<b>2</b>	<b>Materials and methods</b>	<b>15</b>
2.1	Emulsion formation . . . . .	16
2.1.1	WPI emulsion . . . . .	17
2.1.2	Preparation of the emulsion . . . . .	18
2.1.3	Determination of viscosity of emulsions . . . . .	20
2.2	Xanthan gum . . . . .	23
2.3	Zeta potential measurements using a Zetasizer . . . . .	23
2.4	Confocal Imaging . . . . .	26
<b>3</b>	<b>Dependence of the properties of whey protein stabilised emulsions on the physio-chemical conditions and zeta potential.</b>	<b>27</b>
3.1	Gouy-Chapman double layer model and Grahame equation . . . . .	30
3.2	Inter-droplet interactions . . . . .	30
3.3	The development of the theoretical framework for the data analysis . . . . .	31

3.3.1	Gouy-Chapman $pK_a$ model for WPI emulsions . . . . .	31
3.3.2	Theory and calculation . . . . .	33
3.3.3	DLVO theory . . . . .	38
3.4	Materials and methods . . . . .	40
3.4.1	Materials . . . . .	40
3.4.2	Emulsion preparation . . . . .	41
3.4.3	Zeta potential measurements . . . . .	42
3.4.4	Activity measurement for samples with calcium . . . . .	42
3.4.5	Rheological determinations . . . . .	44
3.5	Results and discussion . . . . .	46
3.5.1	Effect of concentration of NaCl and pH on zeta potential . . . . .	46
	Effect of concentration of $CaCl_2$ on zeta potential . . . . .	49
3.5.2	Emulsion rheology with zeta potential . . . . .	51
3.6	Conclusion . . . . .	53
<b>4</b>	<b>Depletion and electrostatic forces in the determination of the cluster kinetics in whey protein stabilised emulsion.</b>	<b>55</b>
4.1	Materials and methods . . . . .	57
4.1.1	Materials . . . . .	57
4.1.2	Sample preparation . . . . .	58
4.1.3	Zeta potential calculation from calcium activity . . . . .	58

4.1.4	Particle size measurements . . . . .	59
4.1.5	Viscosity measurements . . . . .	59
4.2	Theory . . . . .	59
4.3	Results and Discussion . . . . .	63
4.3.1	interaction potentials . . . . .	63
4.3.2	Droplet Size . . . . .	64
4.4	Conclusion . . . . .	71
<b>5</b>	<b>Using Optical Tweezers to Measure the Probability of Aggregation of Pairs of Emulsion Drops: The Development of an Automated Procedure</b>	<b>73</b>
5.1	Emulsion droplet stickiness using OT . . . . .	77
5.2	Probabilistic approach to the measurement of the stickiness of particles . .	78
5.3	Materials and Methods . . . . .	82
5.3.1	Sample preparation . . . . .	82
5.3.2	Optical tweezers . . . . .	82
5.3.3	Microfluidic chip . . . . .	82
5.3.4	Syringe pumps . . . . .	83
5.4	Automation of the stickiness experiment . . . . .	83
5.5	Results and discussion . . . . .	91
5.5.1	Variations in stickiness probability with zeta potential . . . . .	91
5.5.2	Stickiness probability with holding time . . . . .	95

5.5.3 Rheological measurements . . . . .	97
5.6 Conclusion . . . . .	98
<b>6 Conclusion and future directions</b>	<b>101</b>
6.1 Conclusion . . . . .	101
6.2 Future Directions . . . . .	104
6.2.1 Measurement of zeta potential inside the chip . . . . .	104
6.2.2 Stickiness probability measurements with different/modified protein	105
6.2.3 Stickiness probability measurements with xanthan . . . . .	105
6.2.4 Modelling of colloidal aggregation . . . . .	105
Monte Carlo methods . . . . .	107
Molecular dynamics methods . . . . .	107
Brownian dynamics method . . . . .	108
<b>7 Published and to be published work</b>	<b>109</b>
<b>A Appendix to Chapter. 1</b>	<b>111</b>
A.1 Confocal image of emulsion . . . . .	111
<b>B Appendix to Chapter. 3</b>	<b>113</b>
B.1 Eversole and Boardman equation . . . . .	113
<b>C Appendix to Chapter. 4</b>	<b>117</b>



<b>D</b>	<b>Appendix to Chapter. 6</b>	<b>121</b>
D.1	Implementation of simulation . . . . .	121
HOOMD	. . . . .	121
D.1.1	Features and capabilities of HOOMD . . . . .	121
<b>E</b>	<b>STATEMENT OF CONTRIBUTION: DOCTORATE WITH PUBLICATIONS/MANUSCRIPTS</b>	<b>125</b>
	<b>Bibliography</b>	<b>127</b>

# List of Figures

1.1	Gouy-Chapman model . . . . .	4
1.2	Steric Interaction . . . . .	6
1.3	Overall picture . . . . .	13
2.1	Ultra Turrax and Homogeniser . . . . .	19
2.2	Droplet diameter distribution before and after the removal of the large droplets . . . . .	20
2.3	Schematic Cup and Bob and Double Gap Geometry . . . . .	20
2.4	Dilution rheology for emulsion . . . . .	22
2.5	Flow curves of emulsion . . . . .	22
2.6	Zetasizer Nano and folded capillary cell . . . . .	24
2.7	Zetasizer Nano operation . . . . .	25
2.8	Confocal Microscope . . . . .	26
3.1	Graphical representation of the experimental and theoretical work. . . . .	29
3.2	DLVO potential . . . . .	39
3.3	Droplet diameter distribution . . . . .	41

3.4	log Con vs Voltage for measuring Activity . . . . .	44
3.5	Anton Par dynamic shear rheometer 502 . . . . .	45
3.6	Zeta potential dependence on pH and concentration of NaCl . . . . .	46
3.7	Determination of total number of carboxylic and amine groups . . . . .	48
3.8	Zeta potential dependence activity of calcium . . . . .	49
3.9	Results at once . . . . .	50
3.10	Plateau viscosity versus zeta potential squared . . . . .	52
4.1	Interaction potentials as a function of separation . . . . .	63
4.2	Zeta potential and xanthan concentration of samples . . . . .	64
4.3	Droplet size distribution . . . . .	65
4.4	$d_{10}$ values plotted against the characteristic aggregation time . . . . .	66
4.5	droplet size distributions of emulsions . . . . .	67
4.6	The $d_{4,3}$ of samples plotted against characteristic aggregation time . . . . .	69
5.1	Optical Tweezer . . . . .	75
5.2	Ray model to explain forces . . . . .	76
5.3	Stickiness measurement Particles . . . . .	77
5.4	Automation experimental setup . . . . .	80
5.5	Microfluidic chip . . . . .	83
5.6	Syringe pump . . . . .	84

5.7	Flow chart showing the automation of the stickiness experiment . . . . .	85
5.8	Cleaning of the chip . . . . .	86
5.9	Pump plugin of the automation software . . . . .	87
5.10	Stickiness automation plugin . . . . .	88
5.11	Inside the microfluidic chip . . . . .	90
5.12	Stickiness probability with zeta potential . . . . .	92
5.13	Interaction potential for different physio-chemical conditions . . . . .	93
5.14	Stickiness probability with holding time . . . . .	95
5.15	Rheological study on emulsion systems characterised by different zeta potential . . . . .	97
5.16	Summary diagram . . . . .	99
A.1	Confocal image of emulsion . . . . .	111
B.1	Determination of total number of carboxylic and amide groups . . . . .	114
C.1	Particle size distribution for different xanthan concentrations at different zeta potentials. . . . .	118
C.2	Mean size of the droplets with xanthan and added salt . . . . .	119
C.3	Confocal image of emulsion with xanthan . . . . .	119
D.1	Brownian simulation using HOOMD . . . . .	122
D.2	MSD Using HOOMD . . . . .	123



# List of Tables

3.1	Activity coefficient from different models for water at 25°C with A= 0.5, B= 0.33 (James W. Murray [86]) . . . . .	43
-----	---	----



# List of Abbreviations

<b>WPI</b>	<b>W</b> hey <b>P</b> rotein <b>I</b> solate
<b>WPC</b>	<b>W</b> hey <b>P</b> rotein <b>C</b> oncentrate
$\beta$ <b>LG</b>	<b>B</b> eta <b>L</b> acto <b>G</b> lobulin
$\alpha$ <b>LA</b>	<b>A</b> lpha <b>L</b> act <b>A</b> lbumin
<b>SA</b>	<b>S</b> erum <b>A</b> lbumin
<b>Ig</b>	<b>I</b> mmuno <b>g</b> lobulin
<b>IEP</b>	<b>I</b> so <b>E</b> lectric <b>P</b> oint
<b>O/W</b>	<b>O</b> il in <b>W</b> ater
<b>W/O</b>	<b>W</b> ater in <b>O</b> il
<b>EDL</b>	<b>E</b> lectric <b>D</b> ouble <b>L</b> ayer
<b>GC Model</b>	<b>G</b> ouy <b>C</b> hapman <b>M</b> odel
<b>DLVO</b>	<b>D</b> erjaguin <b>L</b> andau <b>V</b> erwey <b>O</b> verbeek
<b>VDW</b>	<b>V</b> an <b>D</b> er <b>W</b> aals
<b>OT</b>	<b>O</b> ptical <b>T</b> weezer
<b>HOT</b>	<b>H</b> olographic <b>O</b> ptical <b>T</b> weezers
<b>DOE</b>	<b>D</b> iffractive <b>O</b> ptical <b>E</b> lement
<b>SLM</b>	<b>S</b> patial <b>L</b> ight <b>M</b> odulator
<b>CGH</b>	<b>C</b> omputer <b>G</b> enerated <b>H</b> ologram
<b>DLA</b>	<b>D</b> iffusion <b>L</b> imited <b>A</b> ggregation
<b>DLCA</b>	<b>D</b> iffusion <b>L</b> imited <b>C</b> olloid <b>A</b> ggregation
<b>RLCA</b>	<b>R</b> eaction <b>L</b> imited <b>C</b> olloid <b>A</b> ggregation
<b>MC</b>	<b>M</b> onte <b>C</b> arlo
<b>MD</b>	<b>M</b> olecular <b>D</b> ynamics



<b>BD</b>	<b>B</b> rownian <b>D</b> ynamics
<b>DMC</b>	<b>D</b> ynamic <b>M</b> onte <b>C</b> arlo
<b>HOOMD</b>	<b>H</b> ighly <b>O</b> ptimized <b>O</b> bject-oriented <b>M</b> any particle <b>D</b> ynamics

# Physical Constants

Boltzmann constant  $k_B = 1.3806 \times 10^{-23} \text{ m}^2 \text{Kgs}^{-1} \text{K}^{-1}$

permittivity of free space  $\epsilon_0 = 8.854 \times 10^{-12} \text{ F m}^{-1}$

Avogadro Constant  $N_A = 6.022 \times 10^{23} \text{ mol}^{-1}$

Charge of an electron  $e = -1.602 \times 10^{-19} \text{ C}$



# List of Symbols

$\Psi$	Surface electric potential
$\sigma$	Surface charge density
$\rho$	local charge density
$n_i$	number concentration of ion $i$
$T$	Temperature, $T = 25^0C(298.15K)$ through out the project
$\kappa$	Debye -Hückel parameter
$\lambda_D$	Debye length
$\zeta$	zeta (potential)
$\epsilon_r$	relative permittivity of medium
$N_{(x)}$	Number of $(x)$ groups on surface
$\lambda_B$	Bjerrum length
$U_E$	Electrophoretic mobility
$\eta$	Viscosity
$f(K_a)$	Henry's function
$m_i$	concentration of the free ion
$a_i$	activity of the free ion
$\gamma_i$	activity coefficient
$A$	Hamaker constant
$a_1, a_2, a$	radius of spheres
$\sigma_d$	collision diameter
$a_p$	particle radius
$\eta(r)$	relative viscosity
$\phi$	volume fraction

xxx

$k$	rate constant
$\alpha$	collision efficiency
$t$	time
$\tau$	coagulation time
$D(i)$	Diffusion coefficient for a particle of radius, $a_i$

# **Chapter 1**

## **Introduction**

## 1.1 Colloidal Systems

The term ‘colloid’ refers to microscopic particles dispersed in a continuous medium or ‘solvent’. Several different forces are potentially operating on these micro particles. Micro particles will settle or rise due to the gravitational force, depending on their density relative to the solvent. This settling or rising is opposed by the viscous drag force which develops when particles move due to externally applied forces, and to the Brownian motion that disperses particles (Pashley and Karaman [1]). Brownian motion is an irregular fluctuation of random motions. It is direct evidence of thermal molecular motion that is the basis of the microscopic theory of the structure of matter. Impacts exerted by the fluid on the particle provide the random forces driving the particles.

Hence, the random influence of the dispersed medium results in giving a random driving force to particles to maintain a sustained irregular motion, and, also gives rise to the above mentioned viscous drag for a forced motion. The frictional force and the random force are related as both come from the same origin. The relationship between the viscous friction and the random diffusion is described by the fluctuation-dissipation theorem (Kubo [2]).

## 1.2 Interaction potentials at the surface

Colloidal interactions are determined by the interaction forces between the particles. These forces, which act over relatively short distances, principally consist of the:

- electrical double layer
- van der Waals forces
- Born repulsion
- hydration effects

- steric interaction
- polymer bridging
- depletion interaction

### 1.2.1 Electrical double layer

A separation of charge and a difference in potential arises when two dissimilar phases come in contact. It can be due to difference in affinity of ions for the two phases, ionisation of surface groups, or physical restriction of certain ions to one phase (Hunter [3]). For electrically charged surfaces in water, surface charges are generated when ions are adsorbed or when surface groups dissociate. The surface charge creates an electric field that attracts counter ions within its vicinity. This layer of surface charges and the second layer of counter ions constitute the “Electric Double Layer”.

German physicist Helmholtz proposed the first theoretical description of the electric double layer by considering counter ions being directly adsorbed to the surface, completely compensating for the surface charge, limiting the electric field generated by the surface charge to the thickness of a molecular layer. However, this treatment contradicted electrokinetic experiments. Louis Gouy and David Chapman came up with a description (by taking the thermal motion of ions into account) that predicts the formation of a diffusive layer. The potential at a distance where the surface molecules start to move (slip plane) is the zeta ( $\zeta$ ) potential (Figure. 1.1).

### 1.2.2 Van der Waals interaction

Van der Waals attraction between molecules arises as a result of correlations between electrons on the different molecules. Negative and positive charges collide with each other continuously in any matter, leading to transient electric and magnetic fields. These



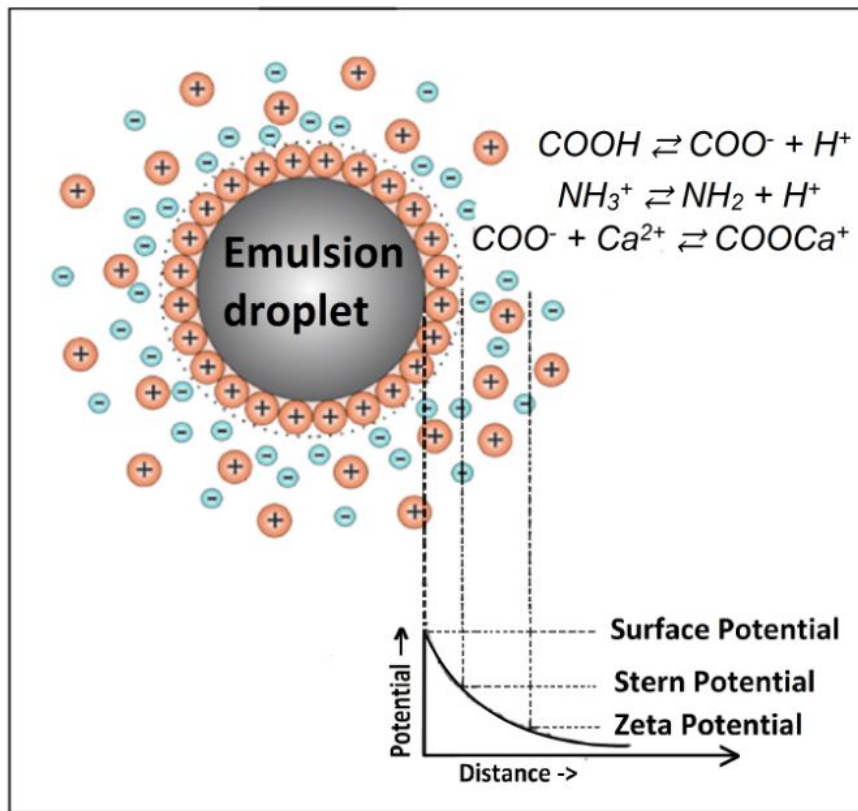


FIGURE 1.1: Illustration of the Gouy-Chapman model for a positively charged emulsion droplet, with possible charge and potential distribution at the interface. Also depicted on this image is an immobilised layer of charge called a Stern layer. This additional Stern layer is a common extension of the Gouy-Chapman model.

fluctuations in charge and field occur due to the thermal agitation, quantum mechanical uncertainties in the positions and momenta of particles, and in the strengths of electromagnetic fields. The collective coordinated interactions of moving electric charges and fields averaged over time creates the Van der Waals or “charge-fluctuation” force (Parsegian [4]).

### 1.2.3 Born repulsion

Born repulsion arises from strong repulsive forces between atoms when the electron shells interpenetrate each other. This short range repulsive force develops when the electron clouds overlap as the particles approach a point of contact, and is very sensitive to the structural details of the surface and the medium making it difficult to estimate. It is the twelfth-order term of the empirical Lennard-Jones 6-12 potential. The Born repulsion ( $\phi_B$ ) between a sphere and a plate is given by:

$$\phi_B(h) = \frac{A\sigma_d^6}{7560} \left[ \frac{8a_p + h}{(2a_p + h)^7} - \frac{6a_p - h}{h^7} \right] \quad (1.1)$$

where  $A$  is the Hamaker constant,  $\sigma_d$  is the collision diameter,  $a_p$  is the particle radius, and  $h$  is the minimum separation distance between particle and the surface. The collision diameter  $\sigma_d$  will be treated as a characteristic property of the solids (Ruckenstein and Prieve [5]).

### 1.2.4 Hydration effect

The presence of polar or charged groups tends to hydrate a surface. This hydration consists of an immobilised water layer. When two particles with hydrated surfaces approach, there will be an extra repulsive interaction distinct from Electric Double Layer (EDL) repulsion. This repulsion arises from the energy cost for the surfaces to be dehydrated so that true contact between particles is able to occur. Hydration effects are expected to be very short ranged; no more than a couple layers of water molecules across.

### 1.2.5 Steric interaction

Steric interactions arise from adsorbed or grafted layers on the surface of colloidal particles, and have an important role in colloidal aggregation and deposition. In the case of

a colloidal particulate dispersion with large adsorbed macro-molecules such as proteins, the stability is enhanced with steric stabilisation.

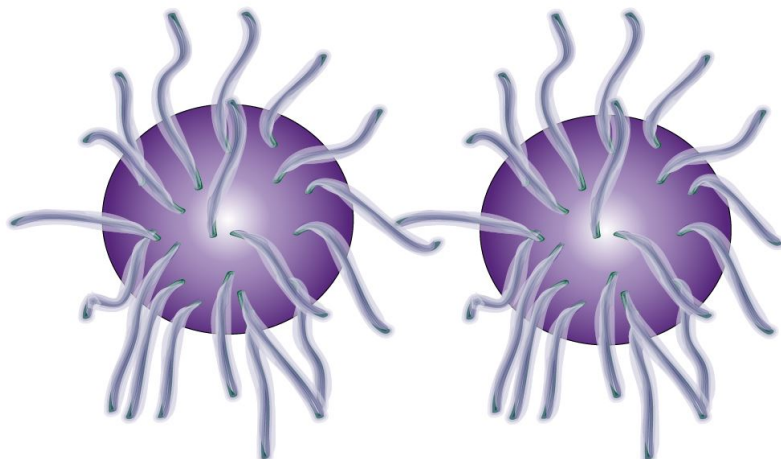


FIGURE 1.2: Steric stabilisation prevents particle contact due to interactions between spatially extended polymer chains (Gennes et al. [6]).

As particles approach, the adsorbed hydrophilic polymer chains interact with one another. Since these chains are hydrated, overlap of the layers causes some dehydration and hence an increase in free energy and a repulsion between particles. The repulsion is so strong that it can be assumed to become infinite as soon as the adsorbed layers begin to overlap, but zero at greater separations. This ‘hard sphere’ assumption is not strictly correct, but is good enough for most practical purposes and leads to some important conclusions. An important factor determining the degree of steric stabilisation is the thickness of the adsorbed layer relative to the particle size.

As Van der Waals attraction energy is proportional to particle size, larger particles will need thicker stabilising layers to confer the same degree of stability (Elimelech et al. [7]). Whey Protein Isolate (WPI), used in this work, is a small molecule and hence the electrostatic force is the key parameter.

### 1.2.6 Polymer bridging

Charge-patch interaction or particle bridging causes polymer bridging in colloids. When relatively low molecular weight, polyelectrolyte molecules adsorb on oppositely charged particle surfaces, an electrostatic “patch” is created. When these oppositely charged areas of different particles come into contact, a strong attractive force is created resulting in flocculation. The common flocculant used for polymer bridging is polyacrylamide. The hydrolysis of polyacrylamide converts amide groups to carboxylic acid groups. Some ions added to the colloids can effect the polymer bridging. If calcium ions are added, the adsorption of hydrolysed polyacrylamide on negatively charged particles is improved by linking carboxylate groups with anionic sites (Elimelech et al. [8] and Hogg [9]).

### 1.2.7 Depletion effect

A depletion force is an attractive force that arises due to the presence of non-adsorbed macro-molecules, micelles or other small particles. A zone of low osmotic pressure occurs between two approaching particles when the separation cannot geometrically accommodate the non-adsorbed macro-molecule. An attraction arises because water flows out of this low osmotic pressure zone to dilute the bulk solution which in turn forces the particles together.

## 1.3 Colloidal aggregation

Colloidal aggregation is a property of many chemical, physical and biological processes (Hidalgo-Alvarez et al. [10]). Aggregation in colloidal dispersions, suspensions, and emulsions plays a key role in many natural phenomena and industrial processes (Kovalchuk and Starov [11]). The stability of these systems can be explained on the basis of interaction forces between particles.

According to DLVO (Derjaguin, Landau, Verwey and Overbeek) theory the net interaction between two colloidal particles can be thought of as competition between attractive van der Waals (vdw) forces and repulsive electrostatic forces, representing the work done in distorting each particle's electrical double layer as they approach (Valleau, J. P et al. [12]). In this project, the aggregation process of an emulsion system is studied. Different interaction forces are generated by changing the physio chemical conditions, such as pH or calcium activity. The aim is to link the physio-chemical conditions to the aggregation stability via a single set of stickiness measurements.

## 1.4 Outline of research project

In this project, the properties of a model emulsion system are studied by measuring the time-evolution of the system's particle interactions under different environmental conditions. Specifically, the individual particle interactions are investigated at high precision using optical tweezers (OT), and these individual particle-pair interactions can be linked to the bulk ensemble behaviour. The aim is to capture complex droplet-droplet interactions with a single stickiness probability parameter. The WPI emulsion is used as a model system. First, a model for the DLVO forces at various conditions is created from a simplified surface equilibrium picture. The applicability of this model is then validated with viscosity measurements. Then the model is further tested by predicting the stability in the presence of additional attractions. The WPI emulsion is then investigated within a microfluidics system using optical tweezers. The stickiness probability is compared against the expected DLVO forces.

### 1.4.1 Surface properties

As described previously, surface properties have a key role in determining colloidal interactions. Emulsified fat is common in many dairy products including beverages and

yogurts. These products are characterised by a high ionic strength (80 *mM*) and are neutral pH (6.5 – 7 for beverages) or acidic pH (4 for yogurt). Proteins can stabilise fat droplets by adding a kinetic barrier to coalescence. In the case of whey protein isolate, this barrier is thought to be mostly electrostatic owing to its small size and high charge density.

This project uses a commercial WPI product (WPI 895) that consists of 76% Beta Lacto Globulin ( $\beta$ -LG), 15% Alpha Lact Albumin ( $\alpha$ -LA), 3% Bovine Serum Albumin (BSA). Compared to other whey protein sources, WPI has low levels of salts.  $\beta$ -LG is a small protein with a molecular weight of 18.5 *kDa* with a radius of gyration around 13.9 Å and has a total net charge of around +10 to around –20 charges per molecule depending on the pH (Roefs and Kruif [13]). The size and conformation of the  $\beta$ -LG can also be manipulated by the absorption of calcium ions. The manner in which calcium affects the interactions and hence stability of protein coated emulsion droplets has frequently been studied in a qualitative manner but has not been subjected to much quantitative analysis. We focus on a model which could explain the surface dependence of interactions effectively.

In this project, the effect of pH and salt concentration on the  $\zeta$  potential of the WPI emulsion is studied in order to gain a better understanding of the surface properties. First, the effects upon  $\zeta$  potential of various concentration of NaCl at different pH levels is investigated and fitted to the Gouy-Chapman (GC) model (Missana and Adell [14] and Oldham [15]). Then, from the fitted parameters, the  $\zeta$  potential is calculated at different concentrations of added calcium at constant ionic strength and pH using the model and verified experimentally. This means that the zeta potential and capture probability can be tuned using the environmental conditions, Na and Ca concentrations and pH.

### 1.4.2 Addition of depletion forces to the system – Application of surface properties

Two big colloidal particles immersed in a fluid of smaller colloidal particles or non-adsorbing polymers or micelles or smaller hard spheres (with the separation of the surfaces of the big particles less than the diameter of the small ones) experience an attractive depletion force proportional to the osmotic pressure of the medium due to the expulsion or depletion of the small particles, leading to an anisotropy of the local pressure (Asakura and Oosawa [16], Mao et al. [17], Götzelmann et al. [18], Roth et al. [19], and Lekkerkerker and Tuinier [20]). The stability of systems are strongly influenced by depletion forces.

Xanthan, commercially known as xanthan gum (a heteropolysaccharide produced by *Xanthomonas campestris* [21, 22]) is used in the experiments. Predicting the shelf life of emulsions is difficult as there is an overwhelming number of phenomena to consider. A good strategy to model the major effects by progressively building up increasingly complex models. The electrostatic interaction which could be characterised by the zeta potential is crucial in the behaviour of the added biopolymer [23]. The initial model that allows the calculation of the zeta potential, and thus interaction forces, based on the calcium levels as well as the ionic strength and pH, could be extended to a system with added biopolymer.

Laser diffraction measurements of droplet size distribution and confocal images are common analysis tools and are implemented. In a system consisting of a hydrocolloid stabiliser and an emulsifier that opposes coalescence, instability can be conceptually laid out in two stages: the aggregation of droplets and the coalescence of droplets. The aggregation of colloidal particles is of great importance in colloid science. Relation of attractive and repulsive forces acting between particles determines stability in these systems (Kovalchuk et al. [24]). Two distinct regimes of irreversible colloid aggregation are, One: Diffusion-limited colloid aggregation, where the repulsive force between the colloidal particles are negligible limiting the aggregation rate only to the time taken for

clusters to collide during diffusion and, Two: Reaction limited colloid aggregation where there is significant repulsive force, which has to be overcome by thermal energy between the particles, limiting the rate by time taken for two clusters to overcome this repulsive barrier by thermal activation (D.J Robinson and J.C Earnshaw [25]). These regimes correspond to the limiting cases of rapid and slow colloid aggregation in colloid science (Klein and Meakin [26]). The process by which two droplets touch and merges to a single bigger droplet with smaller surface area due to the surface tension at contact is known as coalescence (Eggers et al. [27]).

The assumption here is that droplets rest in a secondary minimum due to an attraction much longer in range than the repulsion. Conveniently, confocal images elucidate aggregation while laser diffraction elucidates coalescence. In a dairy system the Debye length, a measure of how far the net electrostatic effect of the charged particle in a solution persists is just over a  $nm$  and a confocal microscope cannot resolve the thin film that would separate charged droplets meaning aggregates appear as one large body. On the other hand, laser diffraction involves extreme dilution which removes any depletion force allowing individual droplets to separate.

### 1.4.3 Stickiness measurements

Optical tweezers are used in biological and physical sciences to precisely manipulate micron sized particles (Grier [28]) and are especially well suited to manipulating emulsion particles. Emulsion droplets are first trapped using the tweezers, then brought together and allowed to be in contact for a particular amount of time, then freed. The particles are then imaged to study the properties (Crocker and Grier [29]).

For this work, optical tweezers were used in conjunction with an automated microfluidic apparatus to measure the capture probability between pairs of particles. This was done in order to obtain statistically valid assessment of the stickiness between particles. The capture probability was determined for droplets with a range of surface charges,



controlled by the bulk ionic conditions. Handy features of microfluidics, such as laminar flow, facile integration with mechanical, electrical, optical systems, and low-cost fabrication (Wang et al. [30]) makes it easier for its integration to the experimental setup. In microfluidics, the proper selection of wavelength and phase of light helps in controlling motions and flows on a length scale that has challenged other technologies, hastening the adoption of lab-on-a-chip devices for a wide variety of applications (Grier [31]). The ideal range for the stickiness measurements will be near the isoelectric point (IEP), where the effect of zeta potential is most dramatic.

The capture probability corresponds to the collision efficiency in the Smoluchowski approach of perikinetic colloidal aggregation. Smoluchowski did initial studies on rates of aggregation assuming it to be second order process, where the rate of collision is proportional to the product of concentrations of two colliding species (Elimelech et al. [7]). The number of collisions between particles,  $i$  and  $j$  in unit time and unit volume with  $n_i, n_j$  referring to the number concentrations of different aggregates and rate constant  $k_{ij}$  is given by,

$$J_{ij} = k_{ij}n_i n_j; \quad ; k = i + j \quad (1.2)$$

Of these collisions, only some of them are effective in producing aggregates (collision efficiency,  $\alpha$ ), depending on the interparticle force between them from a range of 1, where all particle stick, suggesting a strong attractive force between particles, to an  $\alpha$  of 0, where nothing sticks due to strong repulsive force between particles. We are experimentally finding this efficiency of stickiness through the tweezer experiment as capture probability. This capture probability can be related to the low shear viscosity or droplet size.

#### 1.4.4 Application to shelf life

The results from the surface property study, depletion force study and stickiness measurements can be directly applied in industries to predict the shelf life of products. Surface studies gives a quantitative understanding of the zeta potentials which is a key to

predict the shelf life. A higher zeta potential suggests a more stable product ensuring higher shelf life. Adding a depletion force not only helps in regulating the consistency but also the stability of the product. Desired amount of the depletants can be added depending upon the requirement of the products and also to enhance the shelf life. Stickiness measurements can be carried out to products with known or unknown parameters to see how it would behave over time.

### 1.4.5 Approach

The project aims at studying aggregation processes through understanding colloidal interactions and by incorporating a measured capture probability.

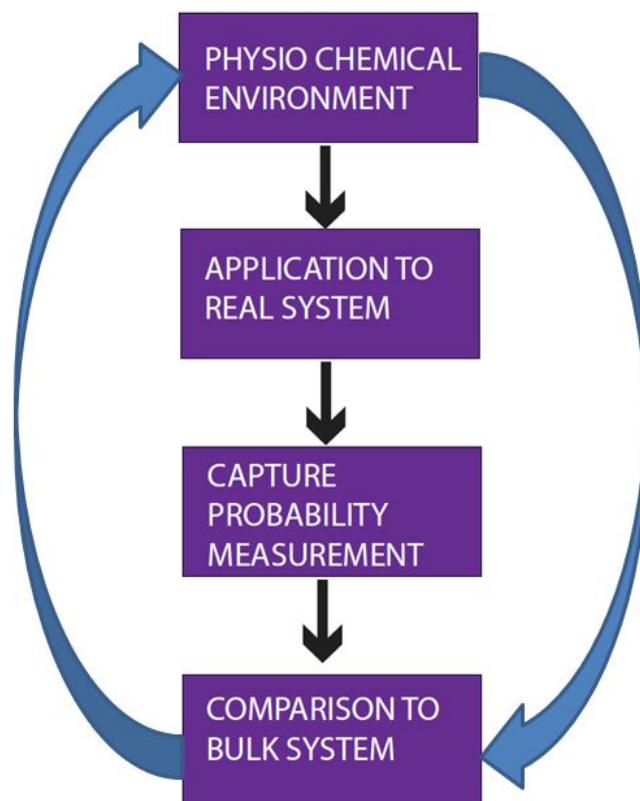


FIGURE 1.3: Basic scheme of the project

Hence, the understanding of one leads to the other. Figure. 1.3 is an illustration

of the plan of the project. The goal is to develop a model which would predict the growth kinetics once the physiochemical environment is known.

## **Chapter 2**

### **Materials and methods**

## 2.1 Emulsion formation

Emulsions contain at least two immiscible liquids, like oil and water, with one of the liquids being dispersed in the other. Emulsions can be classified based on the relative spatial distribution of the oil and water phases. A system consisting of oil droplets dispersed in a water phase is called an oil-in-water (O/W) emulsion (e.g. milk, cream, mayonnaise, beverages) and that consisting of water droplets dispersed in an oil phase is called a water-in-oil (W/O) emulsion (e.g. butter and margarine). Droplets in an emulsion are referred to as the dispersed, or internal phase, and the continuous fluid is called the continuous, external or solvent phase. The process by which two immiscible liquids are converted to droplets dispersed in a continuous phase is called emulsification. During emulsification, droplets are first deformed and broken up. The surfactants are adsorbed on to the surfaces of the deformed or new droplets then the droplets could collide with each other and could coalesce (Walstra [32]).

By dispersing oil and water, an emulsion can be formed, but on their own the particles will soon separate into an upper oil layer and bottom water layer due to merging of the droplets, leading to phase separation (as the contact between oil and water molecules is thermodynamically unstable). This can be overcome by adding kinetic stability enhancers called stabilisers or emulsifiers. Surface active molecules that adsorb to the surface of droplets during homogenisation creating a protective layer of repulsive forces. This prevents the droplets from coming close and aggregating. These surface molecules are known as emulsifiers. Emulsifiers are generally amphiphilic (having polar and non polar regions on same molecule) in nature. Surfactants, phospholipids, proteins, and polysaccharides are some common emulsifiers used in the food industry (McClements [33]).

Proteins are amphiphilic in nature, making them excellent choice in food emulsions. Proteins get adsorbed at the surfaces and forms films at the interfaces and hence lowers the interfacial tension (Van Aken [34] and Perrechil and Cunha [35]).

### 2.1.1 WPI emulsion

Milk proteins are excellent emulsifiers. They can be classified as either caseins or whey proteins. Whey proteins are used in the current study as they are soluble in milk serum or whey and need not consider the steric interactions. Whey proteins are highly structured, and possess a compact globular structure held together by hydrophobicity, covalent links and hydrogen bonding (Euston et al. [36]). Whey Protein Concentrate (WPC) and Whey Protein Isolate (WPI) are the soluble whey products. WPC is obtained by ultra-filtration and diafiltration of whey, and WPI by ion exchange recovery. WPC contains a maximum of about 75% protein, whereas WPI has up to 90% protein (Wong et al. [37]).

$\beta$ -lactoglobulin,  $\alpha$ -lactalbumin, serum albumin, immunoglobulins and proteose-peptone fractions are the major characterised components of whey proteins (Farrell et al. [38]).

$\alpha$ -lactalbumin is a globular metalloprotein consisting of 123 amino acids with a molecular weight of 14,147 (genetic variant A); 14,175 (genetic variant B) and a structure stabilised by 4 sulphur bridges. One atom of calcium is reversibly bound to this protein stabilising the tertiary structure (Baumy and Brule [39]).

$\beta$ -lactoglobulin is another major globular whey protein, consisting of 162 amino acids with molecular weight of 18,362 (genetic variant A) and 18,276 (genetic variant B).  $\beta$ -LG is acid stable without denaturing down to about pH 2 but its surface activity is very much dependent on pH (Wong et al. [37]).

Aggregation of WPI stabilised emulsion droplets is sensitive to the pH and ionic strength of the aqueous phase. Near the isoelectric point (IEP), considerable aggregation occurs resulting in an increase in viscosity of the emulsion and a greater instability due to creaming (Demetriades et al. [40]).

### 2.1.2 Preparation of the emulsion

WPI stabilised emulsions were manufactured for this study. Different methods of preparation were explored by trying different values for the rpm of Ultra-Turrax and pressures for the two stages of the homogenizer so as to reach the desired size of the emulsion droplets (around  $\approx 2 \mu m$  so that it is possible to manipulate the particles in a microfluidic chip and trap using an optical tweezer setup later as described in chapter. 5). Adjusting the pH at different stages of emulsification and the zeta potential of resultant emulsion showed great dependency. The following protocol is culminated so as to maintain the reproducibility of the data.

2 wt% WPI was mixed with milli-Q water and stirred at 50 °C for half an hour. The final pH was measured to be 6.3. Native WPI is almost completely soluble at room temperature from pH 3 to 8 (Damodaran et al. [41]). 20 wt% canola oil was added into the mixture and pre-homogenised at 7,000 rev/min for 6 minutes using an Ultra-Turrax T25 (IKA®-Werke GmbH & Co. KG, Staufen, Germany) to form a coarse emulsion. Subsequently a two-stage high pressure homogenizer (Panda, Niro Soavi, Parma, Italy) was used to emulsify the sample at a pressure of 150 bar on the first stage and 50 bar on the second stage at ambient room temperature (ca. 22 °C).

The solution was dialysed to have a well-defined ionic background and to remove unadsorbed protein preventing any depletion forces that may arise. The emulsion was dialysed against water with 0.02 wt% sodium azide to prevent any bacterial growth. The cellulose membrane had a molecular weight cut off of 20 kDa. Three solution changes reduced the concentration of unadsorbed material by a factor of 5<sup>3</sup>. Large droplets were removed by leaving the emulsion in a narrow graduated cylinder for 24 hours and discarding the upper 25% of the sample. The emulsion was stored at a temperature of 10 °C. The emulsion droplet size was measured using a Malvern Mastersizer (Malvern Instruments Ltd. A general purpose spherical analysis model was used with particle refractive index of 1.47 in water with zero light absorption, and an obscuration



(A) Ultra Turrax



(B) Homogeniser

FIGURE 2.1: Ultra Turrax and Homogeniser

value between 12% to 15%.) The results showed a particle distribution that peaked at around  $2\ \mu\text{m}$  diameter. Figure. 2.2 shows the particle size distribution before and after the removal of the large droplets.

A surface coating of WPI can stabilise emulsions under acidic conditions (round pH 3) and also in a basic condition (around pH 7 and above). The composition of the adsorbed layer at pH 3 contains much higher levels of  $\alpha$ -LA than at pH 7. This difference in conformation could be due to changes in the conformation and quaternary structure of the whey proteins when the pH is lowered (Hunt and Dalgleish [42]). This preferential adsorption at different pH results in different surface properties and hence different zeta potential and stickiness of the emulsion droplets. So the pH of the sample was maintained constant and the method of preparation of emulsion standardised. When the pH was adjusted before mixing with the Ultra Turrax or the pH was adjusted after mixing different zeta potential values were observed. Hence, it does matter how we made the emulsion: the properties are path dependent.



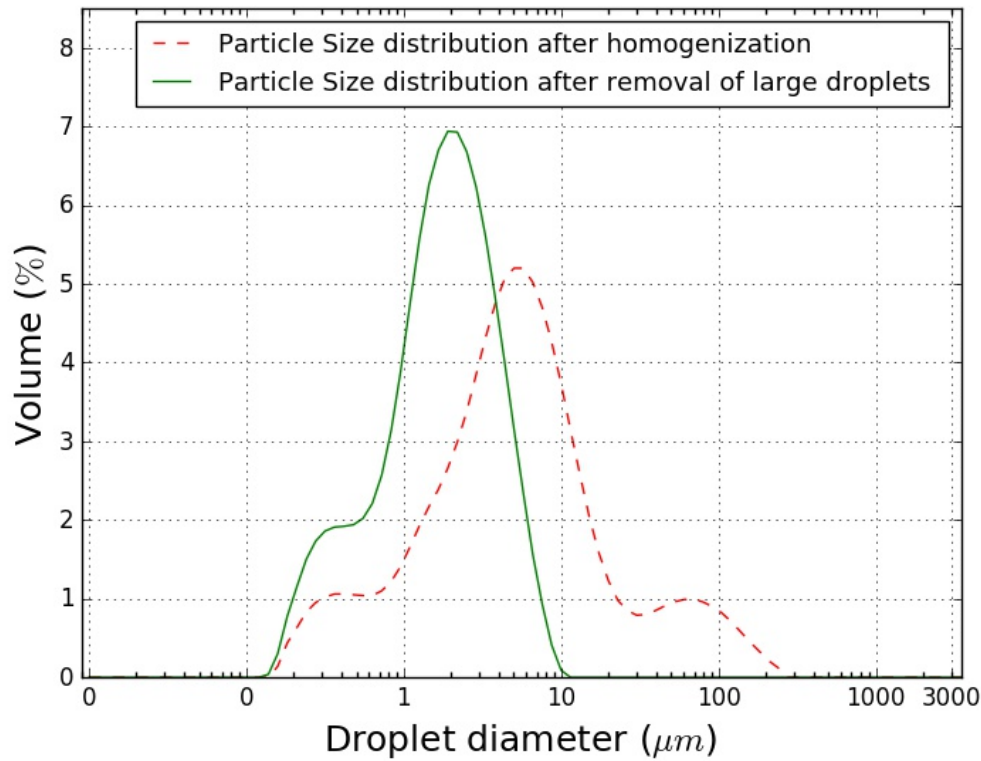


FIGURE 2.2: Droplet diameter distribution, measured using a Malvern Mastersizer before and after the removal of the large droplets.

### 2.1.3 Determination of viscosity of emulsions

The rheology of the sample was measured using a double gap geometry which was found to be better than cup and bob geometry for 20% O/W emulsion.

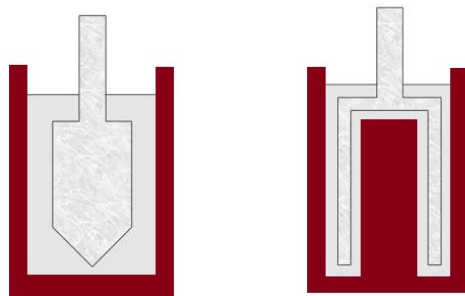


FIGURE 2.3: Schematic representation of left: Cup and Bob Geometry right: Double gap geometry.

When highly viscous oil droplets are dispersed in a medium of low viscosity (water), the relative viscosity  $\eta(r)$  of a dilute O/W emulsion of non-interacting droplets behaves as it would for a suspension. In the above case,  $\eta(r)$  is given by the Einstein equation (Einstein [43]):

$$\eta(r) = \eta_0(1 + 2.5\phi) \quad (2.1)$$

where  $\eta_0$  is the viscosity of suspending medium and  $\phi$  is the volume fraction (total volume of oil in the emulsion divided by the volume of the emulsion) of oil droplets. The prepared emulsion was diluted by one third, one fourth, one fifth and one sixth, and the viscosity was measured and compared to the trend estimated using the Einstein equation to check that the composition didn't change in the emulsification procedure. Figure. 2.4 gives the measured and expected relative viscosity. Which means, the emulsion has almost 20 wt% of oil and is not lost in the process.

A flow curve gives viscosity as a function of shear stress which arises from the parallel force vector component of the cross section of the material. High concentration leads to principle changes in the rheological properties as shown in the flow curve shown in Figure. 2.5. Newtonian viscous flow, where the viscosity is a constant for all the shears is replaced by a viscoplastic behaviour (rate-dependent inelastic behaviour) with a decrease in the apparent viscosity in a small range of applied stresses. The jump in the apparent viscosity at some shear stress can be treated as the yield stress of the emulsion.

Thixotropy (time-dependent shear thinning property) is another rheological behaviour of concentrated emulsions. The interfacial layers in the closely arranged drops produce structures destroyed by deformation and restored at rest. Viscoelastic effects are caused by interaction between drops and the evolution of their shape during flow.

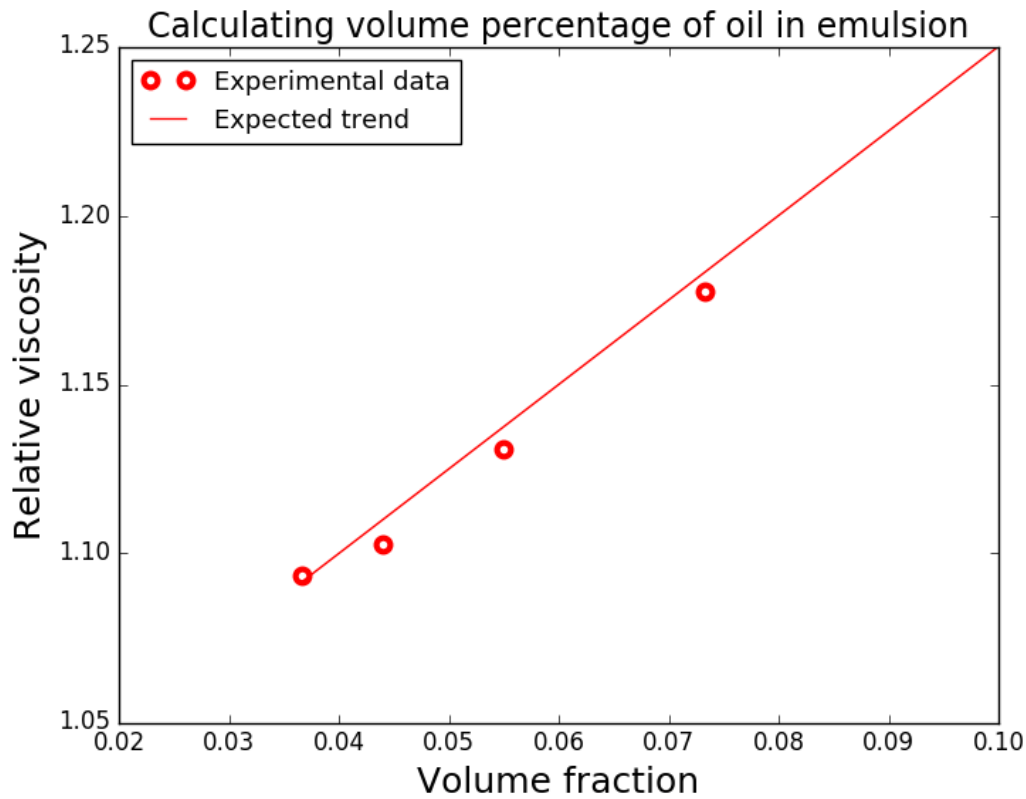


FIGURE 2.4: Dilution rheology: Measured (points) and calculated (Eqn. 2.1) relative viscosity for 20 wt% canola oil in water emulsion using Einsteins equation.

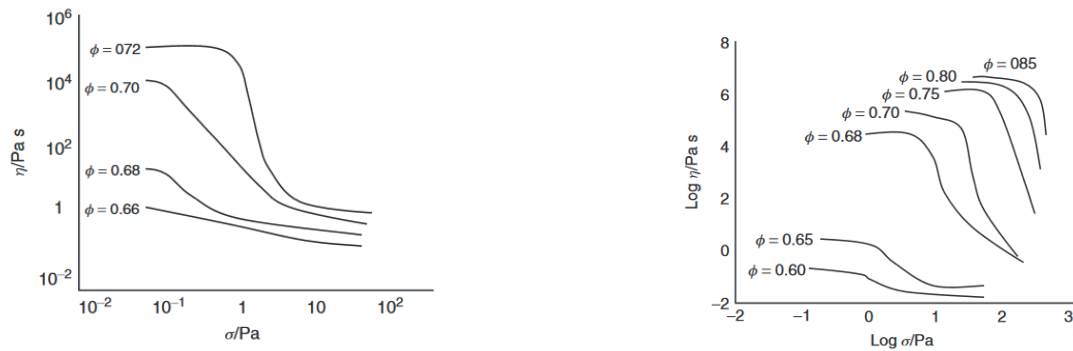


FIGURE 2.5: Left: Flow curves of model O/W emulsion (average drop size of  $4.6\mu\text{m}$ ) at various volume fractions. Right: Flow curves of W/O emulsions when approaching the concentration limit corresponding to the closest packing of spherical drops (Tadros [44])

## 2.2 Xanthan gum

Xanthan gum is a polysaccharide produced by the bacterium *Xanthomonas campestris* found on cabbage plants (Whitcomb and Macosko [45]). It is a heteropolysaccharide with a primary structure consisting of D-glucose, D-mannose, and D-glucuronic acid in the ratio of 2 : 2 : 1 and also of pyruvic and acetic acid (Sandford et al. [46]). X-ray diffraction studies suggest a helical structure for xanthan with side groups folding down along the helix creating a stiff rod-like macro-molecule (OKUYAMA et al. [47]). Xanthan is generally soluble in cold and hot water but forms lumps if not agitated intensely upon introduction into the aqueous medium (Katzbauer [48]).

Xanthan is widely used in food industry due to its properties like emulsion stabilisation, stability at different temperature, rheological properties, long term stability, compatibility with food products, air incorporation and retention etc (García-Ochoa et al. [49] and Sworn [50]). Xanthan is specifically used for the depletion study in this work as it being a large non adsorbing macro-molecule, ensure a depletion flocculation at dosages that are practical (not exceedingly high, therefore diluting the emulsion). The non adsorbing at the surface also means the zeta potential calculations in the absence of the polymer can be applied even when it is present in the samples. It has also been studied before in a qualitative manner, so useful for ensuring confidence in droplet sizes etc.

## 2.3 Zeta potential measurements using a Zetasizer

The Zetasizer Nano series calculates the zeta potential by determining the electrophoretic Mobility and then applying the Henry equation.

$$U_E = \frac{2\epsilon\zeta f(k_a)}{3\eta} \quad (2.2)$$



FIGURE 2.6: Zetasizer Nano used for measuring the zeta potential of the sample and the folded capillary cell to which the sample was injected (Malvern Instruments Ltd [51]).

where  $U_E$  is the electrophoretic mobility,  $\zeta$  is the zeta potential,  $\epsilon$  is the dielectric constant,  $\eta$  is the viscosity,  $f(K_a)$  is the Henry's function (values which varies between 1 and 1.5 were used in Henry's function). In the experiment, Henry's function with a maximum value of 1.5 for measuring zeta potential which is generally used for particles in polar media of moderate electrolyte concentration is used.

The electrophoretic mobility is obtained by performing an electrophoresis experiment on the sample and measuring the velocity of the particles using Laser Doppler Velocimetry (Malvern Instruments Ltd [51]). The Zetasizer Nano consists of

- A laser is used to provide a light source to illuminate the particles within the sample (for zeta potential measurements this light source is split to provide an incident and reference beam).
- An Attenuator to avoid overloading of light to the detector.
- The laser beam passes through the centre of the sample cell.

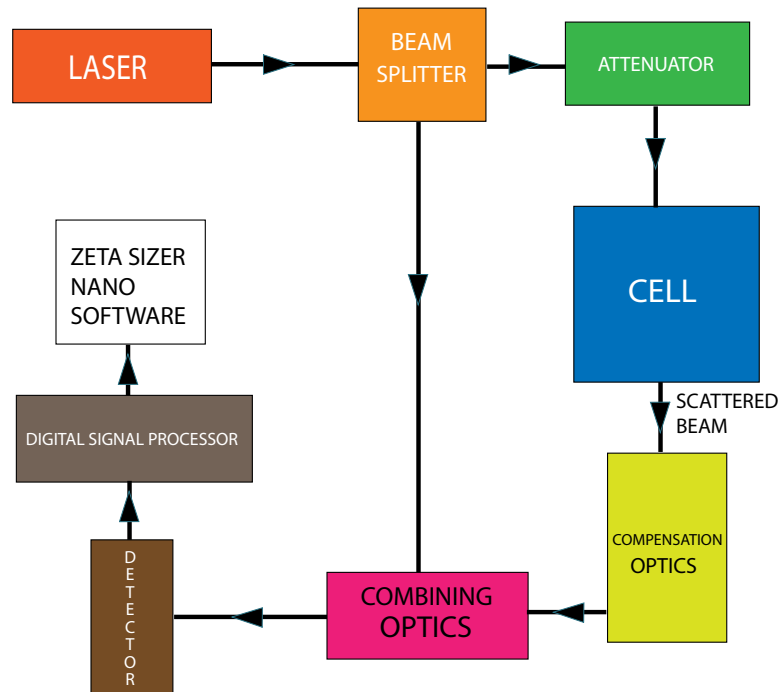


FIGURE 2.7: Zetasizer Nano operation.

- compensation optics, to correct for any differences in the cell wall thickness and dispersant refraction
- A detector.
- Digital signal processor collects the information from detector.
- A computer, where the Zetasizer Nano software produces a frequency spectrum from which the electrophoretic mobility and hence the zeta potential information is calculated from the data.

## 2.4 Confocal Imaging

Microstructure of the emulsions was studied using Leica SP5 DM6000B Scanning Confocal Microscope. Images were acquired sequentially at a resolution of  $1024 \times 1024$  pixels and  $400\text{ Hz}$  with a HCX PL APO 60.0x1.40 oil lens. Fast green was acquired by excitation

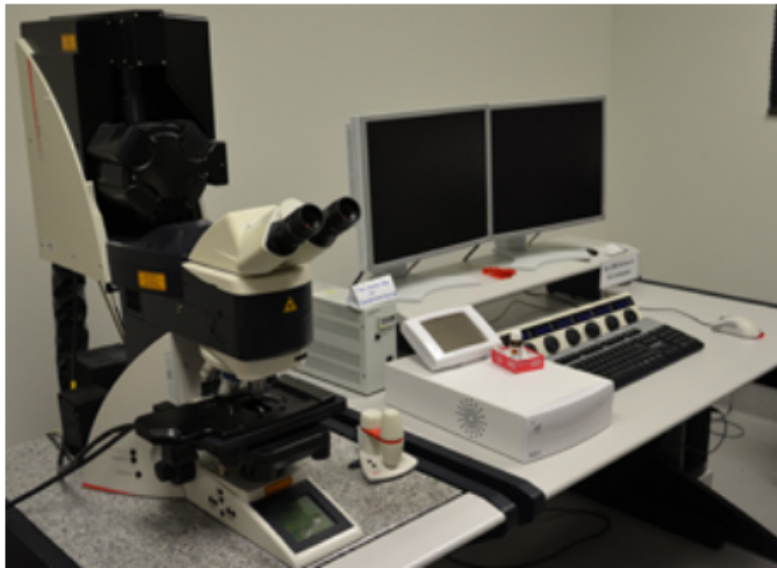


FIGURE 2.8: Leica Scanning Confocal Microscope. Image courtesy: Manawatu Microscopy and Imaging Centre (MMIC)

with the  $561\text{ nm}$  laser and emission collected from  $658\text{ nm} - 625\text{ nm}$ . Nile red was acquired by excitation with the  $633\text{ nm}$  laser and emission collected from  $641\text{ nm} - 800\text{ nm}$ . The confocal images are given in Figure. [A.1](#) of Appendix. [A](#) and Figure. [C.3](#) of Appendix. [C](#)

## **Chapter 3**

**Dependence of the properties of whey protein stabilised emulsions on the physio-chemical conditions and zeta potential.**



A thorough understanding of solid-liquid interfaces is crucial for understanding experimental colloidal aggregation measurements.

For the whey protein stabilised emulsion particles used in this thesis, stability is predominately electrostatic due to the small size and high charge density of its individual interface components (Foegeding et al. [52]). The ionisation degree and hence the stability and aggregation of whey-protein stabilised emulsions depends strongly on pH, ionic strength, and calcium activity of the bulk (Hunt and Dalgleish [53], Ju and Kilara [54], Kulmyrzaev et al. [55], and Spiegel and Huss [56]). In order to produce an emulsion that is stable, it is important to ensure that the pH is far from the isoelectric point (IEP) of the proteins and that the salt concentration is sufficiently low that surface charges are not significantly screened and the zeta potential ( $\zeta$ ) remains high (Kulmyrzaev and Schubert [57] and Sun and Gunasekaran [58]).

The electrostatic interaction between droplets can be predicted from surface potential, ionic strength (a proxy for Debye length) and droplet size. The experimental determination of the surface potential is generally an arduous task but it is well approximated by the more accessible zeta potential. The zeta potential is the electrostatic potential at the slipping plane a few molecules away from the surface (Dalgleish [59]). The manner in which pH, calcium activity and ionic strength affect the interactions, and hence the stability of protein coated emulsion droplets, has frequently been studied (Dickinson and Golding [60], Kulmyrzaev et al. [61], Ye and Singh [62], and Sosa-Herrera et al. [63]) but a complete quantitative analysis that captures all of these terms has not been attempted to date.

In this chapter we highlight the fact that electrostatic interactions between colloidal particles greatly influence their aggregation properties (Elimelech et al. [7]) so we will be focusing on describing electrical double layer forces and how physical models can be applied to the interface.

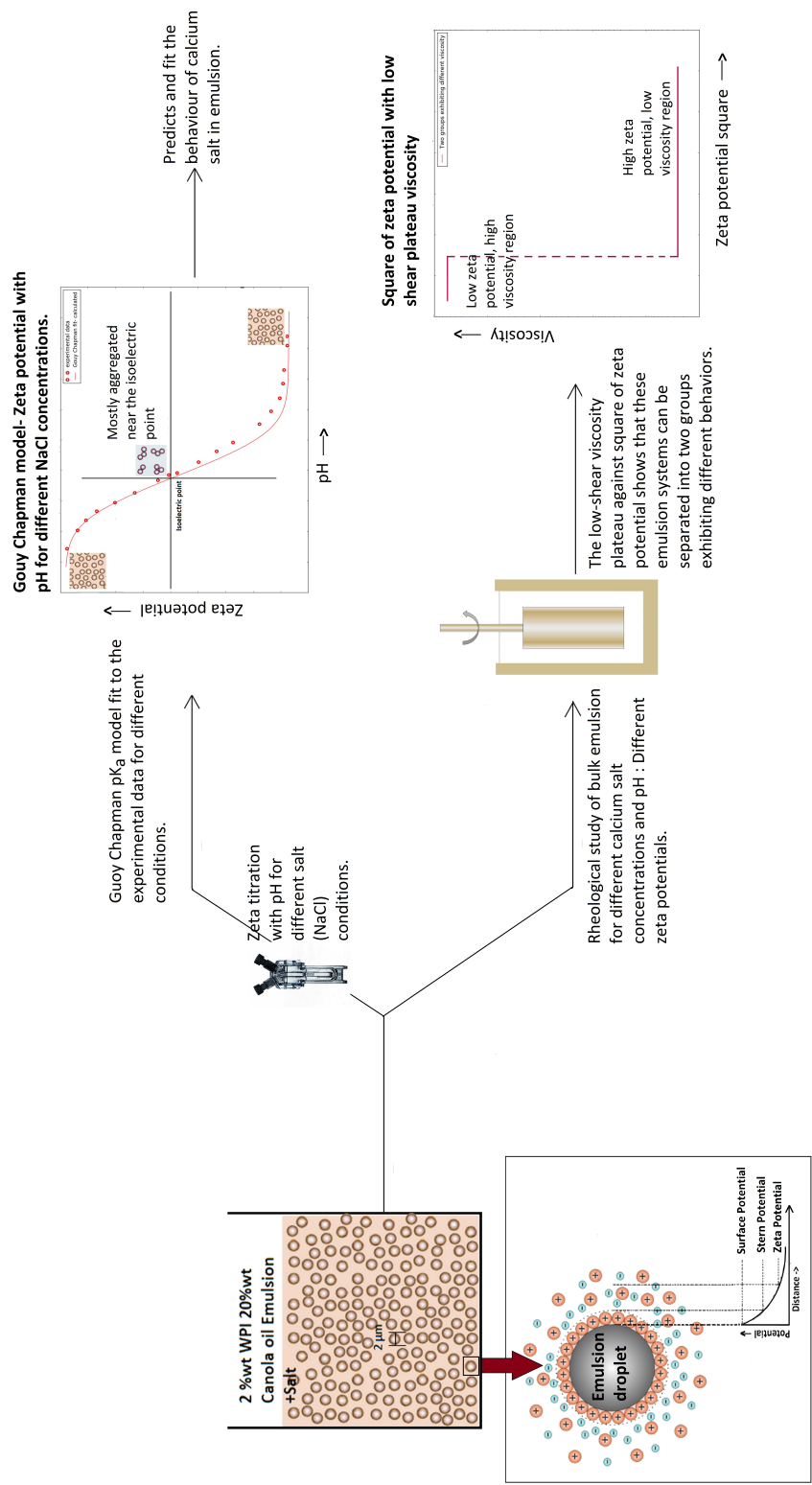


FIGURE 3.1: Graphical representation of the experimental and theoretical work.

### 3.1 Gouy-Chapman double layer model and Grahame equation

Gouy and Chapman independently came up with models to describe the charge and the potential distribution in solution as a function of distance from the surface. They did this by assuming the following:

1. The interface is infinite, flat and impenetrable.
2. The compensating or counter ions are point charges, immersed in continuous dielectric medium.
3. Ion-ion interactions are neglected – only the Coulomb interaction is considered.
4. Surface charge and hence the potential are distributed uniformly over the surface.
5. The solvent or dielectric medium is considered to be uniform throughout.

The Gouy-Chapman model is a good approach for treating electrolytes with concentrations of less than 200 mM and surface potential below 40 mV. For potentials that are greater than this, a Stern layer consisting of adsorbed hydrated ions must be considered.

In the following sections, o/w emulsion particles with WPI on the interface will be examined in light of the Gouy-Chapman model. The model will be adapted using an amino acid charging equilibria to model our WPI emulsion. It will be assumed that the  $\zeta$  potential is equal to the surface potential in this case.

### 3.2 Inter-droplet interactions

For protein-stabilised emulsions, the physio-chemical properties depend on the:

- nature, strength and range of attractive and repulsive forces

- environmental conditions (salt concentration, pH) that influence these forces (Dalglish [64])

The total interaction potential between a pair of emulsion droplets is the sum of the Van der Waals, electrostatic and short-range interaction potentials. When attractive forces dominate, the emulsion droplets tend to aggregate. The electric double layer force and the zeta potential are sensitive to pH and ionic strength. At pH near the isoelectric point of the protein, the net charge on the droplets is low, hence the electrostatic repulsion is weak. Increasing the ionic strength results in more counter ions shielding charges on the droplet surface and decreasing the electrostatic repulsion between droplets. Hence, aggregation of emulsion droplets stabilised by WPI is very sensitive to pH and ionic strength. Near the isoelectric point of the proteins, extensive flocculation occurs which leads to a considerable increase in viscosity of the emulsion and a greater instability due to creaming of aggregated droplets (Demetriades et al. [40]).

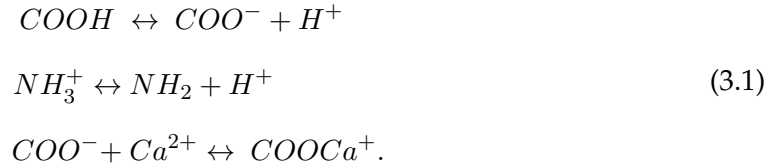
### 3.3 The development of the theoretical framework for the data analysis

#### 3.3.1 Gouy-Chapman $pK_a$ model for WPI emulsions

As described, the stability and aggregation of whey-protein stabilised emulsions depends strongly on pH and concentration of salt added. Relatively low electrostatic repulsion between the emulsion droplets near the isoelectric point causes them to aggregate. To produce an emulsion that is stable, it is important to ensure that the pH is sufficiently far from the isoelectric point of the proteins (Kulmyrzaev et al. [65]) and that the salt concentration is less than that which would cause instability.

The surface of the emulsion droplets are coated with WPI. The charge on the surface is determined by the equilibrium charging behaviour of the amino acids in the

surrounding environment. The hypothesis is that this complex charge behaviour can be approximated by three generic equilibrium: the protonation of carboxylic acids and amine groups and an electrostatic interaction between carboxylic acid groups and calcium ions:



Notably, in the absence of calcium there are only two equilibria of concern. The  $pK_a$  of carboxylic acids is typically around 5, with values of amines much higher, around 12. The large separation between these values means that the separate contributions of the two types of groups to droplet charging behaviour can be easily resolved since the bulk of the charging behaviour occurs within a few pH units of the  $pK_a$ . The charging behaviour of latex particles, metal oxides, metal sulphides, clay, glass and silica has previously been modelled by combining charging estimates using the  $pK_a$  value of ionisable surface groups with the Gouy-Chapman model of the electrical double layer (EDL) (Larson and Attard [66], Behrens and Grier [67], Usui and Healy [68], Leroy and Revil [69], and Hizal and Apak [70]). Such an approach has been shown to work well when the absolute value of the zeta potential is less than 40 mV, above which Stern layers (refer Appendix. B) must be taken into account (Butt et al. [71]). To create this model the effect of pH and ionic strength on the zeta potential is determined, allowing the concentration and  $pK_a$  of surface amino acids to be calculated. Subsequently, the effect of calcium is introduced, allowing the prediction of the zeta potential from any combination of ionic strength, calcium activity and pH (within the limits of the Gouy-Chapman model). The stability of the emulsion can thus be tuned and/or predicted based on pH, calcium concentration [Ca], and I (ionic strength) alone.

### 3.3.2 Theory and calculation

The DLVO theory of colloidal stability (named after Derjaguin, Landau, Verwey and Overbeek) assumes that the total force between colloidal particles is obtained by adding the van der Waals and electrical double layer forces between them (Cosgrove [72]). A quantitative appreciation of the EDL in these systems also provides the opportunity to highlight the significance of any non-DLVO forces in the experimental data.

With a complete picture of the surface electrical behaviour in hand, macroscopic rheological properties and coagulation rates can be compared in light of the predicted DLVO forces operating. The rheological properties of protein solutions can be influenced by concentration, temperature, pH, ionic strength, and previous processing treatments (Tung [73]). Intermolecular interactions between charged protein molecules play a large role in determining the rheological properties in solutions and protein-stabilised emulsions (Goodwin [74]). The consistency index and the flow behaviour index are sensitive to changes in pH and protein concentration (Bazinet et al. [75]). Indeed, flow properties and yield stresses of suspensions have previously been related to electrokinetic measurements (Hunter [76] and Scales et al. [77]). The ionisation of these groups on the protein molecule determines the surface charge of the droplets. The ionisation degree depends on the pH and ionic strength of the bulk. Below the isoelectric point of the WPI, the number density of positively charged groups at the surface will be greater than negatively charged groups. At this point, the amino groups are positively charged ( $-NH_3^+$ ) and carboxyl groups are neutral ( $-COOH$ ). With an increase of pH, the magnitude of positive charge decreases due to some of the carboxyl groups becoming negatively charged ( $-COO^-$ ) and some of amino groups becoming neutral ( $-NH_2$ ). At the isoelectric point, the potential becomes zero indicating that there is a balance of positively and negatively charged groups. If the pH is increased beyond the IEP, a net increase of negative charge will lead to higher negative potential (Kulmyrzaev and Schubert [78]).

In the following,  $N_{S1}$  and  $N_{S2}$  are defined as the total number of carboxylic and amine groups present at the surface per unit area:

$$N_{S1} = N_{COO^-} + N_{COOH} \quad (3.2)$$

$$N_{S2} = N_{NH_2} + N_{NH_3^+}. \quad (3.3)$$

The equilibrium constants are defined as:

$$K_{a1} = \frac{[COO^-][H^+]}{[COOH]} \quad (3.4)$$

$$K_{a2} = \frac{[NH_2][H^+]}{[NH_3^+]}. \quad (3.5)$$

Adapting the equilibrium to a mass action law at the surface allows these to be rewritten (Behrens et al. [79]) as:

$$K_{a1} = \frac{N_{COO^-}[H^+]_S}{N_{COOH}} \quad (3.6)$$

$$K_{a2} = \frac{N_{NH_2}[H^+]_S}{N_{NH_3^+}}. \quad (3.7)$$

$[H^+]_S$  is the *surface* proton concentration. This concentration will be different from that of the bulk on account of the EDL. A negatively charged surface will attract protons and cations that would be repelled from a positive surface. The Boltzmann equation can be used to write the relation between surface or EDL and bulk proton concentrations (Hall et al. [80] and Butt et al. [71]) as:

$$[H^+]_S = [H^+]_{bulk} \times e^{\frac{-e\Psi}{k_B T}} \quad (3.8)$$

where  $e$  is the electron charge,  $\Psi$  is the surface potential,  $k_B$  is the Boltzmann constant and  $T$  the temperature. (Note that  $z = 1$  has been omitted from this equation.) These equations allow the equilibrium concentrations of surface charge groups to be predicted as a function of pH, and subsequently the zeta potential can be calculated using the Grahame equation for surface potential  $\Psi$  and approximating their equivalence which is established experimentally (Popa et al. [81]).

$$\Psi = \frac{2k_B T}{ze} \times A \sinh \left[ \frac{\sigma_{app} z e \lambda_D}{2 \varepsilon_0 \varepsilon_r k_B T} \right] \quad (3.9)$$

where  $\varepsilon_r$  is the relative permittivity of the medium,  $\varepsilon_0$  is the permittivity of free space, with the apparent surface charge density:

$$\sigma_{app} = e \times (N_{NH_3^+} - N_{COO^-}). \quad (3.10)$$

The Debye length is given by:

$$\lambda_D = \left[ 4\pi \lambda_B \sum_{j=1}^N n_j z_j^2 \right]^{-\frac{1}{2}} \quad (3.11)$$

with  $\lambda_B$ , the Bjerrum length, given by:

$$\lambda_B = \frac{e^2}{4\pi \varepsilon_0 \varepsilon_r k_B T}. \quad (3.12)$$

$n_j$  is the ion density.



The Bjerrum length is 7.025 Å at 25 °C, hence  $\lambda_D$  is calculated as 1.08 nm for solutions with an ionic strength of 80 mM.

The model strategy involves plotting the experimentally measured zeta potential against the bulk pH for different concentrations of NaCl and optimising the model fit in order to find the values of the total number of carboxyl and amine groups and their  $pK_a$  values ( $N_{S1}$ ,  $N_{S2}$ ,  $pK_{a1}$ ,  $pK_{a2}$  respectively). Once  $K_{a1}$ ,  $K_{a2}$ ,  $N_{S1}$  and  $N_{S2}$  have been found in this manner, the model can be extended in order to investigate the way in which calcium affects the stability of protein coated emulsions. Such systems have frequently been studied in a qualitative manner, but not subjected to much quantitative analysis.

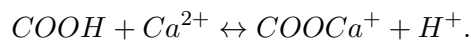
When calcium is added to this WPI stabilised emulsion, the surface ionisation degree is modified by calcium binding, which can be described according to:

$$K_{Ca} = \frac{[COOCa^+]}{[COO^-][Ca^{2+}]_S}. \quad (3.13)$$

where  $[Ca^{2+}]_S$  is the local calcium concentration in the solution directly at the surface or EDL calcium concentration, noting  $z = 2$  given by:

$$[Ca^{2+}]_S = [Ca^{2+}]_{bulk} \times e^{\frac{-2e\Psi}{k_B T}}. \quad (3.14)$$

Calcium binds to  $COO^-$  forming  $COOCa^+$  thus increasing the positive charge at the surface resulting in an increased (more positive) zeta potential. Combining the ionisation of carboxylic and calcium ions then:



Defining the equilibrium on a one-to-one or one-to-two stoichiometry does not

affect basic results of the model but provides algebraic simplicity. A one-to-one stoichiometry will alter the calcium saturation limit, however the model and experiments are more than ten times below this limit.

The overall equilibrium constant for calcium binding  $K_{ov}$  is given by:

$$K_{ov} = \frac{[COOCa^+][H^+]_S}{[COOH][Ca^{2+}]_S}. \quad (3.15)$$

Noting that  $K_{ov} = K_{a_1} \times K_{Ca}$  and replacing the equilibrium with a mass action law for surfaces as before, the apparent surface charge can now be given by:

$$\sigma_{app} = e \times (N_{NH_3^+} - N_{COO^-} + N_{COOCa^+}). \quad (3.16)$$

With the number of carboxylic groups appropriately modified:

$$N_{S1} = N_{COOCa^+} + N_{COO^-} + N_{COOH} \quad (3.17)$$

and substituting  $N_{COOCa^+}$  from equation 3.16, equation 3.17 becomes:

$$N_{S1} = \left( \frac{\sigma_{app}}{e} - N_{NH_3^+} + N_{COO^-} \right) + N_{COO^-} + N_{COOH}. \quad (3.18)$$

Rearranging 3.18 gives:

$$N_{COOH} = N_{S1} - 2N_{COO^-} - \frac{\sigma_{app}}{e} + N_{NH_3^+}. \quad (3.19)$$

$K_{ov}$  can now be re-written as a product of  $K_{a_1}$  and  $K_{Ca}$  with  $K_{a_1}$  expanded. First  $[H]_S$  is substituted by equation 3.8. Then the denominator of  $K_{a_1}$  is replaced by

with equation 3.19

the overall equilibrium constant can be written as:

$$K_{ov} = \frac{N_{COO^-}[H^+]_S}{N_{COOH}} \times K_{Ca} = \frac{N_{COO^-}([H^+]_{bulk} \times e^{\frac{-e\Psi}{k_B T}})}{(N_{S1} - 2N_{coo^-} - \frac{\sigma_{app}}{e} + N_{NH_3^+})} \times K_{Ca} \quad (3.20)$$

To model the zeta potential of WPI stabilised emulsions not only as a function of pH and ionic strength, but also as a function of calcium activity,  $K_{Ca}$  is used as the fit parameter. The combination of equations 3.9, 3.6, 3.7 and 3.20 provides a theoretical framework that can be used. First, the pH and ionic strength need to be predefined, and  $N_{S1}$ ,  $N_{S2}$ ,  $K_{a1}$  and  $K_{a2}$  need to be known. Then a list of  $\sigma_{app}/e$  values is generated and used to calculate an accompanying list of  $\zeta$  potential values. Next,  $N_{NH_3^+}$  is solved for using equation 3.7. Choosing a fit value of  $K_{Ca}$  leaves  $N_{COO^-}$  as the only unknown in equation 3.20 which can now be solved for each  $\sigma_{app}/e$  value. Then equation 3.16 gives  $N_{COOCa^+}$  and likewise,  $N_{COOH}$  can be solved via equation 3.19. Finally the calcium activity is calculated using these values from the fitted value of  $K_{Ca}$  and equations 3.13 and 3.14. Caution must be used to not generate nonsensical negative values for any of the charge group densities when using this approach.

### 3.3.3 DLVO theory

According to DLVO theory, the interaction between two colloidal particles bearing the same charge is comprised of a repulsive EDL potential and an attractive Van der Waals potential.

$$V_{DLVO}(h, \psi) = V_{EDL}(h, \psi) + V_{vdW}(h) \quad (3.21)$$

where,  $h$  is the separation between surfaces of the spheres and  $\psi$  is the surface potential.

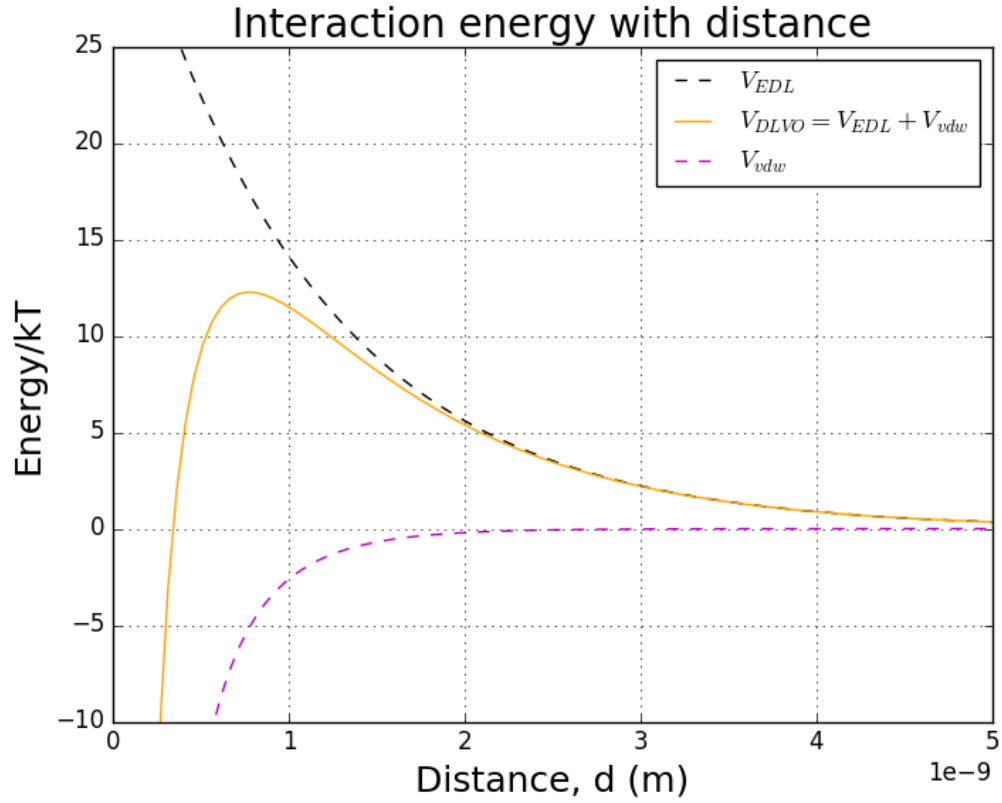


FIGURE 3.2: DLVO interaction profile: The total potential energy as the sum of the attractive Van der Waals potential and the repulsive EDL potential. The DLVO potential calculated here is for a zeta potential of  $-18 \text{ mV}$ .

The DLVO energy profile may show a shallow secondary minimum at larger distances, then increases to a maximum as the distance decreases, before dropping to a deep attractive potential at short distances. Colliding particles must overcome the repulsive energy barrier to come into contact and stick together, leading to coagulation. The relative prominence of attractive and repulsive forces determines the aggregation behaviour in colloidal systems (Israelachvili [82]). The EDL interaction potential between two closely placed spheres is given by (Masliyah and Bhattacharjee [83] and Elimelech et al. [84]):

$$V_{EDL}(h, \psi) = 2\pi\epsilon_r\epsilon_0 a\psi^2 e^{\frac{-h}{\lambda_D}}. \quad (3.22)$$

Here  $a$  is the radius of spheres,  $\lambda_D$  is the Debye length, and as previously mentioned  $\epsilon_r$  is the relative permittivity of the medium and  $\epsilon_0$  is the permittivity of free space.

The Van der Waals potential, arising from spontaneous electric and magnetic polarisation for identical spheres at close approach is:

$$V_{vdW}(h) = -\frac{a}{12h} \times Ae^{\frac{-2h}{\lambda_D}} \quad (3.23)$$

where  $A$  is the Hamaker constant (for canola oil droplets in water,  $A \sim k_B T$  is assumed, typical of many hydrocarbons in water) (Hamaker [85]). The DLVO energy profile is shown in figure. 3.2.

In principle, Van der Waals interaction energy is insignificant at larger distances but attraction becomes very strong on close approach. Other repulsive forces are also present at short ranges (section 1.2.3) and make the attraction finite. Van der Waals attraction is assumed not to change in our experiments.

## 3.4 Materials and methods

### 3.4.1 Materials

Whey Protein Isolate 895 (sold as ALACENTM 895) was supplied by Fonterra Co-operative Group Ltd, Auckland, New Zealand. WPI895 consists of 76%  $\beta$ -lactoglobulin, 15%  $\alpha$ -lactalbumin and 3% bovine serum albumin as determined by the manufacturer.

Canola oil was purchased from Davis Trading Co., Palmerston North, New Zealand. All chemicals used were of analytical grade, obtained from Sigma Chemical

Co. (St Louis, MO, USA) unless otherwise specified. RO water further purified by a Milli-Q system (Millipore, Bedford, MA, USA) was used exclusively.

### 3.4.2 Emulsion preparation

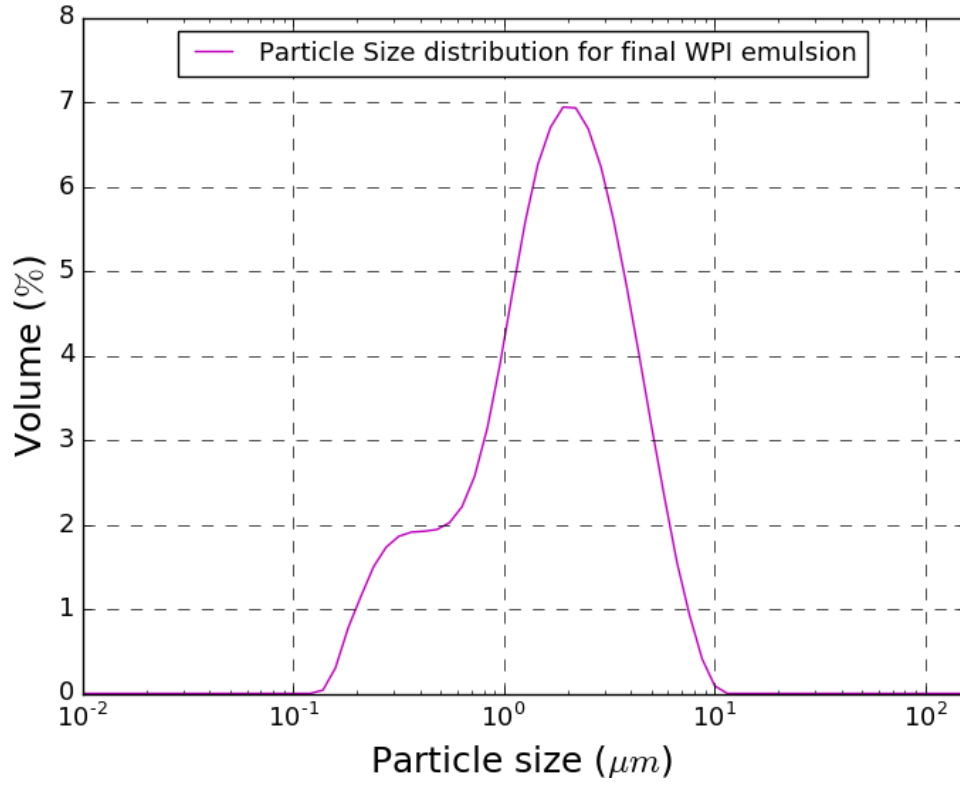


FIGURE 3.3: Droplet diameter distribution of the final WPI emulsion used for the surface property study experiment measured using a Malvern Mastersizer.

The 2 wt% WPI emulsion was made as per the protocol explained in section. 2.1.2. The emulsion was homogenised, fractionised and dialysed to get the desired size distribution. Figure. 3.3 shows the droplet diameter distribution for the experiments.

### 3.4.3 Zeta potential measurements

Electrolyte concentration varied between 50 and 150 *mM* as most dairy products have an ionic strength around 80 *mM* and these ionic strengths maintain the Gouy-Chapman validity with absolute values of the surface potential below  $|40|$  *mV*. 1 *L* NaCl solutions of 50 *mM*, 100 *mM*, and 150 *mM* ionic strength were first prepared. 0.6 *ml* of WPI emulsion was added to each solution. The solutions were adjusted to different pH values using HCl or NaOH solutions with added NaCl to maintain a constant ionic strength. Zeta-potential titration was carried out using a Zetasizer Nano (ZEN3600, Malvern Instruments Ltd.) at each pH at 25 °C. For each zeta potential measurement, 0.75 *ml* of sample was injected to a folded capillary cell.

CaCl<sub>2</sub> solutions at different concentrations (0 *mM*, 0.01 *mM*, 0.05 *mM*, 0.1 *mM*, 0.5 *mM*, 1 *mM*, 5 *mM*, 8 *mM*, 10 *mM*, 20 *mM*) were prepared at a constant ionic strength of 80 *mM* (NaCl being the background salt) at constant pH values and the zeta potentials of the emulsions at these conditions were measured. Making solutions of constant pH near the IEP was a challenge in this experiment.

### 3.4.4 Activity measurement for samples with calcium

The adsorption of calcium ions has a marked effect on the zeta potential, as captured by equations. 3.13 - 3.20. The correct metric in those equations is not the calcium concentration but rather the calcium activity. The calcium activity is defined as the calcium concentration which has units of moles per litre and the unit less activity coefficient. The calcium ions in the solution interacts with the water molecules and shields the charge and interactions between ions hence, at higher salt concentrations ions behave chemically like they are diluted than they are actually. The activity coefficient accommodates the effect of ion-ion and ion-water interactions and tends to one as the ionic strength tends to zero.

Model	Equation	Applicable Ionic Strength (M)
Debye -Hückel	$\log\gamma = AZ^2\sqrt{I}$	$< 10^{-2.3}$
Extended Debye -Hückel	$\log\gamma = AZ^2\frac{\sqrt{I}}{1+Ba\sqrt{I}}$	$< 10^{-1}$
Güntelberg	$\log\gamma = AZ^2\frac{\sqrt{I}}{1+\sqrt{I}}$	$< 10^{-1}$ , for several electrolyte system
Davies Equation	$\log\gamma = AZ^2\left[\frac{\sqrt{I}}{1+\sqrt{I}} - 0.2I\right]$	$< 0.5$

TABLE 3.1: Activity coefficient from different models for water at 25°C with A= 0.5, B= 0.33 (James W. Murray [86])

$$a_i = \gamma_i m_i \quad (3.24)$$

where,  $m_i$  is the concentration of the free ions,  $a_i$  the activity of the free ion and  $\gamma_i$  the free ion activity coefficient.

A short list of theoretical and empirical expressions for the activity coefficient for different models for water at 25°C with the constants,  $A = 0.5$ ,  $B = 0.33$  is given in table. 3.1. Here,  $I$  is the ionic strength and  $a$  is the ion size parameter which takes care of the finite radius of the ions without considering them as point charges.

The activity coefficient is calculated to be 0.38 from the Davies equation for the current experimental study.

In general, equilibrium for all solutions should include consideration of activity coefficients for completeness (Hall et al. [87]). This activity is accommodated for in pH measurements in the absence of calcium, but for calcium the activity has a pH dependence and needs to be measured. Hence, equation 3.13 becomes,



$$K_{Ca} = \frac{[COOCa^+]}{[COO^-]\gamma[Ca^{2+}]} \quad (3.25)$$

Calcium activity of samples with added calcium was determined with a calcium electrode (Thermo Scientific Orion™ Calcium Electrodes-9720BNWP) and the resultant potential was compared to that of four standard buffer solutions, from which the aqueous calcium ion concentration was derived.

The calcium activity of the emulsion is calculated from a calibration curve of  $\log [activity]$  vs  $voltage$  observed on the calcium sensitive electrode. The electrode was considered in good working order when the calibration slope matched the expected result given by the Nernst equation. The  $\log[C]$  vs  $Voltage$  plot is shown in figure. 3.4.

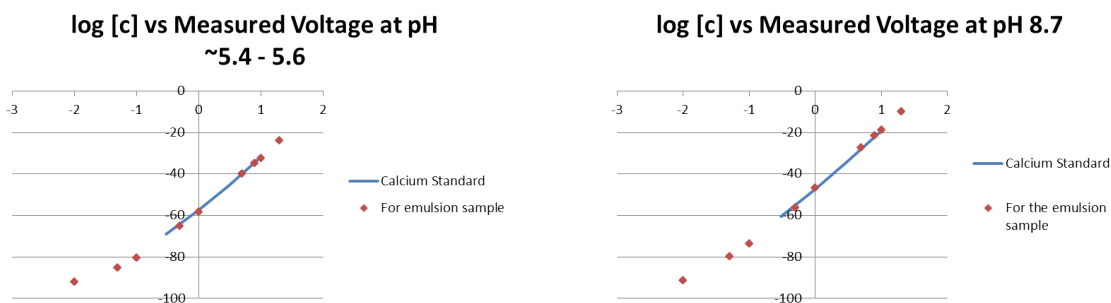


FIGURE 3.4: The logarithm of concentration vs measured voltage for different concentrations of added calcium to sample at two different pH values. The solid blue line shows the activity measured for calcium standard from 0.3 mM to 10 mM.

### 3.4.5 Rheological determinations

Rheological measurements were carried out using Anton Par dynamic shear rheometer (DSR) 502 (figure. 3.5) with an automatic sample changer that consisted of a sample carousel immersed in a waterbath at 20 °C.

Highly concentrated salt solutions with different levels of added calcium with a background of NaCl (to maintain a constant total ionic strength) were added to the

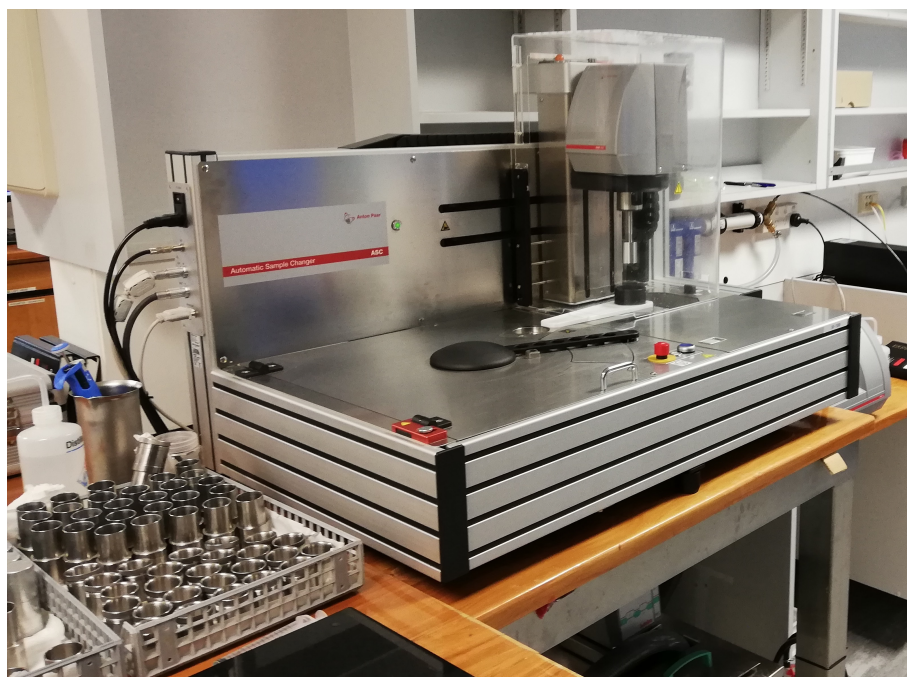


FIGURE 3.5: Anton Par dynamic shear rheometer 502

emulsion with constant stirring, diluting it to 19.4 *wt%* oil to obtain required ionic concentrations for the emulsion samples under investigation. A direct potentiometric measurement was made of the bulk aqueous calcium ion concentration of the solution.

In a parallel experiment, bulk phase separation was examined. Only a minority of samples separated into two layers within a week. Those that did form two layers did so after an initial delay of 20 to 30 hours which was much longer than the  $\approx 12$  hours required by the rheometer to measure all samples. Replicate measurements confirmed that the samples position within the carousel and therefore sample age when measured did not affect the results over the course of the measurement duration.

### 3.5 Results and discussion

#### 3.5.1 Effect of concentration of NaCl and pH on zeta potential

Now that the relevant theoretical frameworks have been examined, the results of the experiments are reported. Figure 3.6 shows the results from zeta potential measurements carried out under different salt conditions as a function of pH. The data are sigmoidal in shape, with the existence of plateau regions about two pH units away from the IEP, consistent with previous works in literature (Kulmyrzaev et al. [61]). The slope of the points near the IEP depends upon the ionic strength of the system.

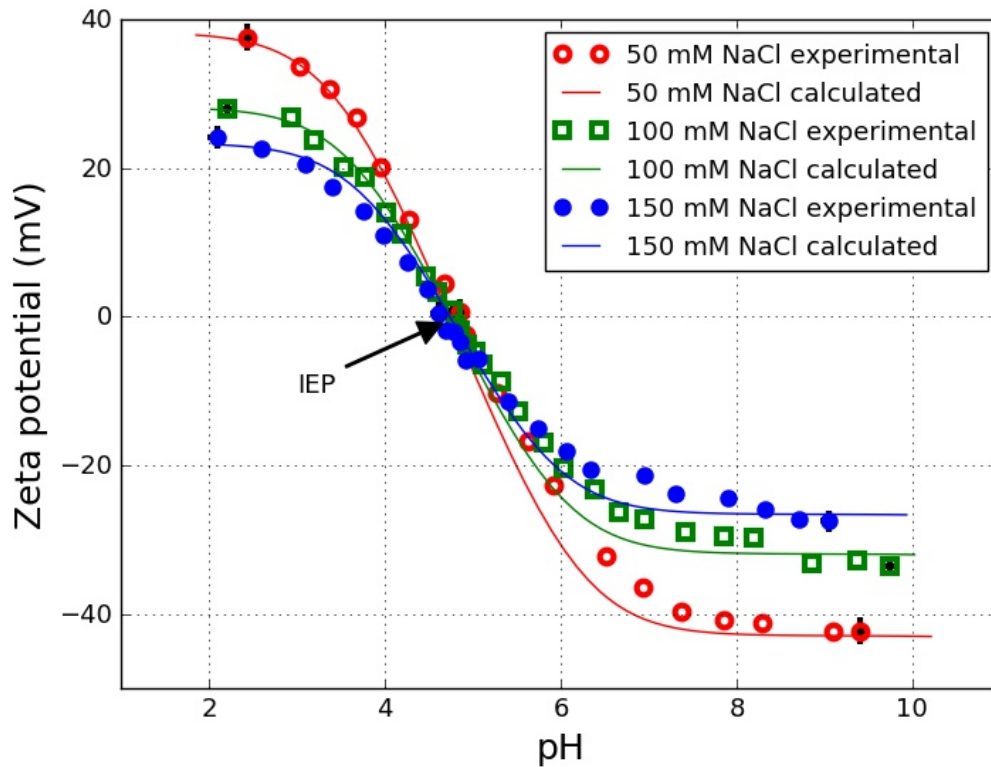


FIGURE 3.6: Droplet zeta potential versus pH for three NaCl concentrations (50 mM, 100 mM, 150 mM). Droplets are canola oil in water stabilised with WPI. The square/circle data points were experimentally measured. The solid lines were calculated using the Gouy-Chapman model. Error bars (shown only on the pH extremes) display typical variations for all data. Fit parameters are  $pK_{a1} = 4.8$  and  $pK_{a2} = 12$ .

The numbers of amine and carboxylic groups per unit surface area, which are essential for the fitting of the experimental data to the Gouy-Chapman model described previously, are calculated from the plateau values shown in Figure. 3.7. At lower pH, in the upper plateau region, the charge density comes solely from the amino groups since effectively all carboxyl groups ( $-COOH$ ) are neutralised allowing  $N_{s2} = (0.135 \pm 0.005)$  groups per  $nm^2$  to be extracted. The surface charge and hence the number densities are calculated from the fit. Increasing the pH, decreases the positive charge as some of the carboxyl groups become negatively charged ( $-COO^-$ ). Between pH 4.5 – 5 the potential decreases to zero indicating the negative carboxyl groups balance the positive amine groups. Further increasing the pH beyond the IEP increases the negative charge until pH 8 where the zeta potential reaches another plateau. This plateau is situated sufficiently far from  $pK_{a1}$  and  $pK_{a2}$  that effectively all the carboxyl and amine groups are charged. This plateau corresponds to a charge density of 0.155 negative charges per  $nm^2$  suggesting  $N_{s1} = 0.290 \pm 0.005$  negative charges per  $nm^2$  (see Figure. 3.7).

An indication of surface protein load can be established from the values of  $N_{s1}$  and  $N_{s2}$  and assuming the surface electrical properties are dominated by  $\beta$ -lactoglobulin.  $\beta$ -lactoglobulin B has 28 Aspartic acid and Glutamic acid residues combined (Creamer et al. [88]) thus  $N_{s1}$  equates to  $1.0 \times 10^{-2}$   $\beta$ -lactoglobulin molecules per  $nm^2$  or  $0.32 \text{ mg}/m^2$ . Likewise  $N_{s2}$  and the combined 21 Arginine, Histidine and Lysine residues corresponds to  $6.4 \times 10^{-3}$   $\beta$ -lactoglobulin molecules per  $nm^2$  or  $0.20 \text{ mg}/m^2$ . These approximate surface coverages are significantly lower than 1.2 to  $1.6 \text{ mg}/m^2$  reported for  $\beta$ -lactoglobulin adsorbing to an air-water (Miller et al. [89]), oil-water (Dickinson and Hong [90], Atkinson et al. [91], Courthaudon et al. [92], and Chen et al. [93]) and polystyrene-water interfaces (Pérez-Fuentes et al. [94]). The discrepancy in adsorbed amount likely arises from the over-simplified nature of the Gouy-Chapman model. The Gouy-Chapman model implemented here is the simplest model for the EDL with the least number of adjustable terms. The Gouy-Chapmann model is limited to low charge densities and the presence of additional sources of charge have been ignored. These additional sources of charge include adsorbed ions in the form of a Stern layer, or absorbed within the protein molecule

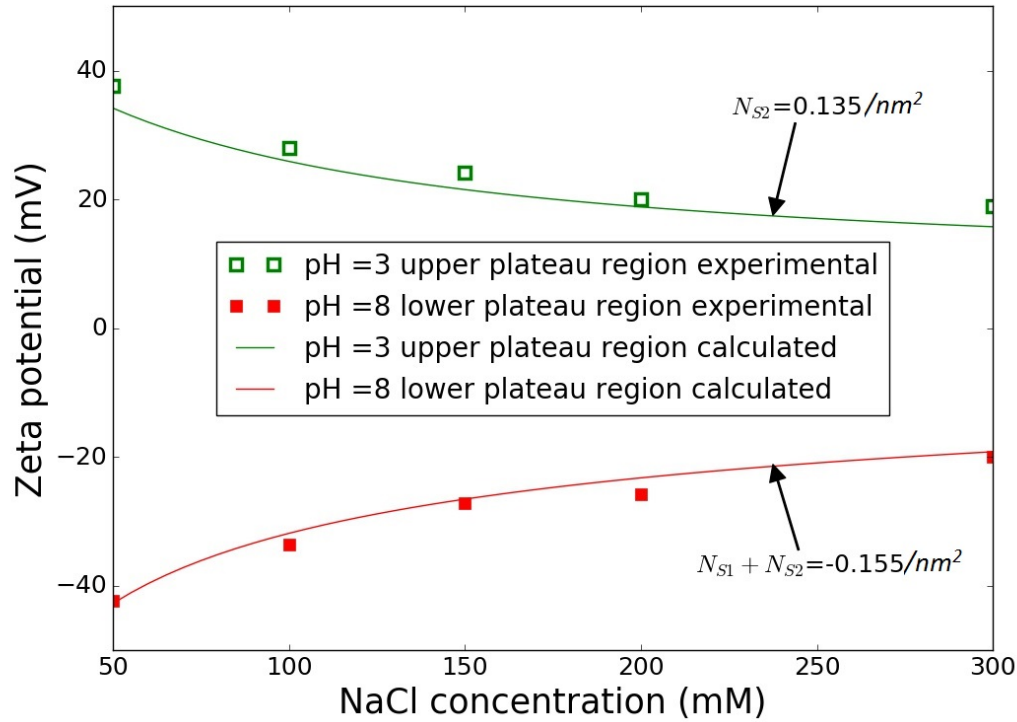


FIGURE 3.7: Determination of total number of carboxylic and amine groups from plateau zeta potential for five different NaCl salt concentrations using equations. 3.2, 3.3, 3.10. The squares are experimentally determined zeta potentials at pH 3 (open squares) and pH 8 (closed squares). The calculated value for  $N_{s1}$  is  $0.290 \pm 0.005$  negative charges per  $nm^2$ .

due to high charge density (Manning [95]). These effects are expected to be due to the high charge density of the proteins and ionic strength of the experiment (Pérez-Fuentes et al. [94]) and would reduce the surface load. Additional sources of error include the use of the Helmholtz-Smoluchowski model for calculating the zeta potential in place of the more complex O'Brien-White model (O'Brien and White [96]) and assuming the equivalence of the zeta potential with the surface potential. In particular at high ionic strength the slip length becomes more significant relative to the Debye length, and the zeta potential will significantly underestimate surface potential. Thus fitted values for  $N_{s1}$   $N_{s2}$  are nominal values not representing the protein adsorption, but are sufficient to describe the zeta potentials and electrical double layer forces within the investigated pH and ionic strength envelope.

With values for  $N_{s1}$  and  $N_{s2}$  estimated, it is possible to fit  $pK_{a1}$  and  $pK_{a2}$  in Figure. 3.6. Acceptable fits were found with  $pK_{a1} = 4.8$  and  $pK_{a2} = 12$ . These values are consistent with average values from the literature [97]. Varying  $pK_{a2}$  between 11 and 13 has little to no effect on the model curve fit. This large variation in  $pK_{a2}$  is not a flaw in the model but rather a consequence of limiting the data set to pH 9 and below where the number of neutral amine groups is negligible.

### Effect of concentration of $\text{CaCl}_2$ on zeta potential

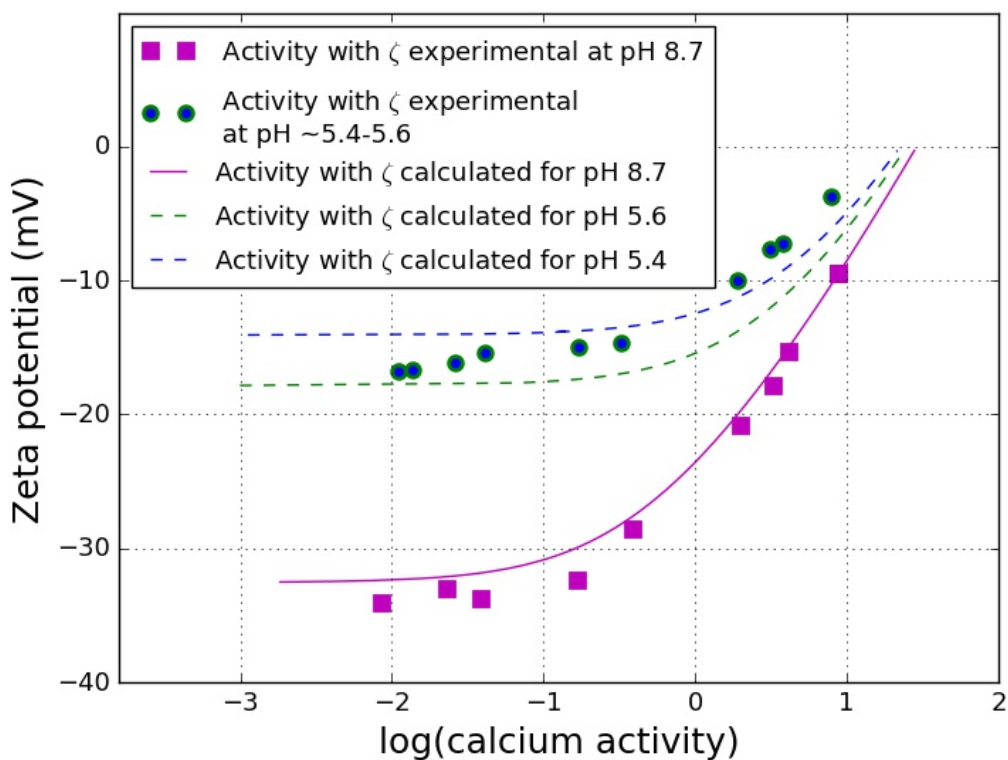


FIGURE 3.8: Droplet zeta potential versus logarithm (to the base 10) of calcium activity in mM. Droplets are canola oil in water stabilised with WPI. The square/circle data points were experimentally measured. The fitting lines were calculated using equations. 3.16, 3.20. All fitting curves used  $pK_{Ca} = 1.9$ . NaCl was used to maintain a constant background ionic strength of 80 mM.

Now that the values of  $N_{S1}$ ,  $N_{S2}$ ,  $pK_{a1}$  and  $pK_{a2}$  have been obtained, the effect of calcium activity could be investigated. The activity of calcium in solution is calculated



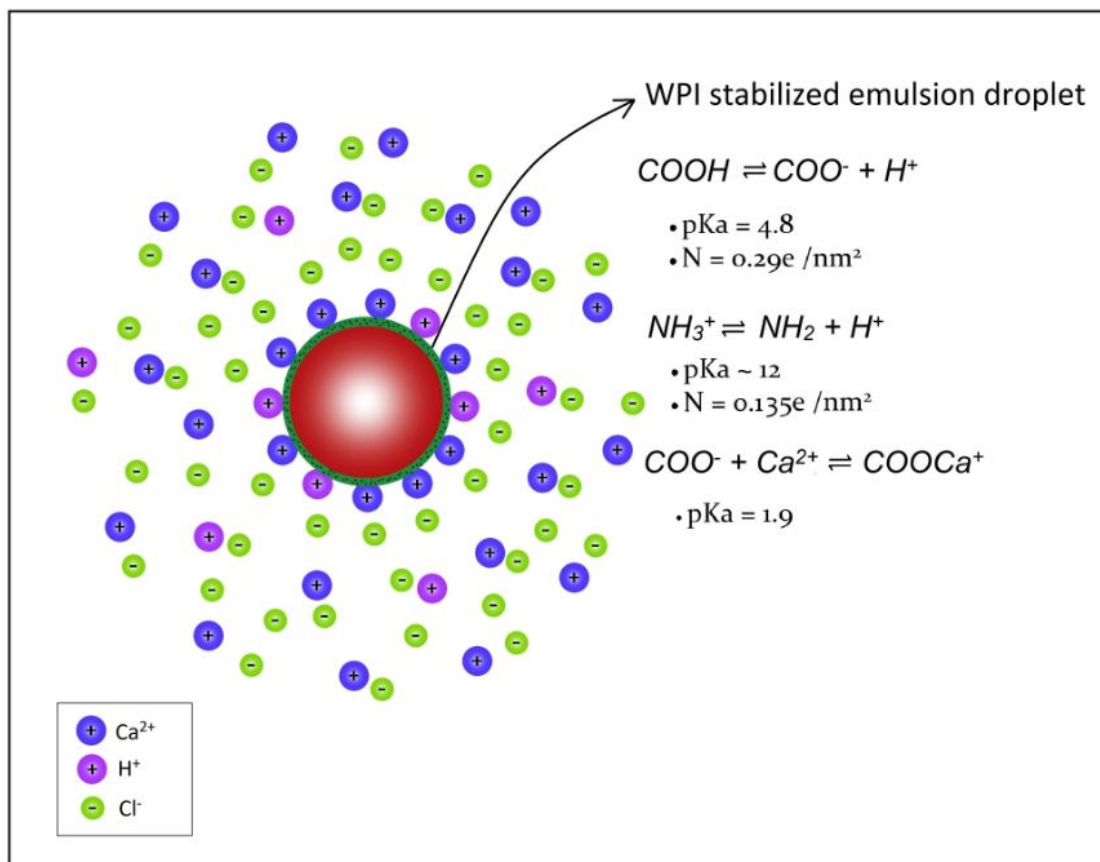


FIGURE 3.9: Results of the experiment at once.

and plotted with measured  $\zeta$  Potential. The zeta potential versus calcium activity for two pH values (5.4-5.6 and 8.7) for activities between 0-10 mM is shown in figure. 3.8. In addition to the parameters extracted from fitting the previous data, a  $\text{pK}_{Ca}$  value of 1.9 was found to provide a good fit of the predictive model to the experimental data, Figure. 3.8 representing the zeta potential.

At the higher pH, variations of  $\pm 1$  pH unit made no obvious difference to the fitting curve. By contrast, at a lower pH, closer to the isoelectric point, a small change in pH influences the magnitude of the predicted trend. Moreover, when titrating the emulsion against calcium, at constant ionic strength, the addition of calcium slightly lowers the pH. This slight variation is dealt with by showing two curves calculated at pH 5.4 and 5.6. All model curves use a  $\text{pK}_{Ca}$  of 1.9.

The outcome of the experiment is depicted in the figure. 3.9. It must be appreciated that the fitted curves of the zeta potential vs calcium activity rely upon the values of  $N_{S1}$  and  $N_{S2}$  which are not reflective of the expected values from the adsorption data (see Appendix. B) but rather nominal values used to fit the EDL forces as simply as possible.

### 3.5.2 Emulsion rheology with zeta potential

The macroscopic flow behaviour of the WPI emulsion system was examined as a function of calcium concentration and pH at an ionic strength of 80 mM. In particular, the flow behaviour of the emulsion sample was investigated by considering the shear stress dependence of the sample viscosity. When the shear stress corresponded to Peclet numbers (ratio of rates of advection to diffusion) much smaller than one, the viscosity was constant as expected. At much larger shear stresses the viscosity was found to decrease in a manner typical of emulsions of 20 wt% (Barnes [98], Tadros [99], and Rao and Rao [100]).

A plot of the magnitude of the low-shear viscosity plateau against  $\zeta^2$  shows that these emulsion systems exhibit two distinct behaviours either side of  $|\zeta| = 15$  mV and can be separated into two groups exhibiting different behaviours as shown in Figure. 3.10. This grouping is consistent with trends seen in more concentrated dispersions that were dominated by the electrical double layer repulsion (Larson [101] and Ong et al. [102]). In those dispersions the yield stress has linear dependence on the square of the zeta potential.

Emulsion viscosity depended almost entirely upon zeta potential, with samples of the same zeta potential behaving similarly, irrespective of whether it was tuned by adjusting pH or by adjusting calcium activity. Such redundancy demonstrates that the possibility of calcium bridging or other calcium-specific effects in these WPI stabilised emulsions is unlikely. When calcium activity was low and the pH was away from the isoelectric point, the viscosity varied between 5 and 15 mPa.s, consistent with a stable



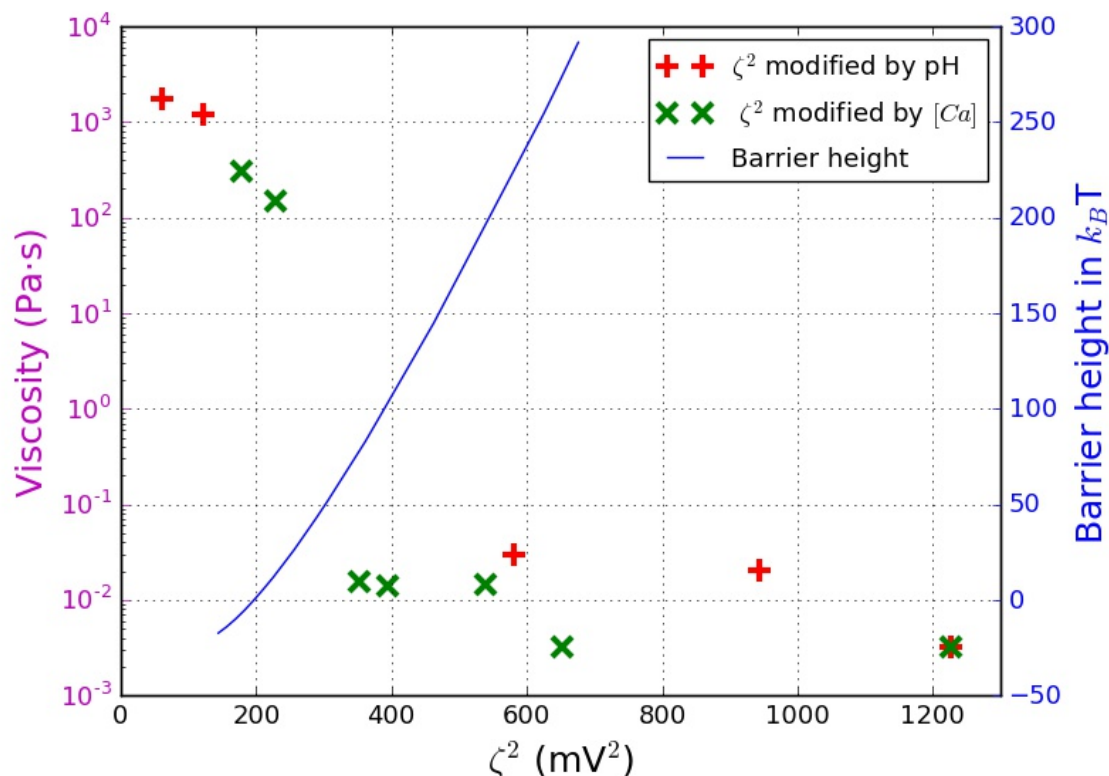


FIGURE 3.10: Plateau viscosity versus zeta potential squared. Droplets are canola oil in water stabilised with WPI. The red "+" data points were experimentally measured at pH = 3.5, 4.4, 5.2, 6.4 and 7.9 without any added calcium. The green "x" data points were experimentally measured using calcium activities of 0, 0.64, 1.06, 1.93, 2.31, 4.03, and 5.18 mM at pH = 7.9. The solid blue line shows the barrier height calculated (equation 4.1) as a function of the zeta potential, its calculation is explained in the text.

emulsion as seen to the right hand side of Figure. 3.10. Under conditions that resulted in more weakly charged droplets, much greater viscosity were observed. These viscosities were  $10^4$  times larger and correspond to extensive droplet aggregation. The transition between the two viscosity groups occurs at  $|\zeta| = (15 \pm 2)$  mV. This critical  $\zeta$  value can be seen to coincide with a zero energy barrier calculated from DLVO potential. Figure. 3.10 also shows the energy barrier height calculated from the (local) maximum in Eqn. 3.21. The barrier height is zero at  $\psi = 14.2$  mV and demarcates, rapid, diffusion limited aggregation. Increasing the  $\psi$  to 14.7 mV adds a  $5k_B T$  energy barrier which is sufficient to prevent any appreciable aggregation. At  $\psi \leq 14.2$  mV the energy barrier is zero or negative indicating the calculated barrier height is only a local maximum. This local maximum

vanishes completely below 11 mV. The agreement between the calculated zero energy barrier and the plateau emulsion viscosity confirms that only DLVO forces are required to understand the behaviour of this system.

### 3.6 Conclusion

The zeta potential of a complex interface such as whey protein isolate can be described by a series of representative equilibrium. The Gouy-Chapman model and realistic pKa values can be used to explain the variation of the  $\zeta$  against pH, ionic strength and calcium activity. Furthermore, changes in  $\zeta$  potential modify the size of the repulsive energy barrier captured by the DLVO interaction energy and are reflected in bulk properties such as coagulation rate and viscosity, irrespective of how  $\zeta$  is modified. With this model, the surface electrostatics and stability can be predicted with a minimum of parameters. This approach can be applied to other complex interfaces as long as the adsorbed layer is flat and the charge is distributed homogeneously.

The Gouy-Chapman model applied here breaks down when attempting to calculate the adsorbed mass, which could be achieved using more complex models of the electrical double layer but would require additional fitting variables and/or experimental data.



## **Chapter 4**

**Depletion and electrostatic forces in the determination of the cluster kinetics in whey protein stabilised emulsion.**

Many UHT foods and beverages are emulsions consisting of many ingredients. The best before date on these products is often defined by the time in which certain functional performances can no longer be guaranteed. The exact definition of shelf life is somewhat arbitrary, but often based on an unaided visual assessment of destabilisation. The formation of separated layers can often be attributed to depletion forces, coalescence and/or creaming while thickening can be attributed to droplet flocculation, where particles come into contact and adhere forming larger sized clusters. Two of the most important ingredients include emulsifiers (which stabilise droplets against aggregation and control droplet size) and stabilisers (generally hydrocolloids) that tailor the rheological properties to prevent or slow down phase separation (Dickinson and Stainsby [103], Garti and Reichman [104], and Hunter [105]). In colloids where the effect of diffusion-induced collisions outweighs gravity-induced sedimentation, shelf life can be established from models of rate limited aggregation (Borwankar et al. [106]). This rate limited aggregation modifies Smoluchowski's aggregation kinetics with a collision based sticking probability that is defined by the relevant interaction forces (Elimelech et al. [84]). A specific model adapted to emulsions assumes dense droplet flocs, described by aggregation kinetics, but goes further to separate the formation of flocs from the film rupture processes that results in coalescence (Borwankar et al. [106] and Tempel [107]). This approach is particularly useful when the interaction forces have a secondary minimum as it defines whether the drops sit in flocs that can be redispersed or whether droplets coalesce into many droplets. The number of droplets in a floc is easily calculated from Smoluchowski's aggregation kinetics minus the effects of film rupture. The rate of film rupture is the product of the lifetime of the single thin film separating two adjacent droplets and the number of films in a floc. Usually, one would consider the rate of film rupture relative to the rate of floc formation (Borwankar et al. [106]). Relatively fast and slow film rupture defines the pure flocculation and pure coalescence extremes respectively. These extremes can be handled using classic aggregation kinetics with Smoluchowski's aggregation kinetics. When considering the shelf life of an emulsion with occasional coalescence it is more practical to separate pure flocculation, pure coalescence, and a mixed regime based on the droplet

population at the end of the desired shelf life.

In this article whey protein stabilised emulsions in the presence of xanthan gum are used. The interactions in this system are well understood; nonetheless, the conditions where these emulsions transition from flocculating to coalescing is not known. Whey protein stabilised emulsions experience electrical double layer forces which can be mediated by the calcium activity, (Kulmyrzaev and Schubert [57], Ravindran et al. [108], McKinley [109], and Deeth and Lewis [110]) depletion forces from the xanthan (Ye et al. [111] and Ye et al. [112]) and van der Waals forces. Previously it was demonstrated that the zeta potential of these droplets can be calculated from the calcium activity, ionic strength and pH (Ravindran et al. [108]). Xanthan is not surface active or does not change the surface tension between the interfaces. (Gunning et al. [113]) and has been shown to increase the coalescence rate of the particles of the emulsion due to the extended range of depletion forces, although this rate increase is offset by a viscosity effect especially at dosages beyond 1 - 1.2 g/L (Ye et al. [111] and Ye et al. [112]). The long ranged nature of depletion forces can trap droplets in a secondary minimum, even if the attraction is relatively weak. Escaping droplets are simply unable to diffuse across the attraction length and tend to get recaptured in the floc.

## 4.1 Materials and methods

### 4.1.1 Materials

Whey Protein Isolate 895 and canola oil was from the same manufacturers as in section. 3.4.1. NovaXan™ 80 NF/FCC Grade Xanthan Gum from ADM (Archer Daniels Midland) was used for the study. All chemicals used were of analytical grade, obtained from Sigma Chemical Co. (St Louis, MO, USA) unless otherwise specified. Milli-Q water (deionised water from a Milli-Q plus R system, Millipore, Bedford, MA, USA) was used for the preparation of the emulsion and salt solutions.

#### 4.1.2 Sample preparation

2 wt% WPI was mixed with Milli-Q water and stirred at 50 °C for half an hour and made into emulsion as per the protocol described in section. 2.1.2 The emulsion droplet size was measured using a Malvern Mastersizer and showed bi-modal distribution consisting of a primary "large" droplet peak around 2  $\mu\text{m}$  and a "small droplet" shoulder 0.3  $\mu\text{m}$ . On occasion a third mode of 30  $\mu\text{m}$  was observed although it should be noted that, this mode was never reproducible and likely a results of adventitious dust entering the sample chamber. 500 ml each of  $\text{CaCl}_2$  solutions at different concentrations (5 mM, 8 mM, 10 mM, 15 mM, 20 mM) were prepared at a constant ionic strength of 80 mM (NaCl being the background salt) at a pH between 7-8. Around 0.3 ml of the emulsion was added to the salt solutions for particle size measurements. 2 wt% of xanthan was made by mixing weighed powder to Milli-Q water, stirring for 12 hours first at room temperature and at a temperature subsequently of 40 °C in an oven for another 12 hours to ensure complete dissolution. 25 different samples were made by mixing the mother xanthan solution at different ratios to yield 0.02 wt%, 0.04 wt%, 0.1 wt%, 0.25 wt%, 0.5 wt% of the xanthan in samples with different salt concentrations by using a vortex mixer at 1000 rpm for 2 minutes. The pH of the emulsion had little to no effect on the final pH of the sample with the addition of xanthan (Sun et al. [114]).

#### 4.1.3 Zeta potential calculation from calcium activity

Adsorption of calcium ions alters the aqueous calcium ion concentration, especially when emulsions are concentrated. Calcium activity of samples with added calcium was determined with a calcium electrode (Thermo Scientific Orion<sup>TM</sup> Calcium Electrodes- 9720BNWP) and the resultant potential was compared to that of four standard buffer solutions, from which the aqueous calcium ion concentration was derived as described in section. 3.4.4. The activity coefficient ( $\gamma$ ) was calculated using the Davies equation (table. 3.1) to find

the activity (effective concentration) of calcium in each sample (Davies [115]).

$$\log \gamma = -0.5z^2 \times \left[ \frac{\sqrt{I}}{1 + \sqrt{I}} - 0.2I \right]$$

where,  $I$  is the ionic strength and  $z$  is the ion valency. Here calcium concentrations are presented as the product of the concentration and the unit less activity coefficient. The zeta potential is then determined from the pH and the calcium activity of the samples by fitting to the Gouy Chapman model (Ravindran et al. [108])

#### 4.1.4 Particle size measurements

The emulsion droplet size was measured using a Malvern Mastersizer (Malvern Instruments Ltd) (using a general purpose spherical analysis model with particle refractive index of 1.47 in water with zero light absorption and an obscuration value between 12% to 15%). Two values are used in this investigation the  $d_{10}$  and the  $d_{4,3}$ . The  $d_{10}$  is the diameter at which 10% of the total mass is comprised of particles with a diameter less than this value and the  $d_{4,3}$  averages diameters,  $d$ , as  $d_{4,3} = \Sigma d^4 / \Sigma d^3$ .

#### 4.1.5 Viscosity measurements

The viscosity of the continuous phase was approximated by recreating corresponding xanthan and salt solutions. Viscosity measurements were carried out using a MCR301 rheometer with a cup and bob geometry and a shear rate of  $0.01 \text{ s}^{-1}$ . To ensure equilibrium measurements the acquisition time was 500 s.

## 4.2 Theory

According to DLVO theory, the interaction between two colloidal particles bearing the same charge is comprised of a repulsive electric double layer (EDL) potential and an



attractive Van der Waals potential. Adding xanthan gum adds an extra depletion force so that the total potential of the system is now given by,

$$V_{total}(h, \psi, c) = V_{EDL}(h, \psi) + V_{vdW}(h) + V_D(h, c) \quad (4.1)$$

$V$  denotes the interaction energy with subscripts, total, EDL, vdW and D denoting the total, the electrical double layer, the van der Waals, and the depletion interaction respectively. Here  $h$  is the separation between the oil water interfaces (any whey protein is thought to adsorb in a flat layer of negligible thickness),  $\psi$  is the surface potential which is approximated by,  $\zeta$ , the zeta potential, and  $c$  is the concentration of xanthan in wt%. The electrical double layer interaction between two droplets is

$$V_{EDL}(h, \psi) = 2\pi\epsilon_r\epsilon_0 a \psi^2 e^{\frac{-h}{\lambda_D}}.$$

The van der Waals potential, arising from spontaneous electric and magnetic polarisations for identical spheres at close approach is:

$$V_{vdW}(h) = -\frac{a}{12h} \times A e^{\frac{-2h}{\lambda_D}}$$

where  $A$  is the Hamaker constant for two bodies of canola oil interacting over a film of water. The value of  $A = 2.2kT$  was calculated assuming canola oil has a refractive index 1.475, the dielectric constant 3.1 and a main electronic absorption frequency of  $3.75 \times 10^{15} s^{-1}$ . The calculation and values for water are outlined in Israelachvili [82]. The exponential term gives the decay specific to systems with high electrolyte concentrations where there is an additional screening effect of the van der Waals interaction (Israelachvili [82]). Without this high salt correction extensive flocculation would be predicted in the absence of any depletion forces but this flocculation was not observed.

The Asakura Oosawa model is used to calculate the depletion potential. The

osmotic pressure creates an attractive force between particles in a medium (Asakura and Oosawa [16]) The depletion potential is given by,

$$V_D(h) = -\rho kT \frac{4\pi}{3} [a + r_g]^3 \left[ 1 - \frac{3}{4} \left[ \frac{2a + h}{a + r_g} \right] + \frac{1}{16} \left[ \frac{2a + h}{a + r_g} \right]^3 \right] \quad (4.2)$$

where  $r_g \approx 100nm$  (Viebke and Williams [116]) describes the radius of gyration for the xanthan.  $\rho$  is the number of xanthan molecules per  $m^3$  which was calculated by using the reported molecular mass of  $3 \times 10^6 g/mol$  (Viebke and Williams [116]). In this article all forces are calculated based on the  $d_{10}$  since these small droplets would have the lowest interaction potential and are therefore the most likely to coalesce.  $\lambda_D = 1.08 nm$  and whereby, in the absence of any xanthan gum, micron sized droplets aggregate when the absolute zeta potential falls within  $\pm(15 \pm (2mV))$ . Depletion forces from added xanthan have a longer range than the electrical double layer force, and create a primary or secondary minimum resulting in flocculation or coalescence.

According to the model of Borwankar et al. [106] when there is no coalescence, the average number of drops in a floc  $N$  and the number of primary droplets not in a floc (per unit volume)  $n_1$  are given by:

$$N = 2 + kn_0t \quad (4.3)$$

$$n_1 = \frac{n_0}{(1 + kn_0t)^2} \quad (4.4)$$

noting  $n_1 = n_0$  when  $t = 0$ . The rate constant for primary droplet collisions,  $k$  is given by,

$$k = 8\pi Da \quad (4.5)$$

These last three equations demonstrate that is more practical to look at emulsion shelf life in terms of  $kn_0t$  rather than time alone. Depletion effects can be accommodated within  $k$  by replacing the radius ( $a$ ) in equation. 4.5 with an effective capture radius

$a_{eff} = a + r_g$ , while maintaining the hydrodynamic radius constant in the diffusion coefficient  $D = kT/6\pi\eta a$  where  $\eta$  is the viscosity of the suspending medium. The depletion effect on  $k$  reduces as droplets coalesce, so for simplicity it has not been added unless otherwise stated. When droplets are coalescing an additional film rupture rate constant,  $K$ , is added. The rate at which the total number of droplets change with time is given by:

$$\frac{dn}{dt} = -Kqmn_{agg} \quad (4.6)$$

here,  $q$ , is the number of films per droplet, or exactly half the number of neighbours, recognising that films are “shared” by two droplets to prevent double counting,  $m$  is the number of droplets per aggregate, and  $n_{agg}$  is the number of aggregates. Note that if there is no coalescence then  $m \equiv N$ . In a concentrated emulsion where droplets are in close proximity to one another and any aggregates are large the number of droplets at any one time is given by:

$$\frac{n}{n_0} = e^{-Gkn_0t} \left\{ 1 + \frac{G}{e^G} \left( 1 - \frac{1}{\theta} \right) + \frac{G^2}{e^G} \ln \theta - \frac{G^3}{2! e^G} (1 - \theta) - \frac{G^4}{2 \cdot 3! \cdot e^G} (1 - \theta^2) \dots \right. \quad (4.7)$$

$$\left. - \frac{G^{j+1}}{(j-1) \cdot j! \cdot e^G} (1 - \theta^{j-1}) \right\}$$

with  $G = Kq/kn_0$ , a dimensionless variable of time and  $\theta = 1 + kn_0t$  and  $j$  is an integer. This is an analytic series solution based on a numerical (Taylor series style) solution to the differential equation (Borwankar et al. [117]).

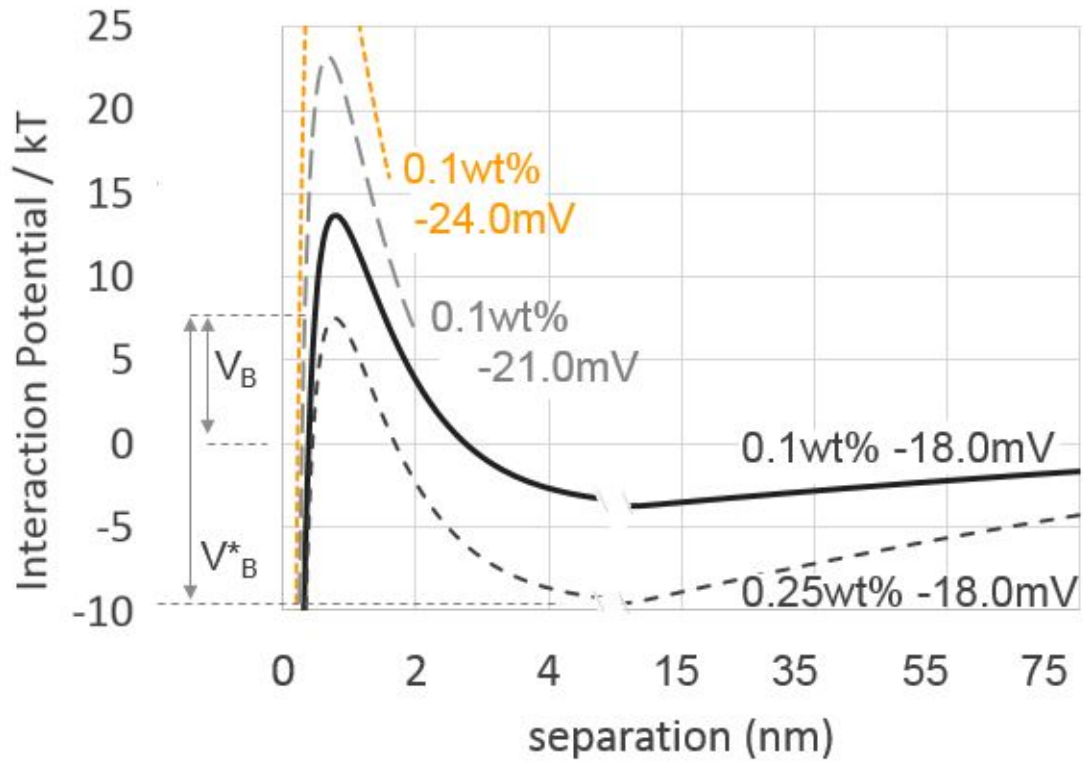


FIGURE 4.1: Calculated interaction potentials as a function of separation. Calculations were based on droplets with a radius of  $150\text{nm}$ . Each interaction potential is labelled with the xanthan dose and zeta potential in close proximity to the curve. Some interactions curves are truncated for clarity.

### 4.3 Results and Discussion

#### 4.3.1 interaction potentials

Interaction potentials were calculated for given values of zeta potential and xanthan concentrations, assuming a radius of  $150\text{ nm}$ , based on the  $d_{10}$  values (Figure 4.1 and 4.2). Changing the zeta potential from  $-18$  to  $-24\text{ mV}$  increased the barrier height by  $22\text{ kT}$ , likewise varying the xanthan dose from  $0.2\text{ wt\%}$  to  $5.0\text{ wt\%}$  altered the depth of the secondary minimum from  $-0.7$  to  $-19\text{ kT}$ . Previously, in the absence of xanthan, droplet flocculation was been observed at zeta potentials somewhere between  $-17$  and  $-13\text{ mV}$  (Ravindran et al. [108]). Such large barriers would normally be considered sufficient to

prevent coalescence. When barrier heights are larger than  $5 kT$  and the secondary minimum is deeper than a few  $kT$ , it becomes necessary to consider the barrier height from the bottom the secondary minimum,  $V_B^*$ , figure. 4.1 (Wiese and Healy [118]). The electrical double layer force and the depletion force dominate the calculated barrier height,  $V_B$ . The small variation in  $V_D(h)$  at close separations means that  $V_B^*$  is a near linear function of  $\zeta^2$ .

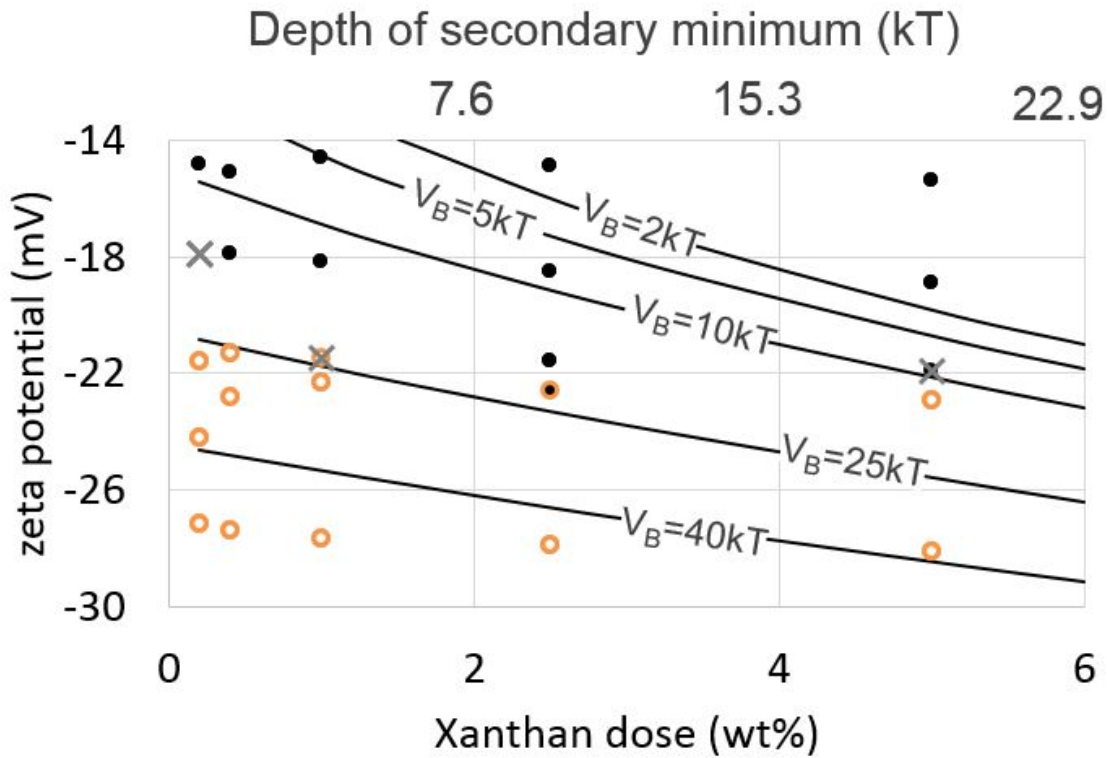


FIGURE 4.2: Zeta potential and xanthan concentration of samples investigated in this study. Samples have been coded as empty circles - flocculation regime, grey crosses - mixed regime and black dots - coalescing regimes. These regimes are discussed later in the text. Contour lines show calculated barrier height as a function of zeta potential and xanthan dose. Contour lines are calculated assuming radii of  $150 \text{ nm}$ .

### 4.3.2 Droplet Size

The stock emulsion showed a bimodal size distribution, (for simplicity, these two populations are referred to as small and large droplets) figure. 4.3. The large droplet peak

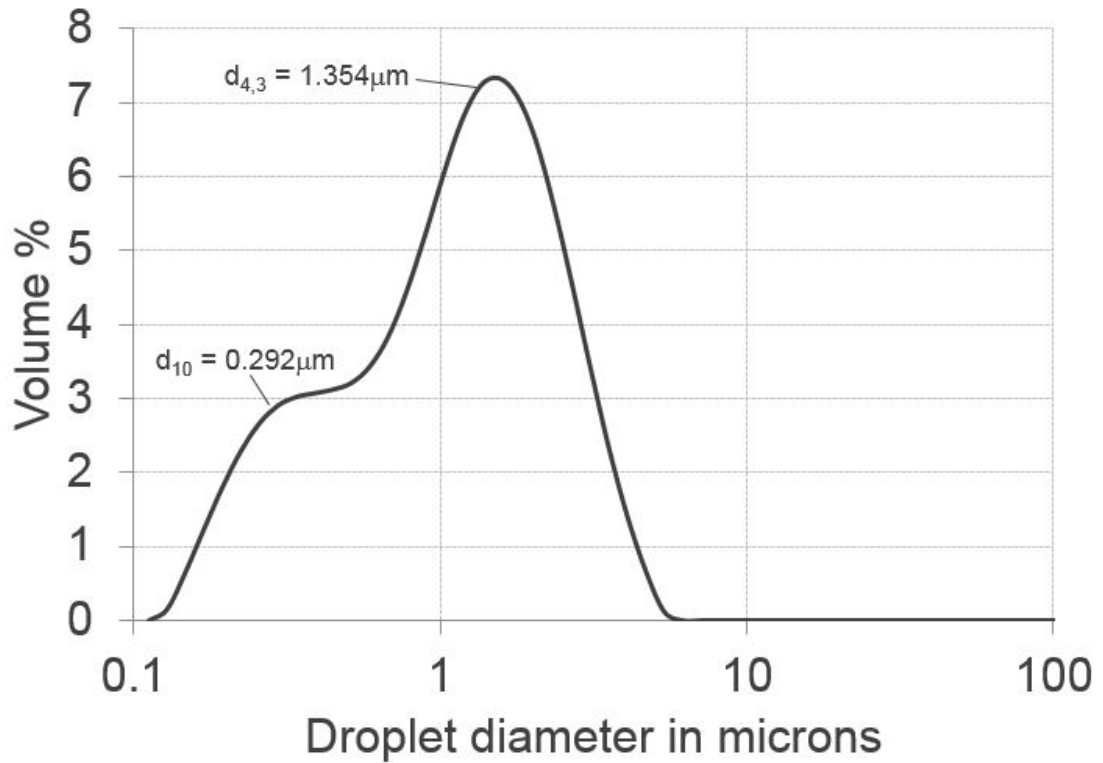


FIGURE 4.3: Droplet size distribution of the stock emulsion showing  $d_{10}$  and  $d_{4,3}$ .

is the dominant peak with a mode close to the  $d_{4,3} = 1.354 \mu\text{m}$ , while the small droplet population is represented by the  $d_{10}$  of 292 nm. The  $d_{4,3}$  was used to calculate  $n_0 = 1.5 \times 10^{17}$  drops per  $\text{m}^3$ , while the  $d_{10}$  is the basis of interaction potentials calculated with  $r = 150 \text{ nm}$ .

Plotting  $d_{10}$  against  $kn_0t$  shows insights in droplet size that aren't clear when plotting against time, zeta potential or xanthan concentration alone, figure. 4.4. With the exception of 4 samples, droplet size data can be categorised into one of two distinct trends. Inclusion or exclusion from these groups was determined by eye. These trends can be separated on zeta potential with a transition between  $-17$  and  $-22 \text{ mV}$ . The first grouping in the data is the flocculation regime, droplet  $d_{10}$  values are independent of  $kn_0t$  and fall below 400 nm with an average of 325 nm. Note 370 nm corresponds to the coalescence of two droplets with size  $d_{10}$ . Although labelled as the flocculation regime, there was a small but consistent loss the small droplet population over time that was

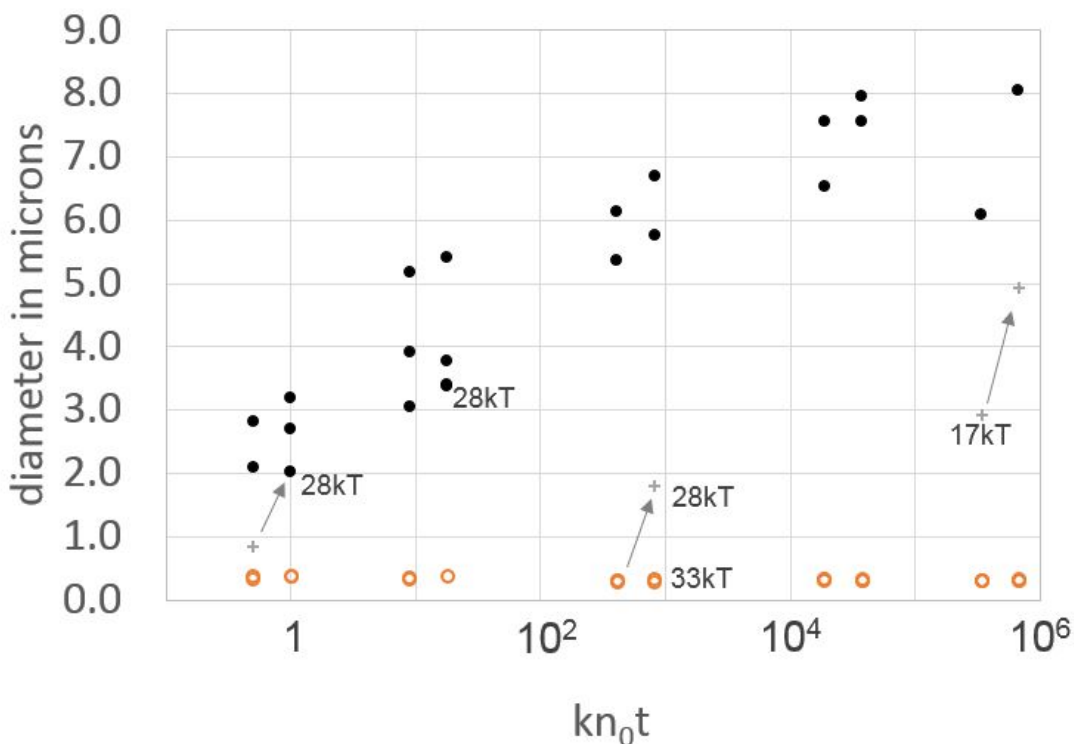


FIGURE 4.4:  $d_{10}$  values plotted against the characteristic aggregation time,  $kn_0t$ . Different symbols show how samples are grouped, but otherwise have no meaning. Empty orange circles show flocculation regime, filled circles coalescing regime, crosses show mixed regime. Arrows show how samples in the mixed regime change over time. Text close to occasional data points shows the calculated barrier height  $V_R^*$ .

more pronounced in the higher xanthan concentrations. This group has large energy barriers on account of the zeta potentials larger (farther from zero) than  $-22\text{ mV}$ . The group also includes three additional samples with a zeta potentials of  $\sim -21\text{ mV}$  but xanthan levels of 0.1% and below.

The second group shows much larger  $d_{10}$  values than the flocculation regime, but also much more scatter in the observed diameter and each  $kn_0t$  value. This second group is labelled as a quasi-coalescing regime. The observed scatter in the quasi-coalescing regimes suggests that the extent of coalescence depends on the calcium dose and as such is not a true coalescing regime where each floc is converts to one colossal

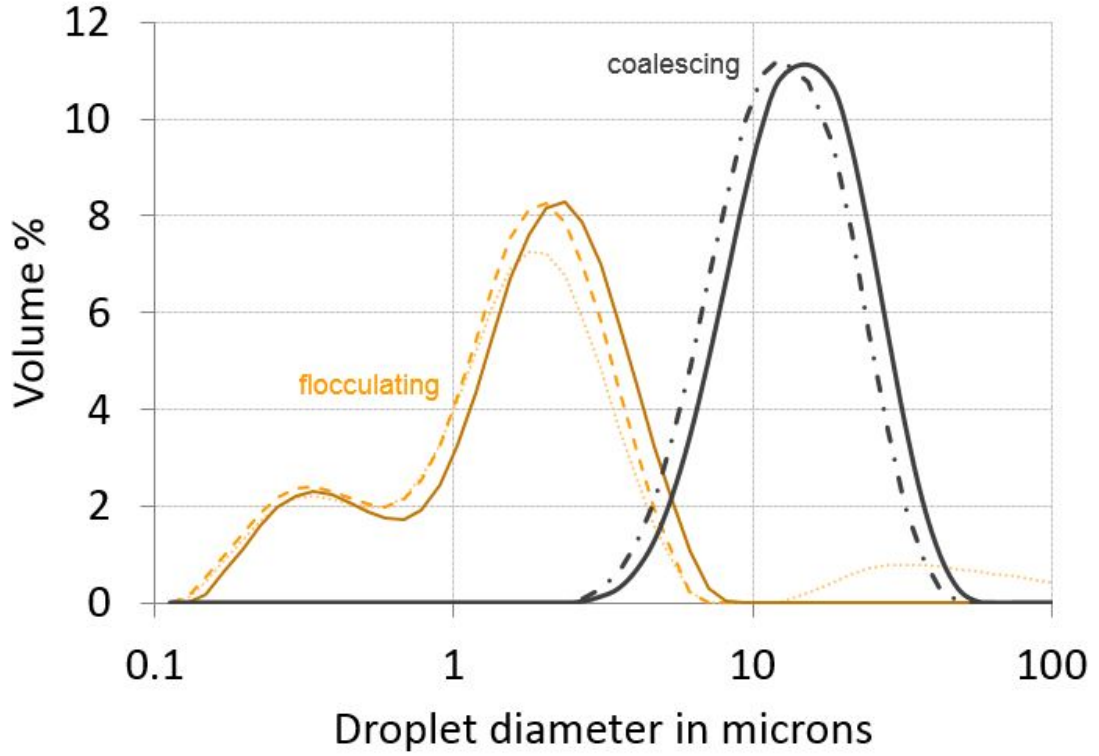


FIGURE 4.5: droplet size distributions of emulsions at  $kn_0t = 410$  or  $0.1wt\%$  xanthan at 4 days. Orange bi-modal curves on the left show the data corresponding to zeta potentials of  $27.7\text{ mV}$  (dotted line),  $22.3\text{ mV}$  (dashed line) and  $21.5\text{ mV}$  (solid line). Black monomodal curves on the right, correspond to  $18.2\text{ mV}$  (dash-dot line) and  $14.6\text{ mV}$  (solid line)

droplet. Nonetheless, the shift in  $d_{10}$  and the the overall droplet size distribution values suggests extensive coalescence, figure. 4.5. Moreover the variation within this group is smaller than the difference between the groups. The quasi-coalescing group shows steadily increasing droplet size with increasing  $kn_0t$  values and zeta potentials smaller (closer to zero) than  $-18\text{ mV}$ . This group has two additional samples characterised by zeta potentials of  $\sim -21\text{ mV}$  but high xanthan levels of  $0.25\%$  and  $0.5\%$ .

Investigating the trends as per the barrier heights,  $V_B^*$ , reveals the smallest barrier height of flocculating samples was  $27\text{ kT}$ , while coalescing samples were all below  $28\text{ kT}$  except one outlier sample with  $32\text{ kT}$ . This outlier was found in the flocculating group at  $kn_0t = 9.0$  but moved into the coalescing group at  $kn_0t = 18.0$ , no other sample moved from the flocculating to the coalescing group. The remaining four samples



points do not appear to not lie in either group and are labelled as being in the mixed regime. This group includes: a sample with  $kn_0t = 0.5$ ,  $\zeta = -21.9 \text{ mV}$ ,  $c = 0.5\%$ . The barrier height of this sample was  $28 \text{ kT}$ . Nonetheless, at these small  $kn_0t$  values, the average aggregate contains only a few droplets and thus  $d_{10}$  is restricted the probability of coalescence and equally small flocs as well as barrier height. Notably, later this sample moved to the coalescing regime when  $kn_0t = 2.5$ . A second mixed regime sample with  $kn_0t = 820$ ,  $\zeta = -21.5 \text{ mV}$ ,  $c = 0.1\%$ . This sample was found earlier in the flocculation regime at  $kn_0t = 410$ . The barrier height of this sample is  $28 \text{ kT}$  and consistent with the separation of coalescing and flocculation regime around  $27 \text{ kT}$ . The final mixed regime sample was found at  $kn_0t = 3.9 \times 10^5$  and  $kn_0t = 7.8 \times 10^5$ ,  $\zeta = -17.9 \text{ mV}$  and  $c = 0.02\%$ . This sample had a barrier height of only  $17 \text{ kT}$ , however, the xanthan dose is particularly low,  $0.02 \text{ wt\%}$ . This low dosage corresponds to a secondary minimum of about  $0.7 \text{ kT}$  and would not trap all of the small droplet population, but notably would trap larger droplets in a floc.

There is a clear trend in the quasi-coalescing regime of increasing  $d_{10}$  with  $kn_0t$ . Naturally, aggregation kinetics predicts larger aggregates at larger  $kn_0t$  values. However, it's not clear how a  $d_{10}$  could be predicted or whether this trend offers any new insight. Below  $kn_0t$  10 equation 4.7 predicts little to no coalescence because flocs are small, and the rate at which films rupture is of the same order of the experimental time scale. Size data at these low  $kn_0t$  values clearly shows some coalescence has occurred. The likely reason for this deviation is that equation 4.7 is based on Smoluchowski aggregation kinetics, and large deviations are known for this high concentration of droplets (Veshchunov and Tarasov [119], Lattuada [120], and Heine and Pratsinis [121]). Nonetheless,  $kn_0t$  remains as the appropriate metric that can be used to understand the aggregation process. It is clear, however, that in order to establish the likelihood of flocculated droplets coalescing the number of drops in a floc must be known. Confocal microscopy was attempted but a sample preparation method that didn't suffer from artefacts such as creaming or the mechanical disturbance of delicate flocs couldn't be devised.

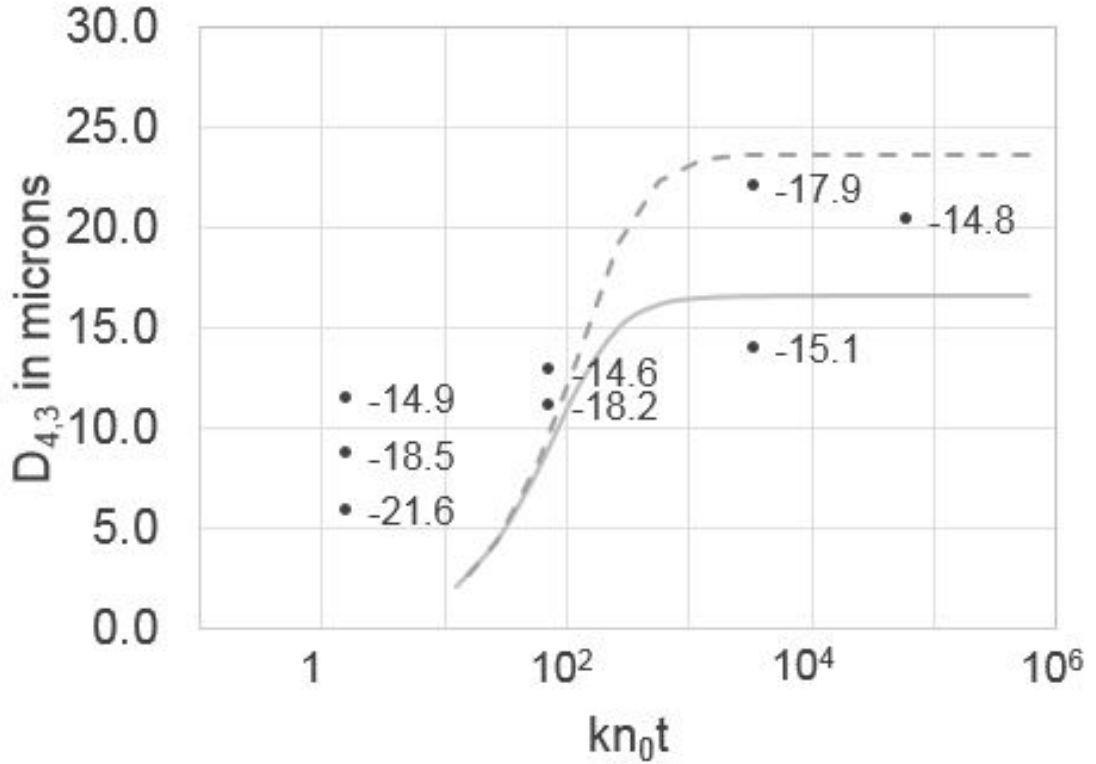


FIGURE 4.6: The  $d_{4,3}$  of samples plotted against characteristic aggregation time. Only samples in the quasi-coalescing regime at 4 days are shown. Lines show calculated diameter 4.7 for  $K^{-1} = 45$  (dashed line) and 50 hours (solid line). Text near data points show the calculated zeta potential in  $mV$

Instead, a comparison is made against equation 4.7 with  $(K)^{-1} = 45$  and 50 hours (As the data coalescence rate must be faster than the time scale of the experiment, 4 and 8 days. The data does not warrant high resolution fit, but a fit of  $k \sim 2$  days seemed to capture the essential ball park. 45 and 50 hours are chosen to demonstrate sensitivity of the fitted  $K$  value.), with each droplet having about 10 neighbours or  $q = 5$ . This equation calculates the number of droplets after coalescence, but can be used to estimate an average droplet size via  $d_{4,3} \sim (n_0/n)^{1/3} d_{4,3stockemulsion}$ . The applied rate constants capture the approximate diameter but does not explain the overall data particularly well. The calculation is only expected to hold for large aggregates, where  $kn_0t$  values are large. Beyond  $kn_0t \sim 1000$  the number of primary droplets is insignificant and growth must come from collisions of colossal flocs. The appropriate rate constant for colossal droplet coalescence is  $kt \times n_0/N$  where the large values of  $N$ , essentially halts any aggregation. Under

these conditions any coalescence is limited by the values of  $K$  and a plateau is observed in the calculated  $d_{4,3}$ . Comparing droplet diameters in the plateau region of equation 4.7 ( $kn_0t > 300$ ) does not reveal any trends in droplet size with the zeta potential.

An energy barrier,  $E_B$  for the rate constant at temperature,  $T$  can be calculated using the Eyring equation.

$$k = \frac{\kappa k_B T}{h} \times e^{\frac{-E_B}{k_B T}} \quad (4.8)$$

where  $\kappa$  is the transmission coefficient and  $h$  the Planck's constant. Assuming a transmission coefficient of 1,  $(50 \text{ hours})^{-1}$  gives an energy barrier of about  $42 kT$  which is not consistent with the calculated here, but consistent with the notion of a large force such as an electrical double layer force. Furthermore, a lack of correlation between zeta potential and droplet size once kinetics has been established suggests a non-DLVO coalescence pathway. Potential explanations could include: a change in the equilibrium conformation surface proteins due the presence of an adjacent charged surface. Any protein conformation changes would be slow as interfacial tension of WPI surfaces are equally high around  $50 \text{ mJ/m}^2$  corresponding to  $\sim 30 kT$  per protein assuming a  $2 \text{ nm}^2$  area. Meyer et al. [122] showed that when charge groups were mobile highly charge surfaces could be attractive. This mobile charge mechanism is somewhat different from the observed behaviour, but does show how a slow structural rearrangement may result in different than expected behaviour. Popa et al. [123] showed patches of opposite charge resulted in a short range attraction that would lower the expected value of  $V_B^*$  even at high zeta potentials and high coverage. At large separations observed force measurements follow the electrical double layer force but with an additional short ranged attraction. This patch charge effect scaled with zeta potential unlike the results here and the underlying mechanism relies on patches larger than the Debye length and it's hard to imagine how a patch of positive charge could be larger than  $1 \times 1 \text{ nm}$  which is close to the native size of a  $\beta LG$  protein. Coalescence pathways may come about by fluctuations in shape which may change  $V_B^*$ . In this instance coalescence would be defined by the rheological properties of the interface. In a related experiment Sun et al. have looked at the coagulation

probability of two particles in an optical trap created by optical tweezers. Sun et al. [124] describe two different probabilities, an instantaneous probability,  $p$ , and an accumulated probability,  $P$  where:

$$P = 1 - e^{-pft} \quad (4.9)$$

here,  $f$  is coalescence attempt frequency and  $t$  is residence time in the optical trap. While  $f$  is not known for colloidal particles it is known for adsorbed atoms on metal surface,  $10^{12-13} Hz$  (Wang and Ehrlich [125]), and surfactant micelle exchange rates,  $10^{11} Hz$  (Tanaka and Edwards [126]). One can imagine that comparatively larger emulsion droplets would be slower still. This optical trapping experiment examines the life time of only one film whereas the experiment here investigates many and  $pf$  essentially mimics  $Kq$ .

## 4.4 Conclusion

Earlier it was found that that droplets flocculate below zeta potentials  $-15 mV$ . By adding a depletion force coalescence can be tested. When the zeta potential is between  $-15 mV$  and  $-21 mV$  the film of water separating droplets in a secondary minimum ruptures at a rate of the order of  $K = (100hours)^{-1}$ . Electrical double layer forces suggest the barrier height at which droplet coalescence is mostly eliminated is surprisingly high at around  $28 kT$ . Even at these high barrier heights the small droplet population was subject to coalescence. Trapping droplets in a secondary minimum results in more coalescence attempts than would occur without a secondary minimum and the coalescence should revert to a first order kinetics with an Eyring style relation. The films separating droplets are only a few  $nm$  across and it's not clear how they rupture. It is clear that the stabilising effect of whey protein emulsions may be dominated by electrostatic effects (Foegeding et al. [52]) non-DLVO behaviour can not be overlooked.



## **Chapter 5**

# **Using Optical Tweezers to Measure the Probability of Aggregation of Pairs of Emulsion Drops: The Development of an Automated Procedure**

In the preceding chapters a framework to understand how the surface properties of emulsion drops depend on environmental conditions was constructed. In this chapter the aim was to understand how surface properties effect the interactions of drops within an emulsion system. In particular an optical tweezer (OT) setup was used to study the stickiness of pairs of particles as their zeta-potential was modified via the environmental conditions. Given the potentially probabilistic nature of the process (different drops may have slightly different amounts or spatial distributions of emulsifier at the surface, and the interaction energies are, in some cases, close to thermal values), it was important that many hundreds of pairs of emulsion drops were tested under each set of global experimental conditions. For this reason developing an automated procedure for carrying out such stickiness measurements with OT became an overriding goal of these studies, and will be an enduring legacy of this project.

Optical tweezers are a great tool for research in the biological and physical sciences (Dufresne et al. [127]). Tightly focused laser beams (typically formed with a high numerical aperture objective (Ashkin [128])) can hold dielectric particles in a so-called optical trap. Here, the dielectric particle experiences forces due to the transfer of momentum from the scattering of incident photons. The resulting optical force can be decomposed into a scattering force in the direction of light propagation (proportional to the optical intensity) and a gradient force in the direction of the spatial light gradient (proportional to the gradient of intensity) (Neuman and Block [129]).

A single-beam gradient trap (referred to herein as optical tweezers), in which the high NA of the focusing lens ensures that the gradient force dominates the scattering force is one of the simplest and most versatile trap types (Ashkin et al. [130]).

If the transverse electric field and intensity distribution of a beam of electromagnetic radiation can be well approximated by Gaussian functions, it is called a Gaussian beam. Most lasers beams are used in a mode where the beam profile can be approximated by a Gaussian function and assuming this then the trapping of a particle at the focus can be understood simply from the transfer of momentum owing to refraction and

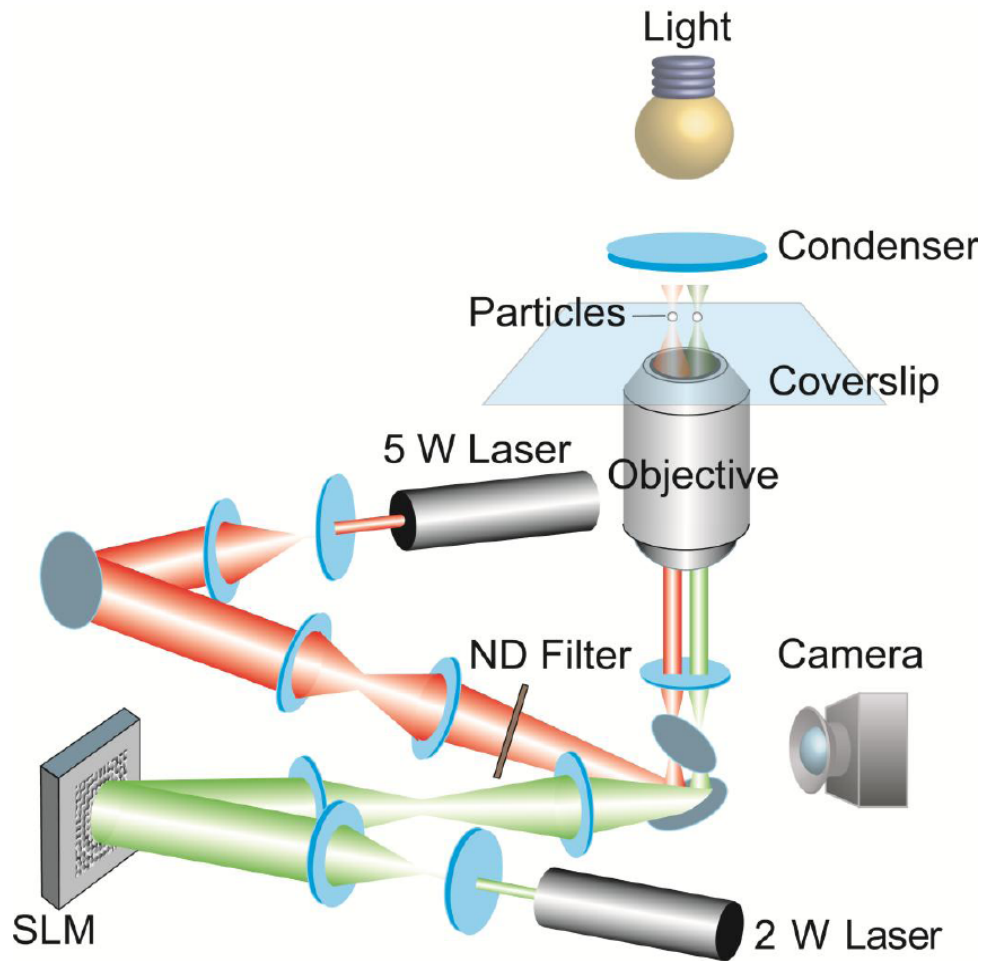


FIGURE 5.1: Optical Tweezers: The current optical tweezer configuration in our lab. In the current study, the 2W laser was used exclusively. Image courtesy: Sandy Suei.

Newton's third law (Jones et al. [131]). In simple gradient traps a Gaussian laser beam is directed into the back aperture of a high numerical aperture objective lens and is brought to a tight focus (Grier [28]).

A simple optical ray model can be used to explain forces in optical tweezers in regimes where the trapped dielectric particle has a size that is larger than the order of the wavelength of the trapping light. Consider a system where light is focused, at high numerical aperture, into a transparent sphere with a higher refractive index than its surroundings. When the particle is at the centre of the trap, it does not experience any force but when there is a lateral or axial displacement from the centre it changes the



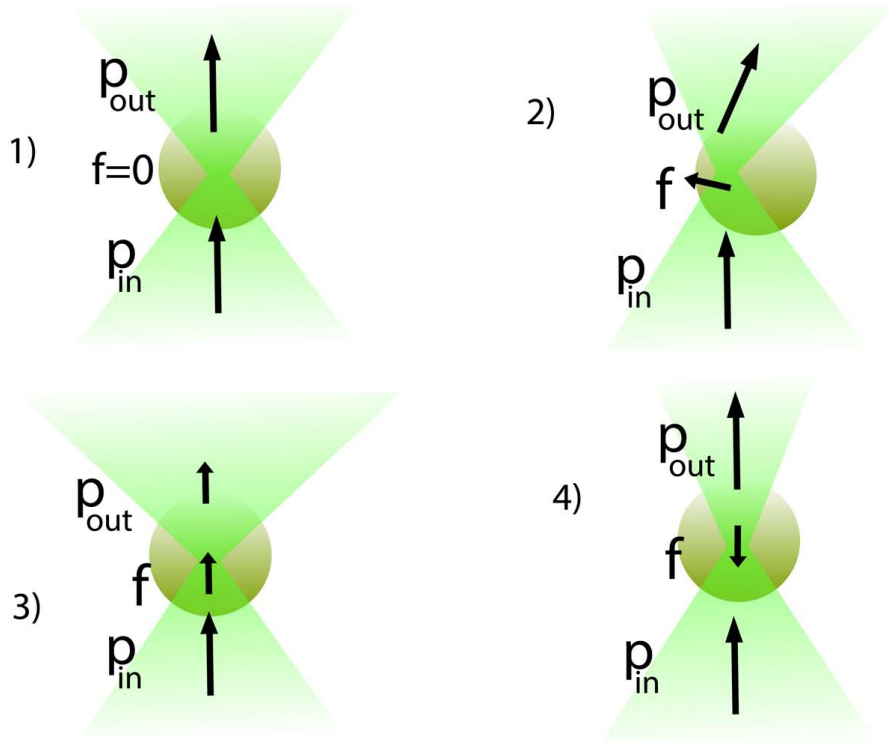


FIGURE 5.2: Optical Tweezers: Ray optics model. Any momentum change from refraction of photons creates a restoring force directing the particle back to the trap centre as shown in (1), (2), (3)& (4)

light's momentum resulting in a restoring force. This restoring force pulls the particle back to the focus (Dholakia et al. [132], Neuman and Block [129], Bowman and Padgett [133], and Polimeno et al. [134]).

In most OT experiments, including the current one, multiple traps are required to be generated. This can be achieved by using multiple beams or by splitting a single beam. A holographic optical tweezers (HOT) uses a computer-designed diffractive optical element (DOE) to split a single expanded and collimated laser beam into a desired distribution of multiple beams, that pass through the strongly converging objective lens and are focused into the optical plane of the microscope (Dufresne et al. [135], Curtis et al. [136], and Jones et al. [131]). Spatial light modulators (SLM) are DOEs that can modulate the phase and/or amplitude of an optical beam (Kuang et al. [137]) (phase of the beam used in the setup in these studies) and as such an optical tweezer setup that includes an SLM is capable of producing multiple traps that can be dynamically controlled.

## 5.1 Emulsion droplet stickiness using OT

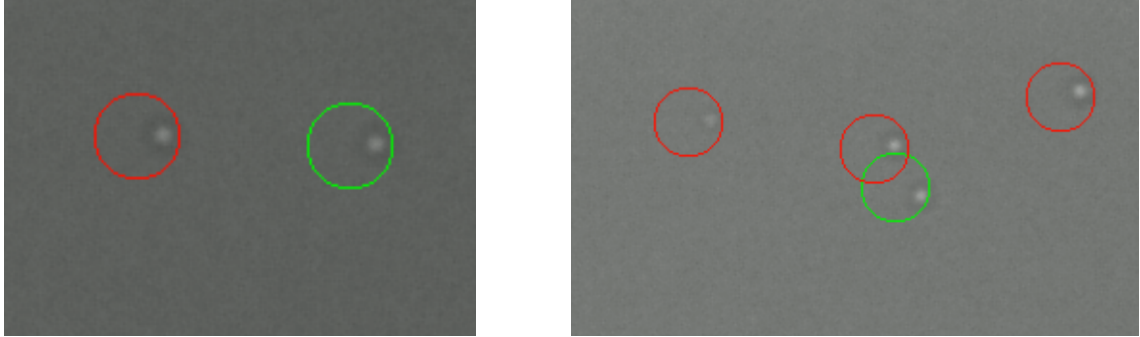


FIGURE 5.3: a) Particles trapped for stickiness measurement. b) Particles trapped in multiple traps.

In principle two individual emulsion drops can be held in place by two optical traps and simply by translating one of the traps they can be brought closer and closer together, allowing the interactions between emulsion droplets to be studied. This method has great potential to increase the understanding of the mechanisms that are important for the stability of bulk emulsions (Nilsen-Nygaard et al. [138] and Griffiths et al. [139]). In reality however, many practical difficulties must be overcome in order to carry out such experiments in a robust manner.

Emulsion droplets either stick together (aggregate) or not when they are allowed to collide in an optical trap, depending on the stability of system, determined by the physio-chemical conditions. The capture probability is a statistical measure of the stickiness of particles under a particular set of environmental conditions. Practically, it is not easy to perform a statistical measurement of stickiness using a traditional well slide arrangement: having many particles being present leads to multiple drops interacting in the traps, interfering with the pairwise measurement, while having few particles present means it is extremely time consuming to isolate multiple pairs of drops for hundreds of repeat experiments. Instead we investigated the use of a microfluidic chip and reservoirs of particles that could be sampled on demand as the basic format of our experiments.

The inherent scale of optical tweezers allows them to be combined easily with

microfluidics (Yao et al. [140]). Having a microfluidic chip format means that once a particle pair has been isolated and trapped from an initially injected particle cloud, flow can be used to wash away any superfluous drops surrounding the trapping area. As such each pairwise stickiness experiment can be carried out in a "clean environment". Herein an *automated* particle collider for measuring particle-particle interactions has been realised by combining elements of microfluidics, holographic optical tweezers (OT with SLM) and image analysis. Each individual measurement consists of confining two particles in close proximity within a pre-determined chemical micro-environment, and observing whether their interactions lead to aggregation in a selected time. To automate the measurements, Red Tweezers and LabVIEW software have been used and a custom plugin written to control pumps (for inject and flush operations), perform particle detection, and manipulate particle positions.

## 5.2 Probabilistic approach to the measurement of the stickiness of particles

In real life colloidal systems, the Brownian motion of particles (and any fluid motion, such as convection or externally imposed flows) can bring particles together, making them collide, and hence can potentially induce aggregation. The short range interactions between particles determines the rate of aggregation once the particles are in close proximity with each other (Adamczyk and Weroński [141], Gregory [142], and Elimelech et al. [84]). The stickiness probability decreases with an increase in the height of the repulsive inter-particle potential barrier (typically governed by electrostatics) and colloidal solutions can become kinetically stable in quiescent systems if these repulsive interactions are many times the available thermal energy. Indeed according to the DLVO theory of coagulation, colloids will remain dispersed if this energy barrier is greater than the average kinetic energy of the particles (Wiese and Healy [118], Kovalchuk et al. [24], and Kovalchuk and Starov [143]).

Colloidal particles with very attractive short range interactions aggregate to form clusters, with size distributions and fractal dimensions falling into one of two limiting cases, depending on whether diffusion of the particles is the rate-limiting step (Diffusion Limited Colloid Aggregation(DLCA)) , or whether the particles can contact each other without always sticking (Reaction Limited Colloid Aggregation (RLCA)). In DLCA, particles stick irreversibly to each other when they come into contact so that the aggregation rate is limited by the time taken for the particles and clusters to collide each other by Brownian diffusion. RLCA occurs when there are repulsive interactions between the particles or clusters, requiring multiple collisions between them before inter-particle bond formation takes place, reducing the aggregation rate. Here the rate is limited by the time taken for two clusters to overcome this repulsive barrier by thermal activation (Lin et al. [144], Klein and Meakin [26], Lin et al. [145], D.J Robinson and J.C Earnshaw [25], Moncho-Jordá et al. [146], and Lu and Weitz [147]).

The stability of a colloidal dispersion is commonly expressed in terms of the stability ratio  $W$ , which is given by the ratio between the total number of collisions experienced and the number of collisions that result in aggregation (McGown and Parfitt [148] and Missana and Adell [14]).(So that  $W=1$  corresponds to diffusion limited cluster aggregation, with larger numbers manifesting reaction limited cluster aggregation). The reciprocal of the stability ratio (the stickiness probability) is measured in the experiments described here. Not all collisions yield aggregation, with only "effective" collisions, those with the right microscopic details (the required thermal kick, and favourable local potentials) able to produce stable doublets. Here an optical tweezer setup is used to investigate this directly. Two particles are brought together using an optical trap, held in close proximity for an experimental contact time, and then subsequently released to see if an "effective collision" had taken place. If attractive forces overpower the repulsive electrostatic interaction then the particle pair will stay stuck together after turning the confining trap off. This microscopic approach to the stickiness gives us direct insight into how stable a colloidal system will be in a quiescent system of Brownian thermally driven collisions.

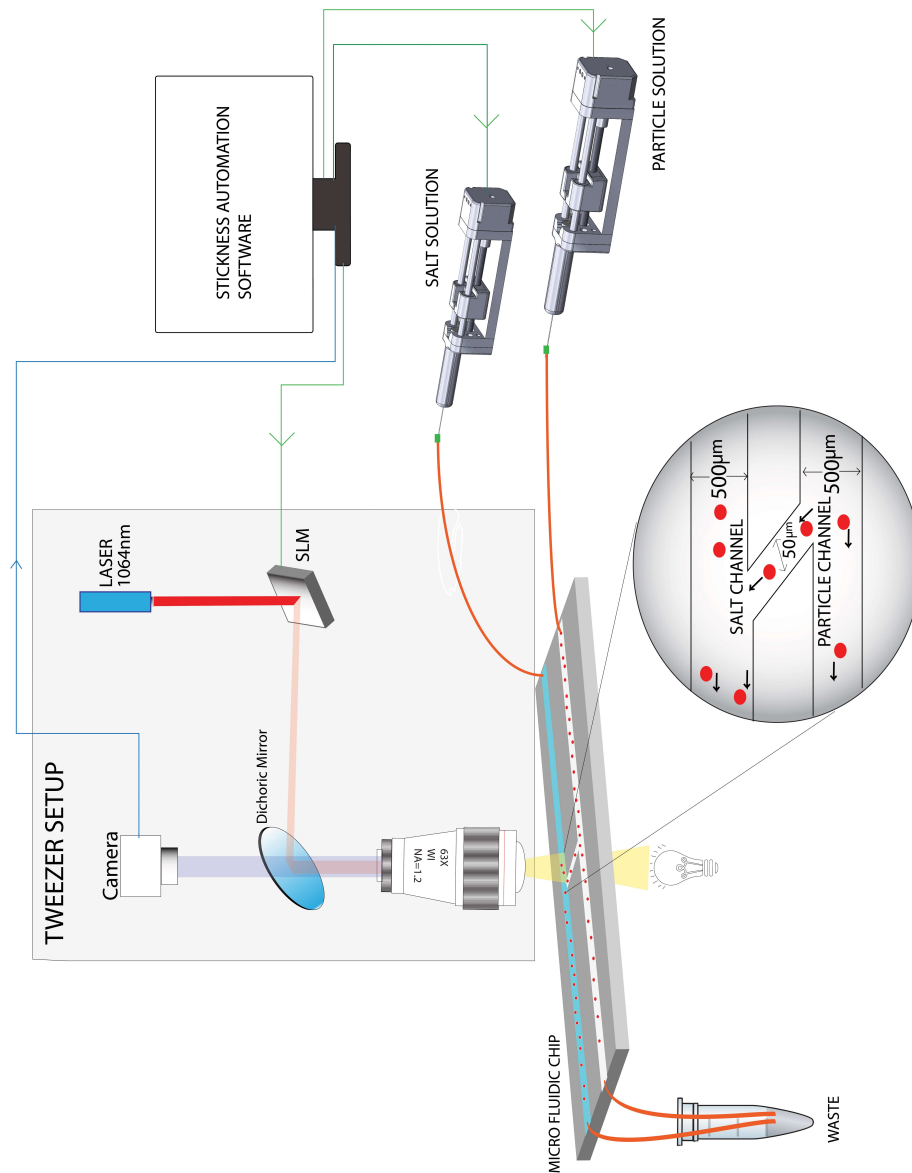


FIGURE 5.4: Experimental setup for stickiness measurements.

The aim of the experiment then is to bring a pair of droplets close to one another to maximise the encounter frequency. This is achieved by optically trapping two droplets in independent traps and then bringing them close together before turning one trap off. Both drops are then drawn into the same trap. As the second particle moves into the pre-occupied trap it first collides with the second particle before occupying a more relaxed state with the two drops held in very close proximity (Xu and Sun [149]). Within the single optical trap, both drops are oriented along the propagation direction of the beam. After a set time the trap is released and whether the two droplets remain stuck together or not is observed.

More specifically, two particles are each optically trapped and then brought together at the time  $t = 0$  into a single trap. The trap is then subsequently turned off, releasing the particles, at the time  $t = \tau$ . Thereby, during this experimental time: one direct collision of the particles is induced through optical forces (at kinetic energies no greater than a fraction of thermal fluctuations (Neuman and Nagy [150])), and subsequently further thermally induced collisions take place owing to the close proximity in which the particles are held. If  $(\tau)$  is longer than the average time taken for one collision (sticking attempt), then the measured probability of sticking ( $P$ ) for the particle pair is an accumulated probability, which is related to  $p$ , the sticking probability after a single collision of the particle pair, by;

$$P = 1 - e^{(-pft)} \quad (5.1)$$

where  $f$  is the collision frequency in the trap (Sun et al. [124]).

## 5.3 Materials and Methods

### 5.3.1 Sample preparation

A stock emulsion was prepared as described in the introduction. It was then diluted using Milli-Q water in the ratio 1:100. Solutions in which the emulsion drops had different zeta potentials were produced by adding analytical grade NaCl, obtained from Sigma Chemical Co. (St Louis, MO, USA) and adjusting the pH.

### 5.3.2 Optical tweezers

The optical tweezers setup used for the trapping of particles consists of a Nikon inverted microscope (Eclipse TE2000-U), 2 W 1064 nm infrared laser, SLM (Boulder Nonlinear Systems, Colorado, USA), and Nikon high numerical aperture water immersion microscope objective lens (MRD07601, CFI Plan Apochromat VC 60XC WI, 60 $\times$ , NA=1.2).

### 5.3.3 Microfluidic chip

The microfluidic chip used was designed in collaboration with, and manufactured by, the Australian National Fabrication Facility. The design consisted of two parallel channels (500  $\mu\text{m}$  wide  $\times$  50  $\mu\text{m}$  deep) connected by a single diagonal channel (50  $\mu\text{m}$  wide  $\times$  20  $\mu\text{m}$  deep). It was manufactured from borosilicate glass that has the low mechanical compliance necessary for high flow stability and a high pressure capability. The high pressure capability, while initially investigated for high temperature applications, turned out to be of critical usefulness in successfully cleaning the channels. Typically eight of these "channel pairs" were machined on one chip, as seen in figure. 5.5. Channels were 4 cm in length and were terminated with tapered holes, that allowed for optimised attachment of PEEK tubing.

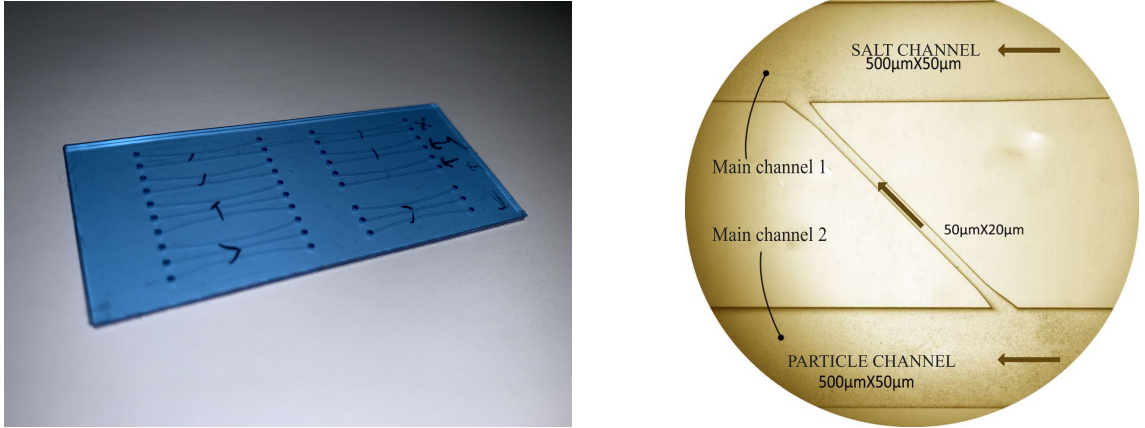


FIGURE 5.5: Microfluidic chip used in the experiment consisting of two parallel channels connected by a single diagonal channel.

### 5.3.4 Syringe pumps

Commercially available syringe pumps were not able to reliably allow the flushing of fluid through the channels of the microfluidic chip while maintaining the optical trapping of emulsion drops, so custom pumps were designed, manufactured and implemented (Figure. 5.6). These syringe pumps, designed and manufactured in our research group, give the option of generating either slow ( $5 \text{ pL}$  injection increments) or very rapid flow ( $1 \text{ /s}$ ) - ideal for either exchanging background solutions while maintaining trapping or for flushing and cleaning respectively. Syringes were thermally shielded in order to remove the effects of temperature fluctuation on the flow. The pumps were controlled using a computer program written in LabVIEW and incorporated into the automation software.

## 5.4 Automation of the stickiness experiment

As described previously, owing both to probable variations between particle pairs, and in some cases potentials with heights close to thermal energies determining the outcome of the interaction, a study of the stickiness of particle pairs demands a large number of pairs of emulsion drops to be considered.



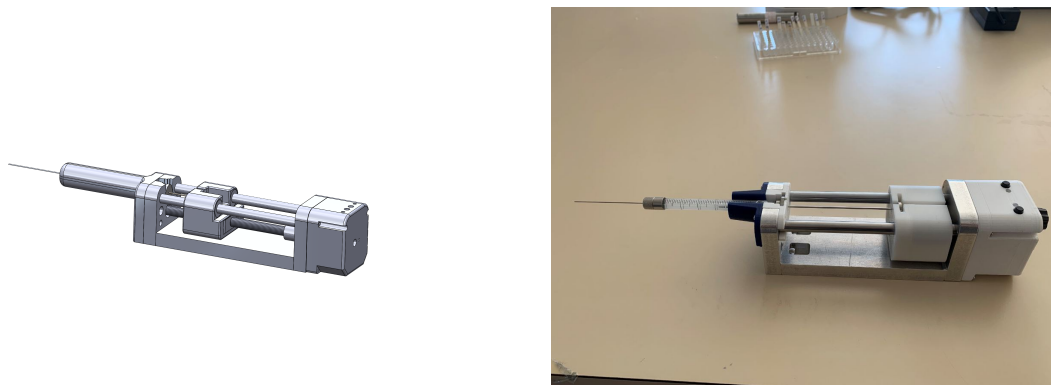


FIGURE 5.6: Syringe pump

Automating the experimental setup, so that pairs of particles can be: automatically selected, brought into a single trap for a fixed time, then released and observed, is crucial in order to make such measurements practicable. An experimental setup incorporating optical tweezers, microfluidic chip and syringe pumps was developed in house and controlled by an automation plugin realised using LabVIEW. The strategy taken is elaborated in Figure. 5.7.

Particle-particle collisions were carried out in a microfluidic chip containing multiple channels as described and outlined in figure. 5.7. The chip consists of main "environmental control" and "particle" channels, that are connected by a narrow diagonal channel, used for transfer of a small amount of particles-of-interest into the desired environment. Solutions corresponding to different physio-chemical conditions, and solutions containing colloidal particle of interest (here emulsion drops) were injected into these two channels respectively, in a controlled manner, using the home-made syringe pumps.

Before starting the automation software, it was important to make sure that the syringes containing the solutions were bubble-free so that a stable flow could be established. The microfluidic chip was also well cleaned before each change of environment. The chips were first washed with 0.1% xanthan solution which was found to remove any stuck particles or aggregates present from previous experiments Figure. 5.8). Subsequently it was rinsed with the detergent DECON-CLEAN, and then with Milli-Q

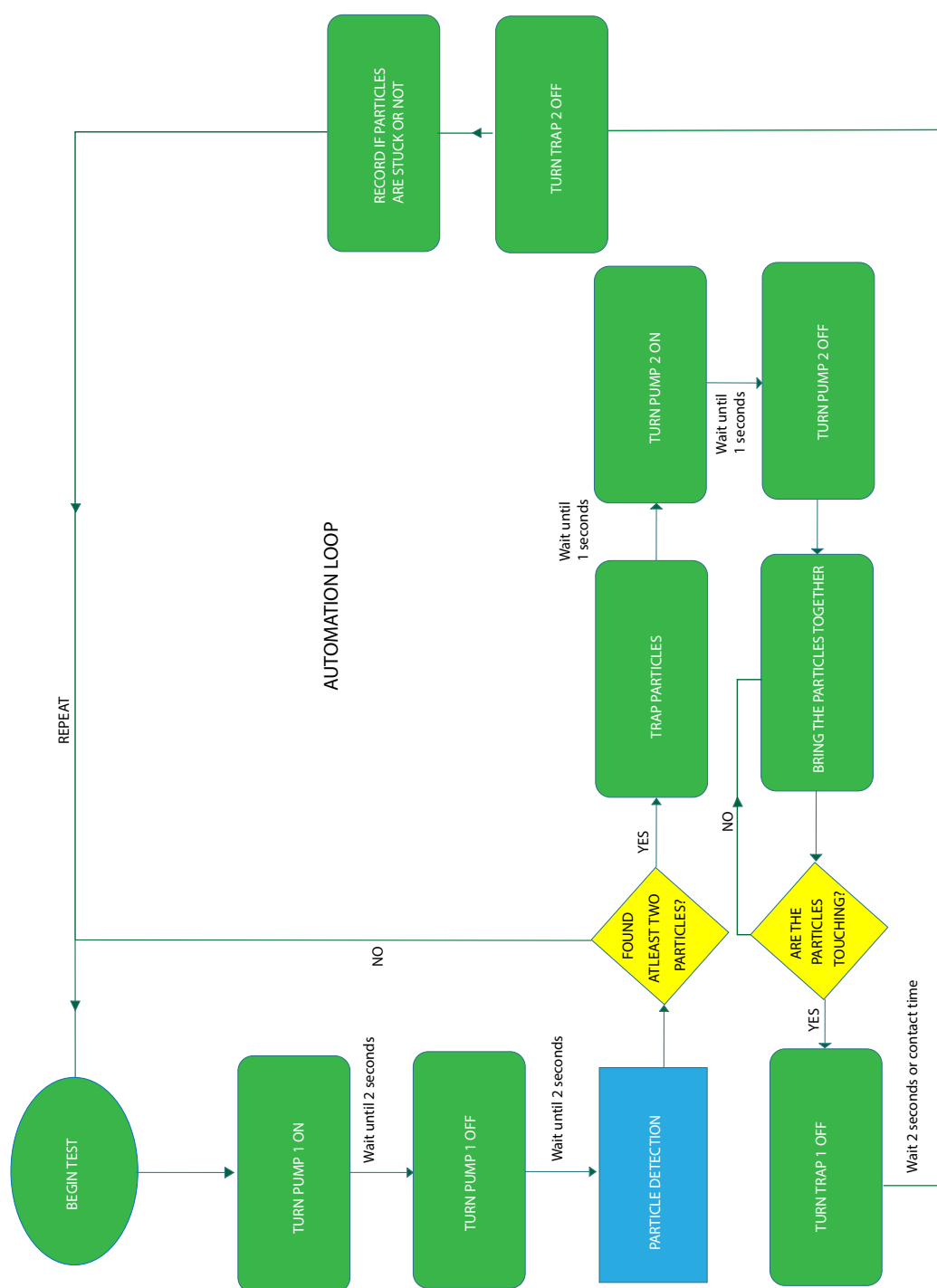


FIGURE 5.7: Flow chart showing different stages of the automation of the stickiness experiment

water multiple times to remove any residues. Finally, syringes containing the relevant emulsion drops and the background electrolyte solutions were inserted into the syringe pumps, and connected via PEEK tubing with zero-dead volume connectors (from the HPLC ecosystem) to the channels on the chip.

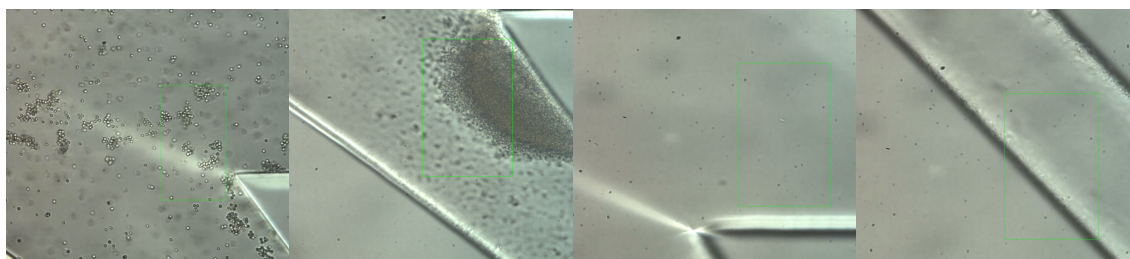


FIGURE 5.8: Cleaning of the microfluidic chip using xanthan: The left hand images show the chip after doing one full set of stickiness measurements. The right hand images show the chip after cleaning.

The microfluidic channels were flushed through with 2-3 mL of degassed Milli-Q water under several bars of pressure. This removed any air bubbles that had attached to surfaces inside the microfluidic chip and tubing. Failure to remove air bubbles can introduce hydraulic capacitance which increases the time required to start and stop flows due to compressability of the gas. Slowed starting and stopping of flows leads to an accumulated increase in experiment time which can be significant over hundreds of iterations of the automation loop. Air bubbles that partially block an upstream channel can redirect laminar flows leading to particle solution bypassing the diagonal channel, or salt solution not sufficiently flushing out unwanted particles. Air bubbles downstream of the diagonal channel can also cause undesirable flows.

Following flushing with Milli-Q water, the pumps controlling the flows of the particle and salt environment solutions are connected to the microfluidic chip and *ca.* 20  $\mu\text{L}$  of sample from each is pumped through their respective channels under several bars of pressure. This displaces any remaining air bubbles and replaces the Milli-Q water previously injected with the actual samples. To mitigate against initial formation of aggregated particles, salt solution is injected first followed by particle solution. This ensures that particles are only exposed to salt solution at the diagonal channel outlet. At this point,

starting and stopping the pumps results in fast, responsive flows. Fluid injection times and amplitudes were determined by running several iterations of the automation loop and gradually adjusting values. Relative flow rates for the particle and salt solutions were configured so that salt solution could never enter the diagonal channel by back-flow, where it could mix with the particle solution. Finally, a region-of-interest (ROI), in which automatic particle detection takes place, was defined by observing the expansion of a small cloud of particles leaving the diagonal transfer channel and entering the environmentally controlled channel. Once the system was primed, and pump values and the ROI were set, the automation protocol was started and used to perform the pairwise stickiness experiments.

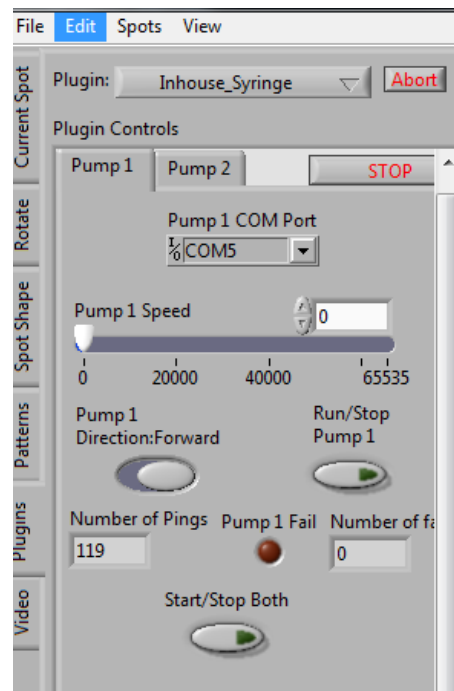


FIGURE 5.9: The "pumps-plugin" of the automation software. The two syringe pumps are controlled using this plugin. The rate of flow and the direction of the syringe motion can be controlled here.

The automation loop begins by switching on the syringe pump attached to the particle channel, at very low flow rate, in order to inject particles onto the chip and to have a fraction of them travel into the other main channel (which contains the controlled

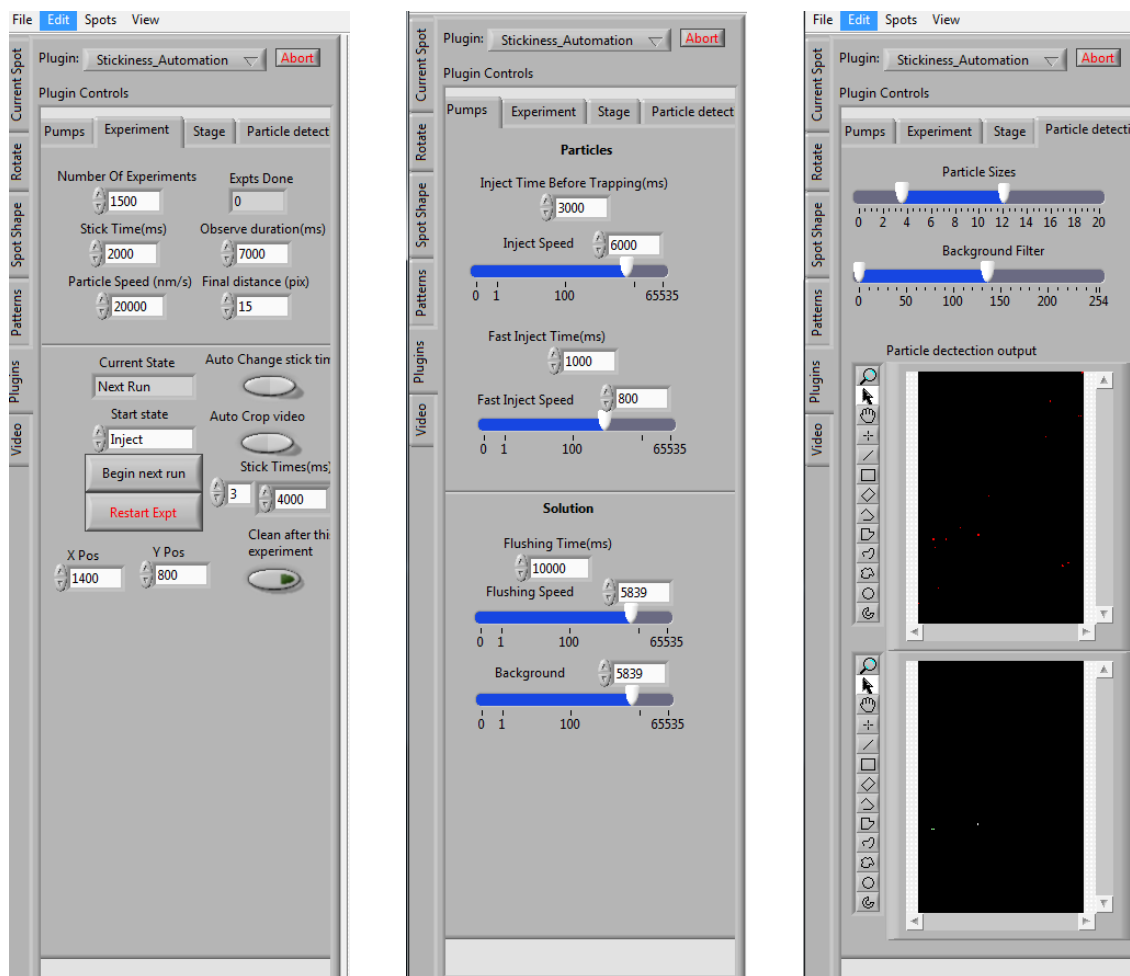


FIGURE 5.10: The "stickiness-automation" plugin

physio-chemical environment) via the diagonal. The could be visualised as a slowly expanding cloud of particles where the diagonal transfer channel joined the environment channel. As there is a significant depth difference between the main channels and diagonal channel, the particles could be observed to rise slightly. An image analysis algorithm was used to detect particles within the expanding cloud that looked like good candidates for performing a stickiness experiment (particles that were stuck to the bottom of the chips were avoided by setting the focal plane around 10  $\mu\text{m}$  above the bottom of the channel).

As described a region of interest for image analysis was selected in the salt channel, near the junction with the diagonal transfer channel. As particles travelled into the

salt channel and approached the ROI, the particle detection algorithm started scanning for particles. The particle detection involved four main steps. First, images captured from the camera were converted to an 8-bit gray-scale and binary threshold was applied. After this step, particles satisfying user-set diameter and eccentricity criteria were filtered out, followed by the simultaneous selection of two in-focus particles, (keeping in mind that they should not be so close to each other that they could not be trapped in two distinct optical traps). The automation software then generates two laser traps using the SLM, in order to capture the two detected and selected particles. If any of the conditions are not satisfied, the algorithm re-scans for particles.

Once the particles were trapped, the pumps-plugin of the automation software was activated, flowing the desired controlled environment (salt solution) through the channel containing the trapped particles, ensuring that all the particles other than those trapped in the ROI were flushed away to the waste outlet at other end of the channel. Simultaneously the application of a background flow in the particle channel was carefully controlled to ensure that 1) the salt solution did not flow back into the particle channel but also 2) that fresh particles (that would interfere with future stickiness measurements) were not injected through the diagonal. Figure. 5.11 shows a schematic of the various steps in the automated stickiness experiment.

The trapped and isolated particles, now surrounded by the desired controlled environment solution, are then moved back downstream to a fixed location (fixed 'x' and 'y' coordinates) where the stickiness measurements were performed. This position was maintained for all experiments in order to ensure consistent laser power was used, (this can vary spatially due to the finite element sizes in the SLM and optical aberrations in the microscope lens). The two particles are now brought very close to each other (the particles are moved with a speed of  $0.02 \text{ mm/s}$  throughout the trials so that hydrodynamic forces owing to flows are negligible) and then one of the traps is turned off so that the two particles become located in the same trap. The time for which the particles are held in the common trap is considered as the "contact time" for the experiment. After this time

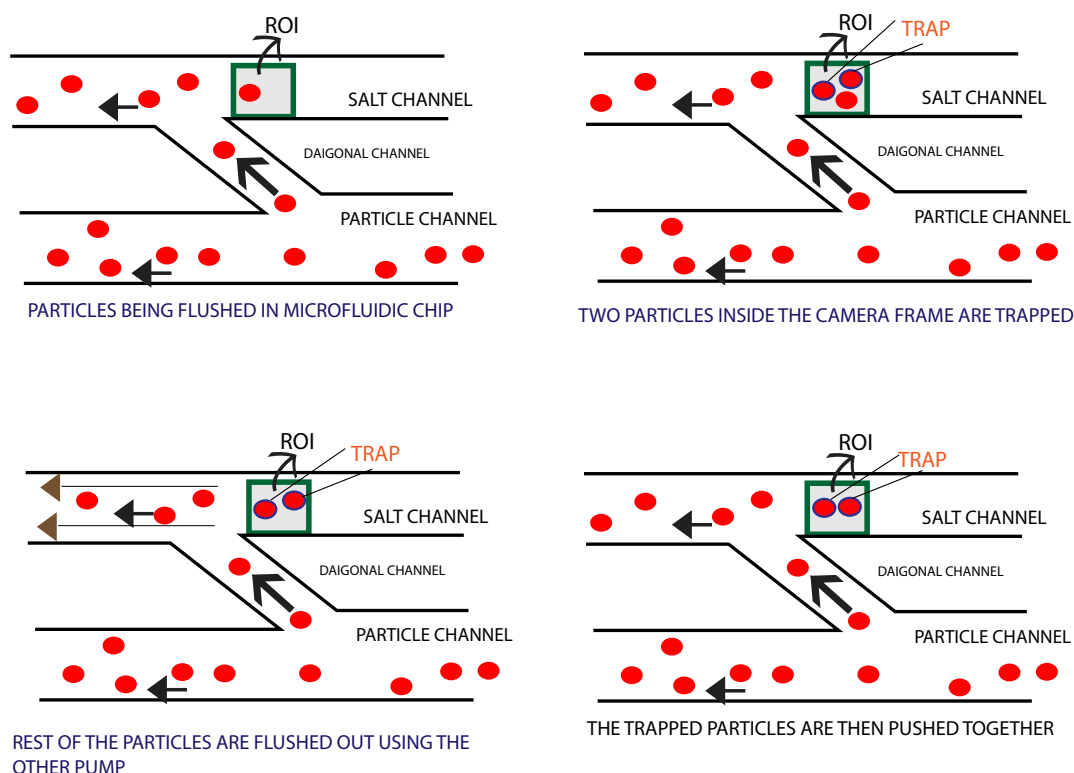


FIGURE 5.11: The schematic representation of the steps involved in the fluids-handling in the microfluidic chip during the experiment. In order: Top left, top right, bottom left, bottom right

the laser power is then switched off so that the particles diffuse freely. The particles are then observed to see if they remain aggregated. The experiment is then repeated automatically hundreds of times, with different pairs of emulsion drops being selected each time. Once all experiment iterations (>500) are completed, a high amplitude pulse was typically applied to purge any stuck particles from the channels. The solution in which the experiments are being carried out (controlling zeta potential and Debye length) was then changed and the whole process repeated.

## 5.5 Results and discussion

### 5.5.1 Variations in stickiness probability with zeta potential

Twelve salt solutions with differing pH values were prepared, each corresponding to the dispersed emulsion drops possessing different zeta potentials as measured on the bulk samples ( $-42\text{ mV}$ ,  $-38\text{ mV}$ ,  $-31\text{ mV}$ ,  $-28\text{ mV}$ ,  $-26\text{ mV}$ ,  $-24\text{ mV}$ ,  $-22\text{ mV}$ ,  $-18\text{ mV}$ ,  $-10\text{ mV}$ ,  $-0.7\text{ mV}$ ,  $21\text{ mV}$ ,  $28\text{ mV}$ ). For each experiment the apparatus was primed as described in the previous section and stickiness data was acquired automatically over many hundreds of pairs of particles. The automation parameters (Figure. 5.7) were set to  $t_{flush} = 15\text{ s}$ ,  $t_{hold} = 2\text{ s}$ , and  $t_{observe} = 5\text{ s}$  and 500 pairwise measurements were acquired under each set of conditions. When the second trap initially holding the second particle is turned off the optically trapped particles initially collide as one particle is drawn into the other particle's pre-occupied trap by optical forces. The particles then relax (Sun et al. [151]) to a situation where they are held in close proximity (even if not in direct contact) allowing Brownian fluctuations to facilitate many collisions over the user-defined duration of  $t_{hold}$  before being released and observed. All experiments were performed at the same location in space in order to ensure the strength of the optical traps remained constant, and were video-recorded. For each pair of drops examined, whether the particles had become aggregated or not was assessed by viewing them during an observation period after the optical trap was removed,  $t_{observe}$ , and recording a '0' for non-stuck, individually diffusing particles or a '1' (stick) when the two drops remained attached and diffused as a single particle. The outcome of each trial was counted in real time or by watching the recorded video offline. The experiments were repeated using all the different salt solutions (corresponding to different zeta potentials of the emulsion drops). Figure. 5.12 shows the stickiness probabilities obtained versus the expected zeta potentials of the emulsion drops, as inferred from prior Zetasizer measurements carried out on the bulk sample. Each point is acquired from studying the result of the experiment for 500 pairs of drops.



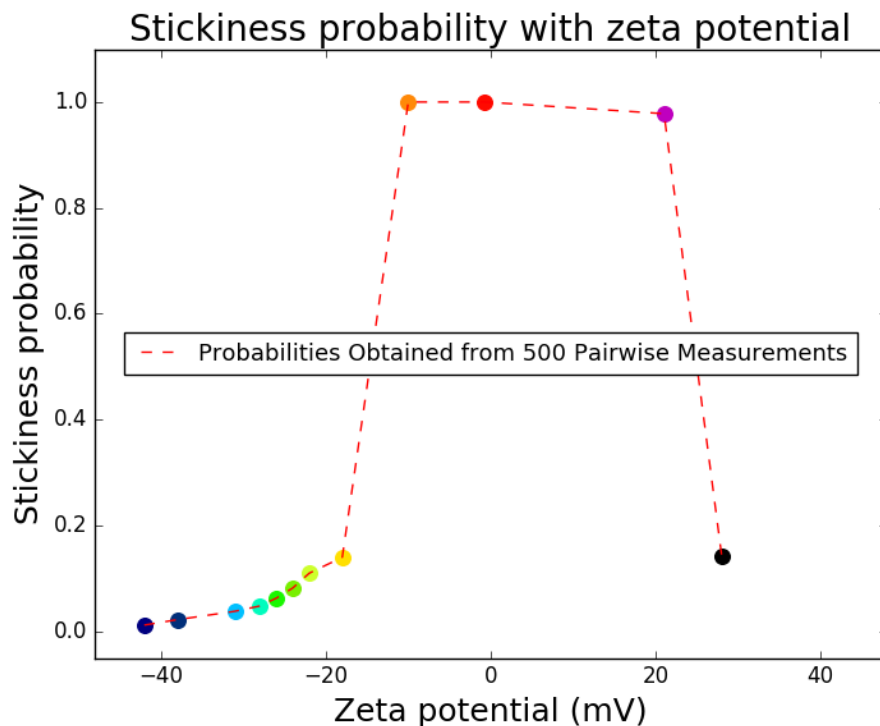


FIGURE 5.12: The stickiness probability with zeta potential, each point obtained from 500 pairwise measurements as described in the text.

As the magnitude of the zeta potential is decreased, the graph initially shows a slow increase in the stickiness probability (for example as it changes from  $-40\text{ mV}$  to around  $-18\text{ mV}$  on the left of the plot). As the magnitude is reduced further, there is a sudden increase in the probability of the droplets becoming attached. As expected as the isoelectric point is approached this reduction eventually results in 100% aggregation as the repulsive electrostatic barrier between the particles is reduced to below thermal energy. Subsequently the sticking probability decreases again as expected as the experiments move away from the isoelectric point to larger positive zeta potentials ( $> 20\text{ mV}$ ).

It should be noted that it is not clear from the stickiness probability data that it is symmetrical about the isoelectric point. The particles appear slightly more sticky at positive rather than negative zeta potentials of the same magnitude. This could be due to protein rearrangement or interaction with the charges on the glass microfluidic chip itself (the pH of the salt solution is very low). Through the dissociation of terminal silanol

groups, the silica at the surface of the microfluidic chip in contact with aqueous solutions is known to acquire a negative surface charge density.



This results in an effective decrease in the pH of the sample (Bender [152] and Behrens et al. [153]) and could result in the observed behaviour in the stickiness data. Nevertheless, the data obtained from our pair-wise experiments (requiring minute amounts of emulsion) are broadly in line with expectations based on zeta-potential measurements made on the bulk emulsion samples.

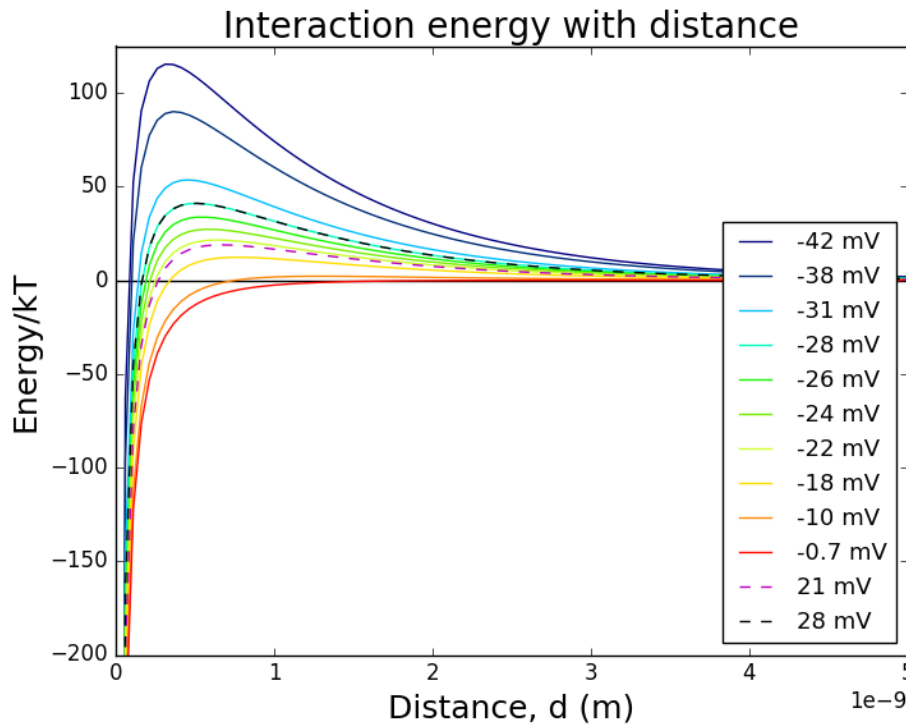


FIGURE 5.13: Interaction potential for different physio-chemical conditions, calculated as described in the text.

An attempt can be made to describe the results more quantitatively, by using the DLVO theory (refer sections. 1.2.1, 1.2.2, 4.1) to calculate the potential between the droplet pairs that has to be overcome for them to stick together and then applying a simple kinetic theory to describe the rate of transition between the aggregated and non-aggregated

states in which the calculated potential barrier plays the role of an activation energy. The sticking probability is expected to be a function of the ratio of the size of the energy barrier between the drops that must be overcome to  $kT$ . Specifically the probability of a collision resulting in successful aggregate formation can be given by (Laidler [154])

$$p = Ae^{-E_b/kT} \quad (5.3)$$

where,  $E_b$  is the barrier height,  $A$  is the attempt frequency, and  $e^{-E_b/kT}$  represents the population of collisions with thermal energy greater than  $E_b$ . It is quite evident that the capture probability increases with a decrease in the barrier height. This barrier has been calculated for the different cases examined experimentally using a screened van der Waals potential (section. 4.2) and can be seen in figure 5.13. The curves have been coloured for easy reference to the relevant experimental data points in the stickiness probability figure. As expected, the zeta potential where the stickiness shows a sharp increase in figure 5.12 in the probability of aggregation corresponds to the repulsive energy barrier becoming comparable to the thermal energy of the particles (orange in figures).

It should be noted however, that while the heights of the calculated repulsive potentials quickly rise to many tens of  $kT$ , suggesting that NO aggregation should be observed at higher zeta potentials (particularly in the range  $-40$  to  $-20$  mV), the results indicate a small but finite number of particles do stick together. This behaviour, where the zeta potential has a high magnitude but where around 5% of the emulsion drops still aggregate is not trivial to explain. We hypothesise that it could be due to "rogue drops" that have not been emulsified to the same degree as the bulk of the samples, and as such have a different (lower) zeta potential. In the Zetasizer measurement an average bulk zeta potential is measured for a large ensemble of particles, whereas in actuality in colloidal suspension, there could be a local drop-to-drop variation in the zeta potential. In the future this hypothesis might be tested by designing an experiment that can measure the zeta potential of the individual drops that are being examined in the OT experiment.

### 5.5.2 Stickiness probability with holding time

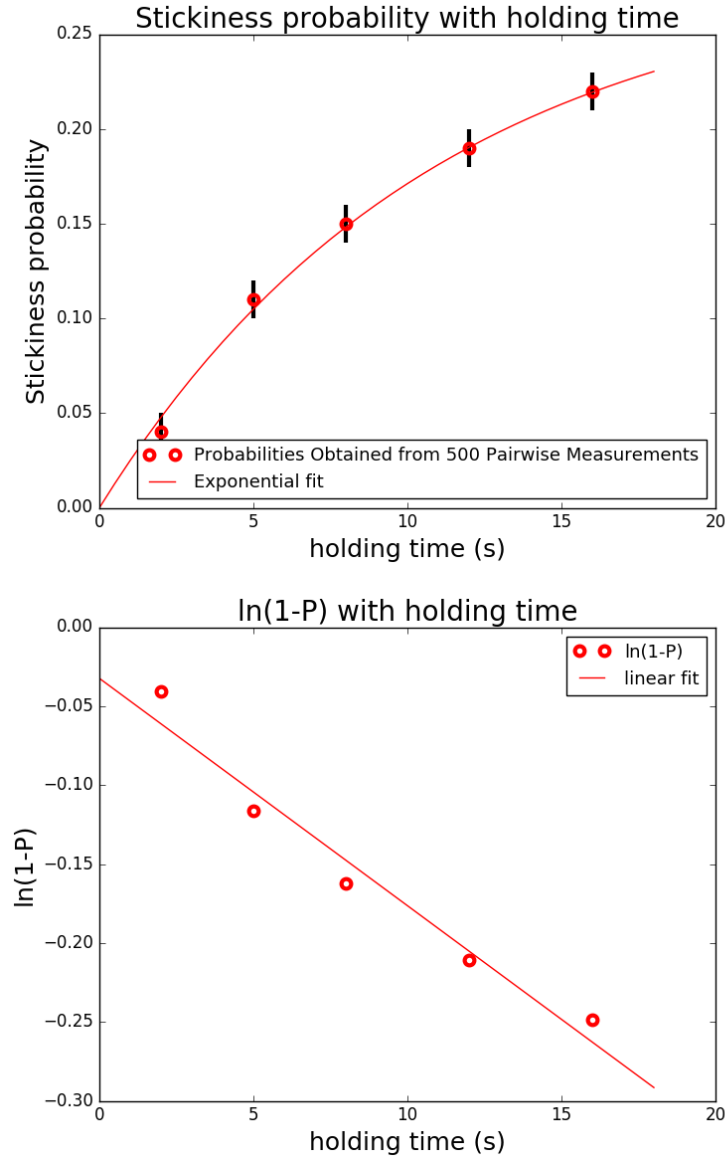


FIGURE 5.14: For 500 pairwise measurements for a zeta potential of  $-31 \text{ mV}$ : a) Stickiness probability with holding time. b)  $\ln(1 - P)$  with holding time.

The stickiness probability measurements for one of the solutions (that with a zeta potential of  $-31 \text{ mV}$ ) were carried out for different holding times, from  $2 \text{ s}$  to  $16 \text{ s}$  (Figure. 5.14). An exponential-like approach was observed with the holding time as previously found (Sun et al. [124] and Sun et al. [114]) and suggested by eqn. 5.1. A plot

of  $\ln(1 - P)$  with the holding time can also be seen in (Figure. 5.14) from which a fit to eqn. 5.1 yields an individual probability for aggregation of  $p \approx 0.025$ .

The exponential-like increase of probability with time is related simply to the fact that, as the drops are confined for longer in the same trapping potential, multiple collision attempts are possible. The probability of observing the event after a certain time is determined by the unchanging probability of an individual event and the time dependent number of attempts (in analogy to the decay of a sample of radioactive nuclei). Holding the drops in close proximity for longer simply increases the chances of observing a barrier-hopping event. The data with the relevant uncertainties allows for a possible small non-zero probability at zero time, that might originate from the fact that even with a zero waiting time there is one collision of the drops when one particle is driven into the other by the optical potential (Sun et al. [151] and Xu and Sun [155]). Correspondingly the value of this intercept is consistent ( $p \approx 0.025$ ) with the probability of aggregation after a single collision obtained from the fit of the data with increasing time. That is; the probability of drops sticking after the initial optically-induced collision is accessible from the intercept, whereas the accumulated probability from Brownian-driven collisions of the drops in the trap is accessible from the slope of how the data changes with holding time. The fact that there appears to be a limiting long-time probability that is different from 1 is however not trivial to explain in this simple model and perhaps suggests that either there is some time dependent changes to the stickiness, or that the long-time exposure to the laser has some effect on the potential stickiness - even that removal of the trap might some how break apart loosely attached drops. While the behaviour is broadly as expected and in line with previous studies, this aspect should be investigated further in future work.

The stickiness measurements can provide insights into the stability of the system that can be compared with findings from bulk measurements sensitive to the aggregation state, made by, rheology, for example.

### 5.5.3 Rheological measurements

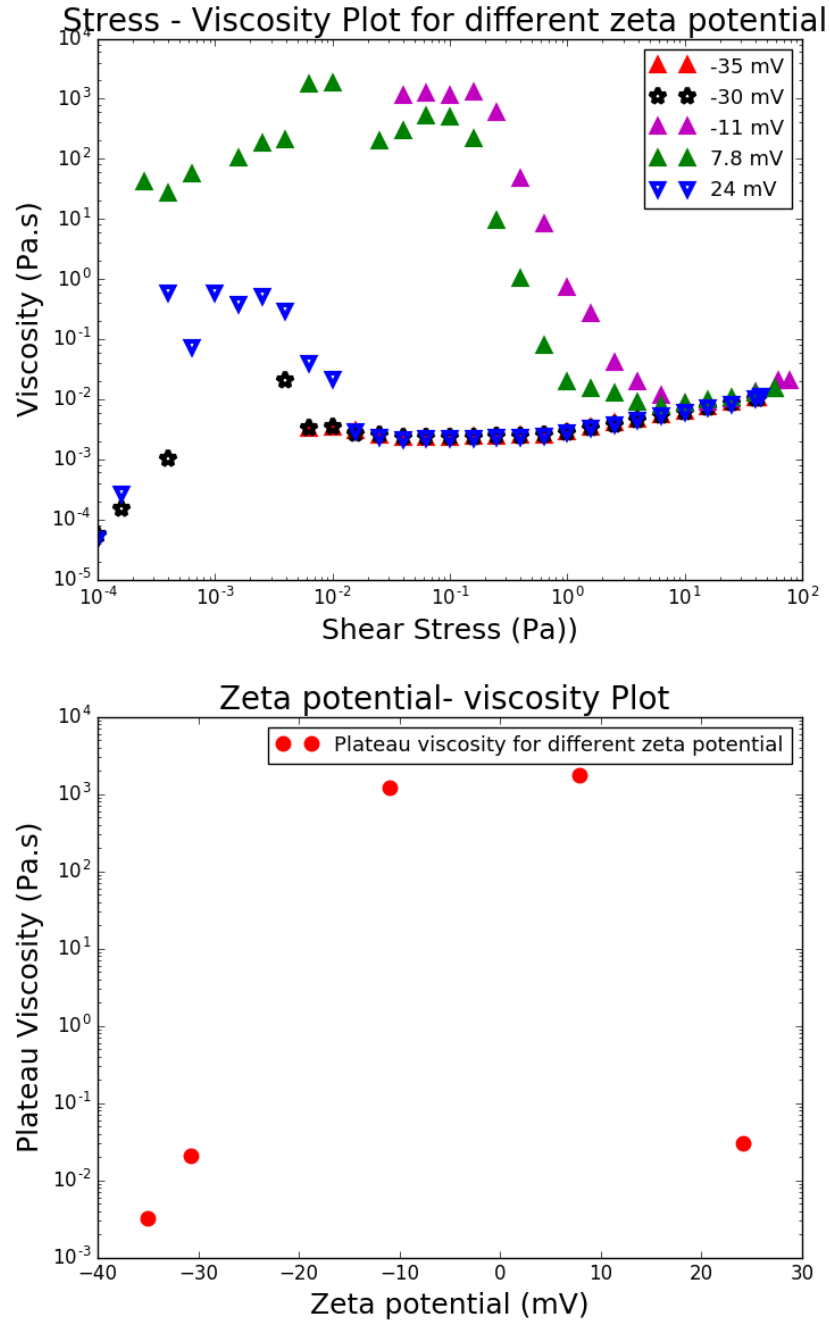


FIGURE 5.15: Rheological study with different zeta potential a) Stress - Viscosity Plot for different zeta potential 20 % O/W WPI emulsion. b) Low-shear plateau viscosity with zeta potential.

The bulk rheological behaviour of the emulsion systems used in the drop wise

stickiness experiments were examined as a function of zeta potential. The flow behaviour of the emulsion samples were studied by varying an applied shear stress and measuring the resultant viscosity of the samples. The viscosity measured at lower shear rates is termed the zero-shear or plateau viscosity and arises from the random orientation of emulsion drops and the effective (charge dependent) phase volume driving their packing. It is typical then to relate the zeta potential of the emulsion to this zero shear viscosity (Barnes [98], Ong et al. [156], Tadros [99], Rao and Rao [100], and Ravindran et al. [108]). As the stress is increased, hydrodynamic factors become dominant with a consequent ordering of the dispersed phase dropping the viscosity to a constant value (Larson [101] and Larsson et al. [157]). A plot of the magnitude of the low-shear viscosity plateau against zeta potential (figure. 5.15) shows a very similar profile to that of the stickiness probability data in figure. 5.12. This is in accordance with our hypothesis that microscopic measurements can be used as a very effective tool in the place of bulk measurements which requires more time, effort and sample.

Figure. 5.16 shows the consistency of behaviour of stickiness probability, the rheology data, and the response to the introduction of depletion forces (chapter. 4); all providing evidence for extensive aggregation near the isoelectric point.

## 5.6 Conclusion

An automated microfluidic setup for studying the interactions of colloidal particles has been discussed in this chapter. The apparatus design consists of a custom glass microfluidic chip, OT, and homemade syringe pumps and computer algorithms which enable fully automated general-purpose experiments to be carried out. In this way hundreds of identical one-at-a-time measurements upon individual particle pairs can be carried out, enabling large data sets to be obtained in a reasonable time and with extremely small amounts of sample.

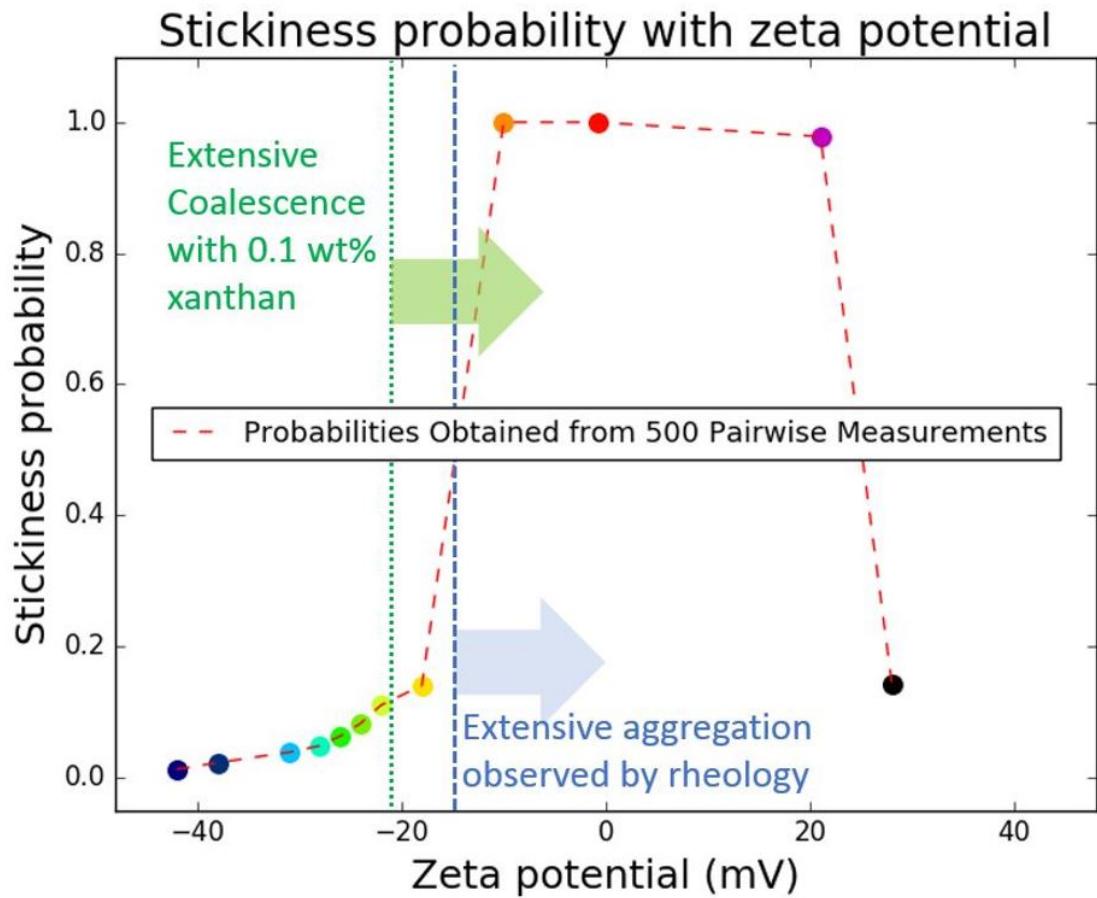


FIGURE 5.16: Summary diagram relating zeta potential to depletion forces and stickiness measurements

Specifically the apparatus was used here to demonstrate quantitative measurements of particle-particle stickiness under different physio-chemical conditions. At each iteration, a cloud of particles was injected into an environment of controlled pH and ionic strength, and two particles were detected and captured. Then a stickiness experiment was performed between the particle pairs and a statistical stickiness probability was obtained from 500 repetitions.

The relationship between the measured stickiness probability and both the bulk zeta potential and the pair contact time was studied. The sharp increase in the stickiness values at zeta potentials of low magnitude could be explained by the fact that the magnitude of the DLVO repulsive barrier between the particles approached  $kT$ . While



more aggregation than predicted simply from the same DLVO theory was observed at high zeta potentials, this was observed both in the stickiness measurements and also in the rheology measurements. It is suggested that this most likely arises from a small population of "rogue drops" being present with much lower zeta potentials than the bulk measurement would suggest.

In conclusion, the one-at-a-time emulsion-pair stickiness measurements have been demonstrated to give a direct assessment of the stability of the system. This has high industrial and commercial relevance as the probability values can be used to measure of the stability of a bulk emulsion system 1) with only micro litres of sample (making high throughput trials possible and reducing costs) and 2) without having to wait extended periods of time for conventional Brownian fluctuations to probe particle stickiness. In addition local drop-to-drop variations can be probed using this methodology, impossible to obtain in conventional bulk experiments.

## Chapter 6

# Conclusion and future directions

### 6.1 Conclusion

In the previous chapters, we described the relationship between stability and zeta potential, and showed how the zeta potential can be varied by changing the concentrations of NaCl, Ca ions and pH. We also showed how such variations explain:

1. behaviour upon addition of other components like polysaccharides.
2. the pairwise sticking probability of drops.
3. the bulk rheology of the system.

While determining the surface properties of the emulsion droplets, the zeta potentials of protein coated oil-in-water droplets were measured and modelled at different pH values, NaCl concentrations and calcium activities. In NaCl solutions without any added calcium at concentrations of 50, 100 and 150 *mM* the isoelectric point was found to be pH  $4.7 \pm 0.2$ . Under strong acid and base conditions (pH 2–3 and pH 9–10) the zeta potential values plateaued between 24 – 40 *mV* at the low pH and –24––42 *mV* at the high pH, with lower absolute values at higher salt concentrations. The Gouy-Chapman model provided an excellent fit to the experimentally measured data. In calcium solutions (with NaCl providing a fixed ionic strength of 80 *mM*) at pH = 5.4 – 5.6, the zeta potential

was found to depend strongly upon calcium activity. At the lower pH (5.4 – 5.6), close to the IEP, the zeta potential was around  $-15\text{ mV}$  at  $0\text{ mM}$  calcium concentration and approached  $0\text{ mV}$  at  $10\text{ mM}$  calcium concentration. The two- $pK_a$  model showed a good fit to these data points, and also showed the zeta potential to be very sensitive to small pH changes. At the higher pH, 4 pH units above the IEP, the zeta potential was around  $-33\text{ mV}$  at  $0\text{ mM}$  calcium concentration and also approached  $0\text{ mV}$  at  $10\text{ mM}$  concentration. The two- $pK_a$  model again showed a good fit to the data points and the zeta potential was found to be insensitive to pH changes, even as large as  $\pm 1$  unit. Changes in the macroscopic behaviour of WPI emulsion drops as pH and concentrations of NaCl and calcium were manipulated could be understood simply by mapping perturbations in the environmental conditions to changes in zeta potential. In turn, changes in zeta potential modify the size of the repulsive energy barrier captured by the DLVO interaction energy and are reflected in bulk properties such as coagulation rate and viscosity, irrespective of the specifics of how zeta potential is modified. Finally, experimental measurements of bulk viscosity versus zeta potential squared (using NaCl and pH, and calcium activity), showed that viscosity (and bulk coagulation time) are dependent only upon the zeta potential, and this led to large changes in rheological behaviour at  $|\zeta| = (17 \pm 2)\text{ mV}$ .

After a good theoretical framework for the physio-chemical properties had been established and verified with experiment, the polysaccharide xanthan was introduced to the emulsion system, adding an extra depletion force between the particles. The longer range of depletion forces as compared to the EDL force created a primary or secondary minimum causing flocculation or coalescence. The barrier height is controlled by the depletion and EDL forces. While the zeta potential was changed from  $-18$  to  $-24\text{ mV}$ , the barrier height increased by  $22\text{ kT}$  and varying the xanthan concentration from  $0.25\text{ wt\%}$  to  $5\text{ wt\%}$  altered the secondary minimum from  $-0.7$  to  $-19\text{ kT}$ . The barrier height at which droplet coalescence was mostly eliminated was very high at  $28\text{ kT}$ , however some of the particles were coalescing even at that barrier height suggesting that coalescence happens as two round droplets climb over the barrier due to the electrical double layer force. It is practically impossible for the particles to overcome this big energy barrier with just

thermal energy, implying some kind of alteration to the interaction energy profile. This unexpected behaviour could be due to a change in the surface protein coverage, or to a change in the conformation of the protein, or an additional short range attraction in addition to the electrical double layer force.

A fully automated microfluidic-optical-tweezer setup was then used to find the statistical capture probability of the emulsion droplets under different physio-chemical conditions. The microfluidic setup was designed in house, and automation algorithms were written using LabView, including the particle detection image processing used to detect individual particles. Syringe pumps were used to inject the particles (in a milli-Q water continuous phase) and salt solutions into the microfluidic chip and to precisely control the flow rates. The automation capability enabled large numbers of particle-particle collision experiments to be performed with minimal human intervention. It also ensured a high level of consistency for the particle-particle collisions because the position of each collision within the camera viewing area was identical, as were the particle approach vectors and collision duration.

For each collision experiment, the particles needed to be delivered to the site of the collision experiment within a salt-free continuous phase to ensure the particles did not form aggregates prior to the controlled collision. After delivery of the particles to the experiment's micro-volume inside the microfluidic chip, a suitable pair of particles were laser trapped with the tweezers, and the remainder of the particles were flushed away by the salt solution. This created a new salt micro-environment around the trapped particle pairs in which the stickiness experiment would be performed.

Sets of 500 pairwise stickiness collision measurements were then performed within the micro-environment as described above. Each measurement set used different salt conditions and holding times. The capture probability obtained showed agreement with the DLVO energy profile calculated for the physio-chemical environment at which the measurements were taken. The higher stickiness values at low zeta potentials were explained with the thermal energy of the particles overcoming the low repulsive energy

barrier. The particles at higher zeta potential exhibited some (although small) stickiness which was not expected from the high repulsive energy barrier they had to overcome. This could be due to an uneven protein surface coverage or a variation in local zeta potential. This effect was observed in the case of depletion forces also. The plateau viscosity data of the emulsion also showed a very similar profile to that of the stickiness measurements, suggesting that capture probability could indeed be used as a tool to predict the bulk behaviour of the system.

A combined study of the surface properties, added polymer and capture probabilities has great scientific and commercial implications. Introducing capture probability, which is a microscopic property efficiently reduces the time and work load in predicting the stability. The model system used in the project could be extended to lot of dairy and industrial products.

## 6.2 Future Directions

### 6.2.1 Measurement of zeta potential inside the chip

An accurate assessment of the droplet zeta potential in a microfluidic chip could be a problem in the execution of the experiments as it depends on solution pH, buffer concentration, surface charge density and also on the size and surface coverage of individual droplets. A small variation could affect the stickiness probability drastically, especially near the isoelectric point where properties can change dramatically. An experimental setup which could measure the zeta potential of the individual droplets just before they come into contact with each other could reduce the uncertainties in the source of the variations in stickiness probability. There are experimental protocols in the literature which could be incorporated to the current microfluidic setup to measure the individual zeta potential. A capacitor model which uses an external electric potential for controlling the electro-osmotic flow could be used for this (Lee et al. [158]).

### 6.2.2 Stickiness probability measurements with different/modified protein

The stickiness probability measurements are used to predict the bulk behaviour of a system. This thesis talks about the development of a model system, whose surface properties are well determined and then linked to stickiness probability and rheological measurements. A stickiness probability study of emulsions generated using modified proteins, such as those dephosphorylated and succinylated  $\alpha_{s1}$ -caseinate, developed by Nazmi et al. [159], would be interesting to pursue in the future. The same method could also be extended to other systems like commercial beverages and other products. This could potentially be used to play a role in prediction of shelf life experiments for those products.

### 6.2.3 Stickiness probability measurements with xanthan

The effect of xanthan gum to the WPI emulsion is already illustrated in Chapter. 3. It would be interesting to see how the capture probability of the emulsion particles changes in the presence of xanthan, which induces a depletion force in addition to the DLVO forces, hence giving a different interaction potential. A hydrodynamic study and temperature regulated study inside the microfluidic chip is also proposed as a project extension.

### 6.2.4 Modelling of colloidal aggregation

This project can be used to provide a theoretical framework for connecting different parameters discussed using simulations of aggregation. As discussed earlier, aggregation of colloidal particles is of great importance in colloid science. Smoluchowski did initial studies on rates of aggregation, leading to the foundations of the subject. Aggregation is thought of as initially similar, primary particles forming aggregates of various sizes and different number densities after a period of aggregation.  $n_i$  particles of size  $i$ , referring to the number concentrations of different aggregates and 'size' means the number of primary particles in the aggregate ( $i$  fold aggregates). Aggregation is basically assumed to

be a second order rate process, where the rate of collision is proportional to the product of concentrations of two colliding species (Elimelech et al. [7]).

The number of collisions between particles,  $i$  and  $j$  in unit time and unit volume according to Smoluchowski, where collisions are considered to be second order rate process with rate constant  $k_{ij}$  is given by,

$$J_{ij} = k_{ij}n_i n_j; \quad ; k = i + j \quad (6.1)$$

Of these collisions, only some of them are effective in producing aggregates (collision efficiency,  $\alpha$ ), depending on the interparticle force between them from a range of 1, where all particle stick, suggesting a strong attractive force between particles, to an  $\alpha$  of 0, where nothing sticks due to strong repulsive force between particles.

Experimentally found efficiency of stickiness through tweezer experiments of the type described here could be used as the input in such simulation models in the future.

By neglecting the hydrodynamic interactions for the time being as the emulsion is at low concentration, just three important transport mechanisms, Brownian motion giving rise to perikinetic aggregation, fluid motion resulting orthokinetic aggregation and differential settling would need to be considered in the model.

The input of the simulation would be the stickiness measurements from the tweezer setup, measured for enough number of times, so as to get a statistical capture probability. Also, after considerable aggregation, the different size of aggregates will need to be considered. In that case, the collision rate constant also need to be changed accordingly.

Real practical problems can be solved using simulation tools with an appropriate degree of rigour and complexity and looking at the microscopic properties that generate the equilibrium as well as dynamic properties of the system. Stochastic methods or ensemble averaged methods can be used to find the equilibrium properties of systems but cannot be scaled to meaningful time dimensions. Instead, generally dynamic methods are used for obtaining kinetics of a phenomena (Elimelech et al. [7]).

### **Stochastic approach**

- Monte Carlo (MC) methods

### **Dynamic approach**

- Molecular Dynamics (MD) methods
- Brownian Dynamics methods

### **Monte Carlo methods**

The core idea in Monte Carlo methods is to use random samples of parameters or inputs to explore the behaviour of a complex system or process. It relies on sampling a given statistical ensemble by generating a succession of configurations (Chen and Kim [160]). MC method is easier to implement but can provide only information on systems in their equilibrium state, unless a dynamic monte carlo method is applied (Patti and Cuetos [161]).

### **Molecular dynamics methods**

Molecular Dynamics methods provides a way of solving a set of coupled equations of motion to get dynamic or time depended properties (Nosé [162]). The configurations are



generated by solving a set of Newton's equation of motion for each of the interacting particles (Potter [163]). There is a big difference between the time scales describing the solvent motion and that of colloidal particles. Hence, it would demand high computing time if MD is to be used for simulating colloidal system. So MD is not a good choice of method for colloidal simulation if the solvent is to be included atomistically (Allen and Tildesley [164]).

### Brownian dynamics method

In the BD method, Newton's laws are replaced by the Langevin equation. The effects of solvent particles are represented by a combination of a random force term and a frictional term. For Brownian Dynamics simulations in the over-damped limit, the position Langevin equation is numerically integrated:

$$\frac{dr_i}{dt} = \frac{1}{\gamma} f_i(t) + \theta_i(t) \quad (6.2)$$

where  $\gamma$  is the friction constant which is the same for all the particles,  $f_i(t)$  is the force acting on particle  $i$  due to the interaction with the other particles, and  $\theta_i(t)$  is a random noise with  $\langle \theta_i(t) \theta_j(t) \rangle = 2\delta_{ij} \delta(t) k_B T / \gamma$ . Here  $k_B$  is the Boltzmann constant and  $T$  is the absolute temperature.

The Stokes-Einstein relation establishes the connection between the diffusion process and the thermal energy (Santos et al. [165]):

$$D = \frac{k_B T}{\gamma} = \frac{k_B T}{6\pi\eta a} \quad (6.3)$$

A suitable interaction potential can be used in modelling colloidal interaction between particles using BD.

## Chapter 7

### Published and to be published work

1. Understanding how the properties of whey protein stabilized emulsions depend on pH, ionic strength and calcium concentration, by mapping environmental conditions to zeta potential.

S.Ravindran et al.

In: *Food Hydrocolloids* 79 (2018), pp. 572–578. ISSN: 0268005X.

2. Depletion and electrostatic forces in the determination of the cluster kinetics in whey protein stabilized emulsion.

*to be submitted.*

3. Using Optical Tweezers to Measure the Probability of Aggregation after the Pair-wise Contact of Emulsion Drops: The Development of an Automated Procedure.

*to be submitted.*



## Appendix A

### Appendix to Chapter. 1

#### A.1 Confocal image of emulsion

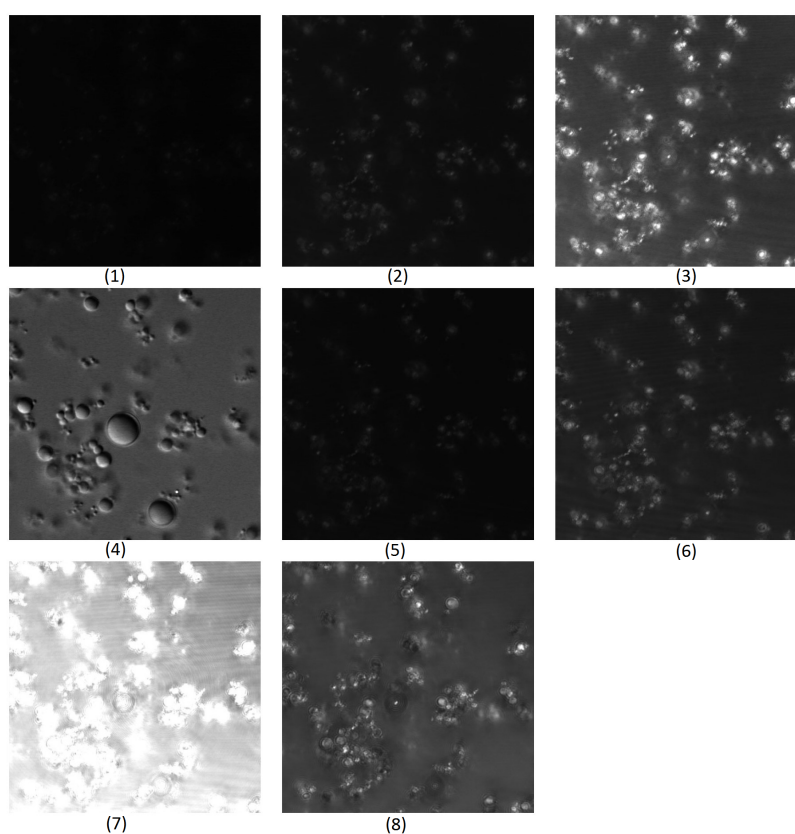


FIGURE A.1: image courtesy: Manawatu Microscopy and Imaging Centre (MMIC)

A 63x NA 1.4 oil lens was used with a zoom of 6 resulting in a pixel size of 80nm. Laser power was kept identical for all images (50% of maximum output). All gain settings were similar ( $307 \pm 1$  volt) and gain was identical being kept at a default value of 0.0%. There was no image averaging.

All of the images except 4, were acquired using the reflectance mode on the scanning confocal. Image 4, is a DIC (Differential Interference Contrast transmitted light image) with matrix parameters as below:

Image	Laser (nm)	Detection Range (nm)
1	458	450-466
2	476	468-484
3	488	480-496
4	488	Transmitted Light Detector
5	496	488-504
6	514	506-522
7	561	553-569
8	633	625-641

## Appendix B

### Appendix to Chapter. 3

#### B.1 Eversole and Boardman equation

Assuming the surface electrical properties are dominated by  $\beta$ -lactoglobulin with  $\approx 10$  to 20 charges per molecule  $N_{s1}$  and  $N_{s2}$  lead to a unrealistically low surface coverage of 0.24 to 0.42  $mg/m^2$  at pH 8 and 3 respectively. The discrepancy in adsorbed amount is likely arise from the over-simplified nature of the Gouy Chapman model. The Guoy-Chapman model implemented here is the simplest model for the EDL with the least number of adjustable terms. However, it does assume that the zeta potential and the surface potential are interchangeable. In detail the zeta potential and the surface potential are related by the via the Eversole and Boardman equation. (Elaissari [166]).

$$\tanh \frac{e\zeta}{4K_B T} = \tanh \frac{e\Psi}{4K_B T} e^{\frac{-\Delta}{\lambda_D}} \quad (B.1)$$

where  $\Delta$  is the distance between the shear plane from the surface layer. The Eversole Boardman equation is not limited by low potentials like the Gouy Chapman model, however, the low potentials explored ( $e\zeta/k_B T \leq 1.5$ ) here the following approximations are valid. First the tanh terms can be simplified noting that  $\tanh(x) \approx x$  when  $x < 0.4$ . Then

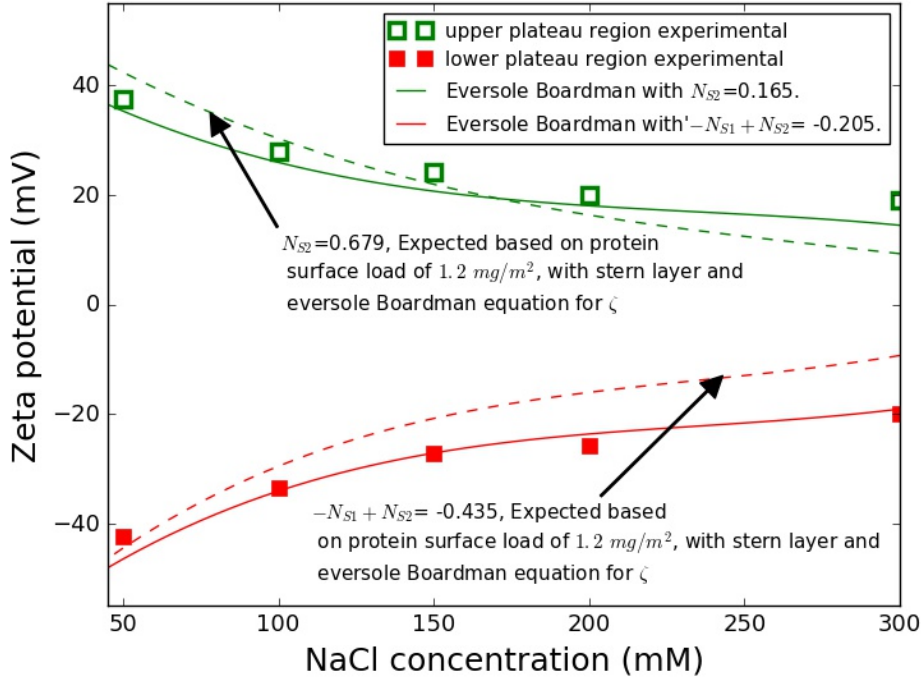


FIGURE B.1: Experimental data from figure 3.7 replotted with a fit using the zeta potential calculated from the Eversole Boardman equation (solid lines) and the expected zeta potential from by assuming a protein surface load of  $1.2 \text{ mg/m}^2$  assuming the presence of a Stern layer (dotted lines) both calculations assume a slip length of  $0.16 \text{ nm}$ . Positive data represents pH 3 and negative data represents pH 8.

substituting equation 3.9 the potential with the surface charge density and acknowledging  $\sinh(x) \approx x$  when  $x \leq 1$  leaves

$$\zeta \sim \frac{\sigma \lambda_D}{\epsilon_0 \epsilon} e^{\frac{-\Delta}{\lambda_D}} \quad (\text{B.2})$$

Thus fitting a straight line on a log - log plot of  $\zeta/\lambda_D$  vs  $1/\lambda_D$  yields the surface potential and the slip length (not shown). The determined slip length was  $0.18$  and  $0.14 \text{ nm}$  at pH 3 and 8 respectively. These values are close to the  $0.25 \text{ nm}$  typically assumed, (Behrens et al. [79]). Extrapolated values of  $\sigma$  do not give good fit to the zeta potential data, the difference between the fitted values presented in this paper and those extrapolated using equation B.2 is comparable to the accumulated error from approximating the hyperbolic functions.

Separating zeta and surface potentials does increase the calculated charge density and therefore the apparent surface coverage. However, at the ionic strength investigated, typical of dairy systems, the exact slip length can have a significant effect on the calculated values on account of the small Debye length. Furthermore surface potentials are now sufficiently high that formation of a Stern layer cannot be ignored. A Stern layer is a layer of immobilized ions, still treated as point charges, on account of the surface potential. The incorporation of Stern layer requires some relabeling of most of the equations presented, details given in the appendix, but in short the zeta potential and interaction forces are calculated from the potential at the Stern plane, while surface equilibria are calculated from the surface potential. The Stern layer can be treated like a capacitor with the drop given by Gauss's law. The Stern layer capacitance is an additional fit term that needs to be determined. For the sake of comparison Fig. 3.7 has been redrawn with a Gouy-Chapman fit line incorporating a slip length of 0.16 nm, and a Gouy Chapman Stern model fixing the surface coverage to be 1.2 mg/m<sup>2</sup>, typical of  $\beta$ -lactoglobulin, figure. B.1 (Dickinson and Hong [167]). Here 1.2 mg/m<sup>2</sup> corresponds to  $N_{s1}$  and  $N_{s2}$  having values of 1.11 negative charges per nm<sup>2</sup> and 0.679 charges per nm<sup>2</sup> and the Stern layer capacitance was assumed from a thickness of a hydrated sodium ion 0.36nm (Israelachvili [82]), and a dielectric constant equal to that of water. Incorporating the slip length increases the values of  $N_{s1}$  and  $N_{s2}$  to 0.165 charges per nm<sup>2</sup> and 0.370 negative charges per nm<sup>2</sup> respectively, giving an average apparent surface coverage of 0.54 mg/m<sup>2</sup>. The curve generated from a surface coverage 1.2 mg/m<sup>2</sup> assuming a Stern layer provides a reasonable fit at 50 - 150 mMol/L but underestimates the data at higher salt concentrations. This last curve is sensitive to the two new fit factors introduced. While it is clear that the actual surface load could be used as a source of  $N_{s1}$  and  $N_{s2}$  validating the Stern layer capacitance and slip length would be required since a large variation in surface charge can be accommodated based on the choice of model, slip length and/or any Stern layer capacitance. This validation could be achieved by titrating the pH against a known volume of the emulsion.



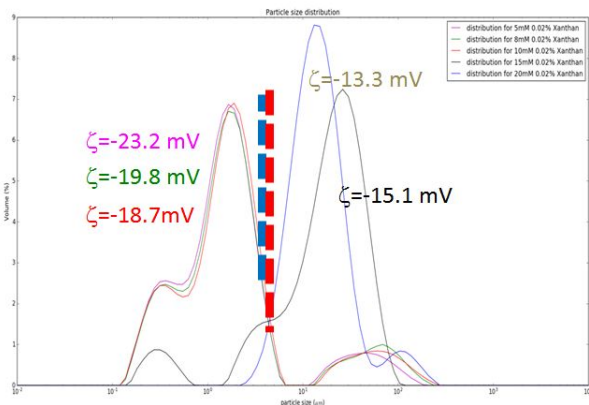


## Appendix C

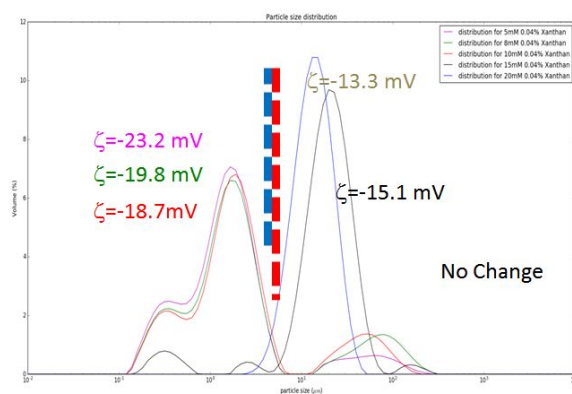
### Appendix to Chapter. 4

Xanthan gum was added in different concentrations to the WPI emulsion at different zeta potentials. Five different zeta potentials and five xanthan concentrations were considered resulting in 25 samples. Malvern mastersizer was used to measure the size distribution of the samples. The particle size distribution curves for different xanthan concentrations (0.02 wt%, 0.04 wt%, 0.1 wt%, 0.25 wt%, 0.5 wt%) at different zeta potential is shown in figure. C.1. At 0.02 wt% and 0.04 wt% of xanthan, the particle size profiles for different zeta potentials look similar with increased particle sizes as the EDL forces decreased after a zeta potential of around  $|\zeta| = 18 \text{ mV}$ . But as the concentration of xanthan is increased, the depletion forces increase, resulting in an attractive potential and thereby causing coalescence of particles gradually. This effectively removes the two distinct behaviour of size distribution around  $|\zeta| = 18 \text{ mV}$  as shown in figure. C.1.

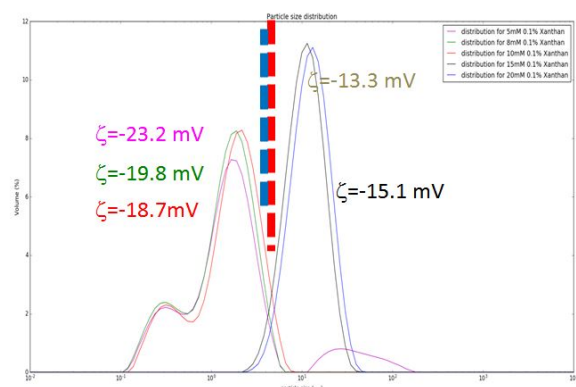
The radius of the particles at the distribution peak for 25 samples is as in figure. C.2. It can be seen that the plot assumes different regions depending on the amount of xanthan and the zeta potential. The samples are in a stable region when the zeta potential and xanthan concentrations are low. Then there is a middle region where there are big fat clusters with limited coalescence after which there is a critical barrier (reddish part in the figure) after which there is evident coalescence. At the lower part of the plot, where the xanthan concentration is high, gradual coalescence is observed as the zeta potential increases.



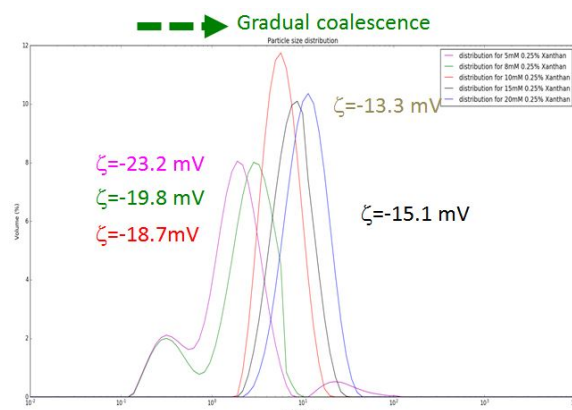
(A) 0.02 wt%



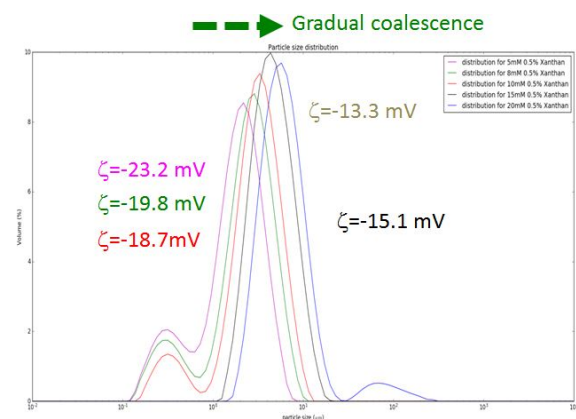
(B) 0.04 wt%



(C) 0.1 wt%



(D) 0.25 wt%



(E) 0.5 wt%

FIGURE C.1: Particle size distribution for different xanthan concentrations(0.02 wt%, 0.04 wt%, 0.1 wt%, 0.25 wt%, 0.5 wt%) at different zeta potentials.

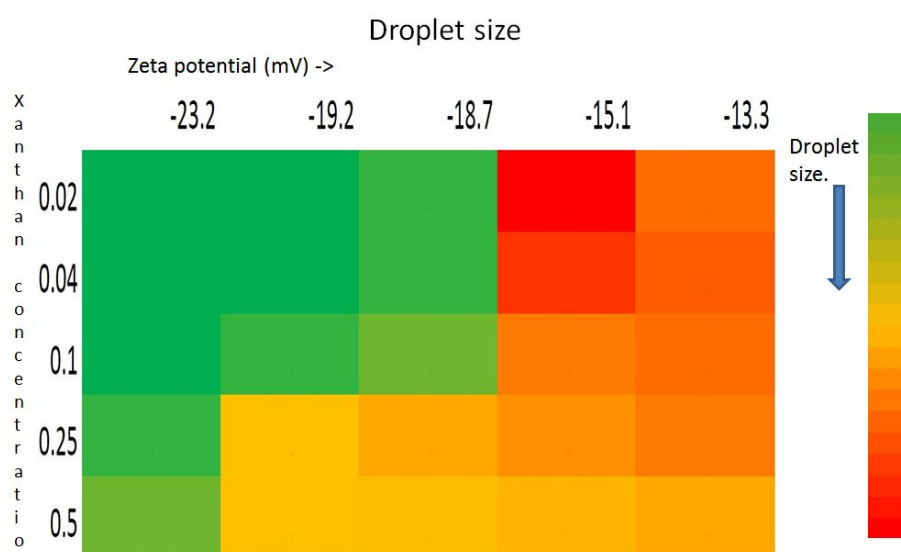


FIGURE C.2: Mean size of the droplets with xanthan and added salt

## Confocal and particle size distribution

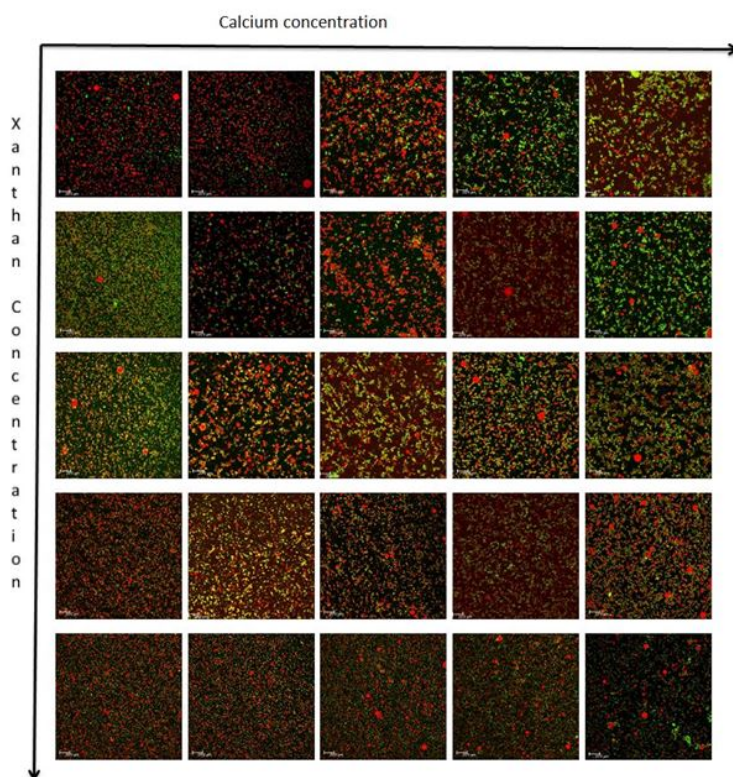


FIGURE C.3: Confocal image of emulsion with added salt and xanthan

The confocal images corresponding to each of the samples is given in figure. C.3.

## Appendix D

# Appendix to Chapter. 6

### D.1 Implementation of simulation

Brownian dynamics method can be implemented using a particle simulation kit called HOOMD-blue, copyrighted by The Regents of the University of Michigan.

#### HOOMD

HOOMD-blue is an open source general purpose particle simulation toolkit scaling from a single CPU core to thousands of GPUs. Particle initial conditions and interactions are defined in a high-level python script. HOOMD-blue has integrators built in for many different thermodynamic ensembles and energy minimization.

#### D.1.1 Features and capabilities of HOOMD

- Advanced neighbour list algorithms
- Pair potentials, Bond potentials, Angle potentials
- Long-ranged potentials, External potentials
- Long-ranged potentials, Many-body potentials

- Simulation box

The box is a parallelepiped with arbitrary lengths and angles allowing for generic triclinic symmetry with periodic boundary conditions in all directions (Derkach [168]).

There are many papers using HOOMD-blue as the tool for simulation (Risbud and Swan [169]), (Varga et al. [170]), where it is used for implementing Brownian Dynamics simulation. An initial simulation using HOOMD has been performed for a system of 1000 identical particles in brownian motion. The bdnvt integrator with verlet algorithm was used for the simulation. Figure D.1 shows snapshot at every 1500<sup>th</sup> step of simulation.

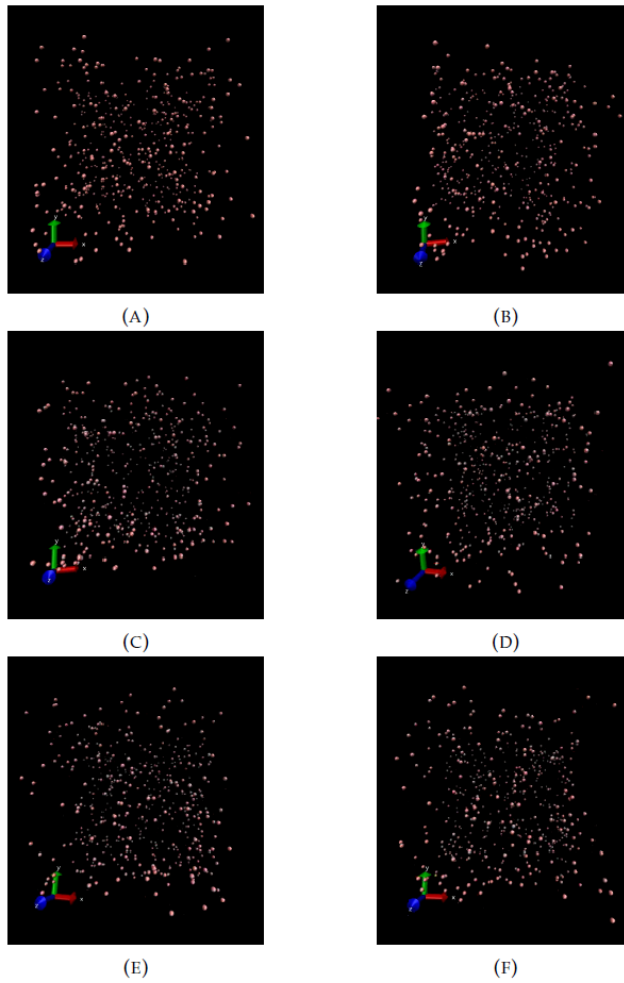


FIGURE D.1: Brownian simulation using HOOMD: Screenshot at each 1500<sup>th</sup> step of simulation using brownian integrator in HOOMD

The position of particles at every  $100^{th}$  step of total 10000 steps is taken to calculate the MSD. Here the units are in reduced Lennard Jones units. MSD is calculated for different volume fractions (corresponds to different particle size effectively) and different reduced temperatures.

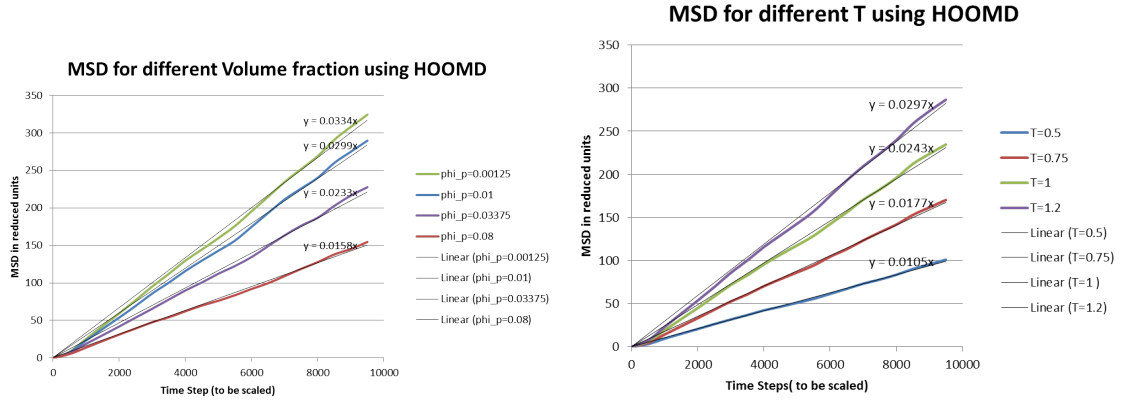


FIGURE D.2: MSD for different Volume fraction and Temperature Using HOOMD

The MSD values obtained by HOOMD is to be tested experimentally to see if it could be used as an effective tool for the implementation of simulation. A plugin to incorporate the stickiness could to be written in future work to realize the aim of the project to predict growth kinetics of colloidal aggregation.






## **Appendix E**

# **STATEMENT OF CONTRIBUTION: DOCTORATE WITH PUBLICATIONS/MANUSCRIPTS**



## STATEMENT OF CONTRIBUTION DOCTORATE WITH PUBLICATIONS/MANUSCRIPTS

We, the candidate and the candidate's Primary Supervisor, certify that all co-authors have consented to their work being included in the thesis and they have accepted the candidate's contribution as indicated below in the *Statement of Originality*.

Name of candidate:	Sapna Ravindran	
Name/title of Primary Supervisor:	Professor Bill Williams	
Name of Research Output and full reference:		
Understanding how the properties of whey protein stabilized emulsions depend on pH, ionic strength and calcium concentration, by mapping environmental conditions to zeta potential, Food Hydrocolloids, Volume 79, 2018, Pages 572-578, ISSN 0268-005X, <a href="https://doi.org/10.1016/j.foodhyd.2017.12.003">https://doi.org/10.1016/j.foodhyd.2017.12.003</a>		
In which Chapter is the Manuscript /Published work:	Chapters 1, 2	
Please indicate:		
<ul style="list-style-type: none"> <li>The percentage of the manuscript/Published Work that was contributed by the candidate:</li> </ul>	80	
and		
<ul style="list-style-type: none"> <li>Describe the contribution that the candidate has made to the Manuscript/Published Work:</li> </ul>		
Carried out the experiments, Did calculations and analysis, primary author of the paper		
For manuscripts intended for publication please indicate target journal:		
Foodhydrocolloids		
Candidate's Signature:	 Digitally signed by Sapna Ravindran DN: cn=Sapna Ravindran, o=Massey University, ou=IFG, email=ssapnaa@gmail.com, c=NZ Date: 2019.05.07 18:35:18 +05'30'	
Date:	07/05/2019	
Primary Supervisor's Signature:	Williams, Martin         Digitally signed by Williams, Martin Date: 2019.05.15 13:44:40 +12'00'	
Date:	15/05/2019	

(This form should appear at the end of each thesis chapter/section/appendix submitted as a manuscript/ publication or collected as an appendix at the end of the thesis)

# Bibliography

- [1] Richard Pashley and Marilyn Karaman. *Applied Colloid and Surface Chemistry*. en. John Wiley & Sons, July 2005. ISBN: 978-0-470-86884-3.
- [2] Rep Kubo. "The fluctuation-dissipation theorem". In: *Reports on progress in physics* 29.1 (1966), p. 255.
- [3] Robert J. Hunter. *Zeta Potential in Colloid Science: Principles and Applications*. en. Academic Press, Apr. 1981. ISBN: 978-1-4832-1408-5.
- [4] V. Adrian Parsegian. *Van der Waals Forces: A Handbook for Biologists, Chemists, Engineers, and Physicists*. en. Cambridge University Press, Nov. 2005. ISBN: 978-1-139-44416-3.
- [5] Eli Ruckenstein and Dennis C. Prieve. "Adsorption and desorption of particles and their chromatographic separation". In: *AIChE Journal* 22.2 (1976), pp. 276–283.
- [6] Pierre-Gilles de Gennes, Francoise Brochard-Wyart, and David Quere. *Capillarity and Wetting Phenomena: Drops, Bubbles, Pearls, Waves*. en. Springer Science & Business Media, Mar. 2013. ISBN: 978-0-387-21656-0.
- [7] M. Elimelech, J. Gregory, and X. Jia. *Particle Deposition and Aggregation: Measurement, Modelling and Simulation*. en. Butterworth-Heinemann, Oct. 2013. ISBN: 978-1-4831-6137-2.
- [8] M. Elimelech et al. *Particle Deposition and Aggregation: Measurement, Modelling and Simulation*. Colloid and surface engineering series. Elsevier Science, 1998. ISBN: 978-0-08-051357-7.

- [9] Richard Hogg. "Bridging flocculation by polymers". In: *KONA Powder and Particle Journal* 30.30 (2012), pp. 3–14. ISSN: 02884534. DOI: [10.14356/kona.2013005](https://doi.org/10.14356/kona.2013005).
- [10] R. Hidalgo-Alvarez et al. "Electrokinetic properties, colloidal stability and aggregation kinetics of polymer colloids". In: *Advances in colloid and interface science* 67 (1996), pp. 1–118.
- [11] N. M. Kovalchuk and V. M. Starov. "Aggregation in colloidal suspensions: Effect of colloidal forces and hydrodynamic interactions". In: *Advances in Colloid and Interface Science*. Interfaces, Wettability, Surface Forces and Applications: Special Issue in honour of the 65th Birthday of John Ralston 179–182 (Nov. 2012), pp. 99–106. ISSN: 0001-8686. DOI: [10.1016/j.cis.2011.05.009](https://doi.org/10.1016/j.cis.2011.05.009).
- [12] Valteau, J. P, Ivkov, R, and Torrie, G. M. "Colloid stability: The forces between charged surfaces in an electrolyte." In: *The Journal of Chemical Physics* 95 (1991).
- [13] P. F. M. Roefs and Kees G. de Kruif. "Association behavior of native \s s-lactoglobulin". In: *Biopolymers* 49 (1999), pp. 11–20.
- [14] Tiziana Missana and Andrés Adell. "On the applicability of DLVO theory to the prediction of clay colloids stability". In: *Journal of Colloid and Interface Science* 230.1 (2000), pp. 150–156. ISSN: 00219797. DOI: [10.1006/jcis.2000.7003](https://doi.org/10.1006/jcis.2000.7003).
- [15] Keith B. Oldham. "A Gouy–Chapman–Stern model of the double layer at a (metal)/(ionic liquid) interface". en. In: *Journal of Electroanalytical Chemistry* 613.2 (Feb. 2008), pp. 131–138. ISSN: 15726657. DOI: [10.1016/j.jelechem.2007.10.017](https://doi.org/10.1016/j.jelechem.2007.10.017).
- [16] Sho Asakura and Fumio Oosawa. "On interaction between two bodies immersed in a solution of macromolecules". In: *The Journal of Chemical Physics* 22.7 (1954), pp. 1255–1256. ISSN: 00219606. DOI: [10.1063/1.1740347](https://doi.org/10.1063/1.1740347).
- [17] Y. Mao, M. E. Cates, and H. N.W. Lekkerkerker. "Depletion force in colloidal systems". In: *Physica A: Statistical Mechanics and its Applications* 222.1-4 (1995), pp. 10–24. ISSN: 03784371. DOI: [10.1016/0378-4371\(95\)00206-5](https://doi.org/10.1016/0378-4371(95)00206-5).
- [18] B. Götzelmann et al. "Depletion potential in hard sphere fluids". In: 47.August (1999), pp. 398–404. ISSN: 0295-5075. DOI: [10.1209/epl/i1999-00402-x](https://doi.org/10.1209/epl/i1999-00402-x).

- [19] R. Roth, R. Evans, and S. Dietrich. "Depletion potential in hard-sphere mixtures: Theory and applications". In: *Physical Review E - Statistical Physics, Plasmas, Fluids, and Related Interdisciplinary Topics* 62.4 B (2000), pp. 5360–5377. ISSN: 1063651X. DOI: [10.1103/PhysRevE.62.5360](https://doi.org/10.1103/PhysRevE.62.5360).
- [20] H N W Lekkerkerker and R Tuinier. *Colloids and the Depletion Interaction*. Lecture Notes in Physics. Springer Netherlands, 2011. ISBN: 9789400712232.
- [21] F. García-Ochoa et al. "Xanthan gum: Production, recovery, and properties". In: *Biotechnology Advances* 18.7 (2000), pp. 549–579. ISSN: 07349750. DOI: [10.1016/S0734-9750\(00\)00050-1](https://doi.org/10.1016/S0734-9750(00)00050-1).
- [22] Yuvaret Viturawong, Piyada Achayuthakan, and Manop Suphantharika. "Gelatinization and rheological properties of rice starch/xanthan mixtures: Effects of molecular weight of xanthan and different salts". In: *Food Chemistry* 111.1 (2008), pp. 106–114. ISSN: 03088146. DOI: [10.1016/j.foodchem.2008.03.041](https://doi.org/10.1016/j.foodchem.2008.03.041).
- [23] Eric Dickinson. "Stability and rheological implications of electrostatic milk protein-polysaccharide interactions". In: 9.1998 (1998).
- [24] Nina Kovalchuk et al. "Colloidal dynamics: Influence of diffusion, inertia and colloidal forces on cluster formation". en. In: *Journal of Colloid and Interface Science* 325.2 (Sept. 2008), pp. 377–385. ISSN: 00219797. DOI: [10.1016/j.jcis.2008.06.017](https://doi.org/10.1016/j.jcis.2008.06.017).
- [25] D.J Robinson and J.C Earnshaw. "Experimental study of colloidal aggregation in two dimensions. I. Structural aspects". In: *Physical Review A* Volume 46, Number 4 (Aug. 1992).
- [26] R. Klein and P. Meakin. "Universality in colloid aggregation". In: *Nature* 339.3 (1989).
- [27] Jens Eggers, John R. Lister, and Howard A. Stone. "Coalescence of liquid drops". In: *Journal of Fluid Mechanics* 401 (Dec. 1999), pp. 293–310. ISSN: 00221120. DOI: [10.1017/S002211209900662X](https://doi.org/10.1017/S002211209900662X).

- [28] David G Grier. "Optical tweezers in colloid and interface science". In: *Current Opinion in Colloid & Interface Science* 2.3 (1997), pp. 264–270. ISSN: 13590294. DOI: [10.1016/s1359-0294\(97\)80034-9](https://doi.org/10.1016/s1359-0294(97)80034-9).
- [29] J. C. Crocker and David G. Grier. "Methods of Digital Video Microscopy for Colloidal Studies". In: *Journal of Colloid and Interface Science* 310.179 (1996), pp. 298–310.
- [30] Xiaolin Wang et al. "Enhanced cell sorting and manipulation with combined optical tweezer and microfluidic chip technologies". In: *Lab on a Chip* 11.21 (2011), pp. 3656–3662. ISSN: 14730189. DOI: [10.1039/c1lc20653b](https://doi.org/10.1039/c1lc20653b).
- [31] David G Grier. "A revolution in optical manipulation." In: *Nature* 424.6950 (2003), pp. 810–6. ISSN: 1476-4687. DOI: [10.1038/nature01935](https://doi.org/10.1038/nature01935).
- [32] Pieter Walstra. "Principles of emulsion formation". In: *Chemical Engineering Science* 48.2 (Jan. 1993), pp. 333–349. ISSN: 0009-2509. DOI: [10.1016/0009-2509\(93\)80021-H](https://doi.org/10.1016/0009-2509(93)80021-H).
- [33] David Julian McClements. *Food Emulsions: Principles, Practices, and Techniques, Third Edition*. en. CRC Press, Aug. 2015. ISBN: 978-1-4987-2669-6.
- [34] George A. Van Aken. "Flow-induced coalescence in protein-stabilized highly concentrated emulsions". In: *Langmuir* 18.7 (2002), pp. 2549–2556. ISSN: 07437463. DOI: [10.1021/la011540s](https://doi.org/10.1021/la011540s).
- [35] F. A. Perrechil and R. L. Cunha. "Oil-in-water emulsions stabilized by sodium caseinate: Influence of pH, high-pressure homogenization and locust bean gum addition". In: *Journal of Food Engineering* 97.4 (2010), pp. 441–448. ISSN: 02608774. DOI: [10.1016/j.jfoodeng.2009.10.041](https://doi.org/10.1016/j.jfoodeng.2009.10.041).
- [36] Stephen R. Euston, Suzanne R. Finnigan, and Robyn L. Hirst. "Kinetics of droplet aggregation in heated whey protein-stabilized emulsions: effect of polysaccharides". In: *Food hydrocolloids* 16.5 (2002), pp. 499–505.

- [37] Dominic W.S. Wong et al. "Structures and functionalities of milk proteins". en. In: *Critical Reviews in Food Science and Nutrition* 36.8 (Dec. 1996), pp. 807–844. ISSN: 1040-8398, 1549-7852.
- [38] H. M. Farrell et al. "Nomenclature of the proteins of cows' milk—sixth revision". In: *Journal of dairy science* 87.6 (2004), pp. 1641–1674.
- [39] J. J. Baummy and G. Brule. "Binding of bivalent cations to alpha lactalbumin and beta lactoglobulin: effect of pH and ionic strength". In: *Le Lait* 68.1 (1988), pp. 33–48.
- [40] K. Demetriades, J. N. Coupland, and D. J. McClements. "Physical properties of whey protein stabilized emulsions as related to pH and NaCl". In: *Journal of Food Science* 62.2 (1997), pp. 342–347.
- [41] Srinivasan Damodaran, Kirk L. Parkin, and Owen R. Fennema. *Fennema's Food Chemistry, Fourth Edition*. en. CRC Press, Sept. 2007, p. 1158. ISBN: 978-1-4200-2052-6.
- [42] Josephine A. Hunt and Douglas G. Dalgleish. "Effect of pH on the stability and surface composition of emulsions made with whey protein isolate". In: *Journal of Agricultural and Food Chemistry* 42.10 (1994), pp. 2131–2135.
- [43] A. Einstein. "Effect of suspended rigid spheres on viscosity". In: *Ann. Phys* 19 (1906), pp. 289–306.
- [44] Tharwat F. Tadros. *Emulsion formation and stability*. John Wiley & Sons, 2013.
- [45] P. J. Whitcomb and C. W. Macosko. "Rheology of Xanthan Gum". In: *Journal of Rheology* 22.5 (1978), pp. 493–505. ISSN: 0148-6055. DOI: [10.1122/1.549485](https://doi.org/10.1122/1.549485).
- [46] P.A. Sandford et al. "Variation in *Xanthomonas campestris* NRRL B 1459: characterization of xanthan products of differing pyruvic acid content". In: *ACS Symp Ser Amer Chem Soc* v. 45 (1977), pp. 192–210.
- [47] K. OKUYAMA et al. "Fiber Diffraction Studies of Bacterial Polysaccharides". In: (1980), pp. 411–427. DOI: [10.1021/bk-1980-0141.ch026](https://doi.org/10.1021/bk-1980-0141.ch026).



- [48] Barbara Katzbauer. "Properties and applications of xanthan gum". In: *Polymer Degradation and Stability* 59.1-3 (Jan. 1998), pp. 81–84. ISSN: 0141-3910. DOI: [10.1016/S0141-3910\(97\)00180-8](https://doi.org/10.1016/S0141-3910(97)00180-8).
- [49] F. García-Ochoa et al. "Xanthan gum: Production, recovery, and properties". In: *Biotechnology Advances* 18.7 (2000), pp. 549–579. ISSN: 0734-9750 (Print)\r0734-9750 (Linking). DOI: [10.1016/S0734-9750\(00\)00050-1](https://doi.org/10.1016/S0734-9750(00)00050-1).
- [50] G. Sworn. "Xanthan gum". In: *Handbook of Hydrocolloids: Second Edition* (2009), pp. 186–203. ISSN: 10920110. DOI: [10.1533/9781845695873.186](https://doi.org/10.1533/9781845695873.186).
- [51] Malvern Instruments Ltd. *Zetasizer Nano user manual — Man0317-1.1.pdf*. 2003.
- [52] E. Allen Foegeding et al. "Advances in modifying and understanding whey protein functionality". In: *Trends in Food Science & Technology* 13.5 (2002), 151–159.
- [53] Josephine A. Hunt and Douglas G. Dalgleish. "Adsorption behaviour of whey protein isolate and caseinate in soya oil-in-water emulsions". In: *Food Hydrocolloids* 8.2 (1994), 175–187.
- [54] Zhi Yong Ju and Arun Kilara. "Gelation of pH-aggregated whey protein isolate solution induced by heat, protease, calcium salt, and acidulant". In: *Journal of Agricultural and Food Chemistry* 46.5 (1998), 1830–1835.
- [55] Asylbek Kulmyrzaev, Ratjika Chanamai, and D Julian McClements. "Influence of pH and CaCl<sub>2</sub> on the stability of dilute whey protein stabilized emulsions". In: *Food Research International* 33.1 (2000), pp. 15–20. ISSN: 0963-9969.
- [56] T. Spiegel and M. Huss. "Whey protein aggregation under shear conditions—effects of pH-value and removal of calcium". In: *International journal of food science & technology* 37.5 (2002), 559–568.
- [57] A.A. Kulmyrzaev and H. Schubert. "Influence of KCl on the physicochemical properties of whey protein stabilized emulsions". en. In: *Food Hydrocolloids* 18.1 (Jan. 2004), pp. 13–19. ISSN: 0268005X. DOI: [10.1016/S0268-005X\(03\)00037-7](https://doi.org/10.1016/S0268-005X(03)00037-7).

- [58] Changhui Sun and Sundaram Gunasekaran. "Effects of protein concentration and oil-phase volume fraction on the stability and rheology of menhaden oil-in-water emulsions stabilized by whey protein isolate with xanthan gum". en. In: *Food Hydrocolloids* 23.1 (Jan. 2009), pp. 165–174. ISSN: 0268005X. DOI: [10.1016/j.foodhyd.2007.12.006](https://doi.org/10.1016/j.foodhyd.2007.12.006).
- [59] Douglas G. Dalgleish. *Adsorption of protein and the stability of emulsions*. en. Apr. 1997. DOI: [10.1016/S0924-2244\(97\)01001-7](https://doi.org/10.1016/S0924-2244(97)01001-7).
- [60] Eric Dickinson and Matt Golding. "Influence of calcium ions on creaming and rheology of emulsions containing sodium caseinate". In: *Colloids and Surfaces A: Physicochemical and Engineering Aspects* 144.1 (1998), pp. 167–177. ISSN: 09277757. DOI: [10.1016/S0927-7757\(98\)00573-1](https://doi.org/10.1016/S0927-7757(98)00573-1).
- [61] Asylbek Kulmyrzaev, Marialice P.C. Sivestre, and D.J. McClements. "Rheology and stability of whey protein stabilized emulsions with high CaCl<sub>2</sub> concentrations". In: *Food Research International* 33.1 (2000), pp. 21–25. ISSN: 09639969. DOI: [10.1016/S0963-9969\(00\)00019-3](https://doi.org/10.1016/S0963-9969(00)00019-3).
- [62] A. Ye and H. Singh. "Influence of calcium chloride addition on the properties of emulsions stabilized by whey protein concentrate". In: *Food Hydrocolloids* 14.4 (2000), 337–346.
- [63] M.G. Sosa-Herrera et al. "Effect of added calcium chloride on the physicochemical and rheological properties of aqueous mixtures of sodium caseinate/sodium alginate and respective oil-in-water emulsions". en. In: *Food Hydrocolloids* 29.1 (Oct. 2012), pp. 175–184. ISSN: 0268005X. DOI: [10.1016/j.foodhyd.2012.02.017](https://doi.org/10.1016/j.foodhyd.2012.02.017).
- [64] Douglas G. Dalgleish. "Adsorption of protein and the stability of emulsions". In: *Trends in Food Science & Technology* 8.1 (Jan. 1997), pp. 1–6. ISSN: 0924-2244. DOI: [10.1016/S0924-2244\(97\)01001-7](https://doi.org/10.1016/S0924-2244(97)01001-7).
- [65] Asylbek Kulmyrzaev, Ratjika Chanamai, and David Julian McClements. "Influence of pH and CaCl<sub>2</sub> on the stability of dilute whey protein emulsions.pdf". In: *Food Research International* 33 (2000), pp. 15–20.

- [66] Ian Larson and Phil Attard. "Surface Charge of Silver Iodide and Several Metal Oxides. Are All Surfaces Nernstian?" en. In: *Journal of Colloid and Interface Science* 227.1 (July 2000), pp. 152–163. ISSN: 00219797. DOI: [10.1006/jcis.2000.6847](https://doi.org/10.1006/jcis.2000.6847).
- [67] Sven H. Behrens and David G. Grier. "The charge of glass and silica surfaces". en. In: *The Journal of Chemical Physics* 115.14 (Oct. 2001), pp. 6716–6721. ISSN: 0021-9606, 1089-7690. DOI: [10.1063/1.1404988](https://doi.org/10.1063/1.1404988).
- [68] S. Usui and T.W. Healy. "Zeta Potential of Stearic Acid Monolayer at the Air–Aqueous Solution Interface". en. In: *Journal of Colloid and Interface Science* 250.2 (June 2002), pp. 371–378. ISSN: 00219797. DOI: [10.1006/jcis.2002.8340](https://doi.org/10.1006/jcis.2002.8340).
- [69] P. Leroy and A. Revil. "A triple-layer model of the surface electrochemical properties of clay minerals". en. In: *Journal of Colloid and Interface Science* 270.2 (Feb. 2004), pp. 371–380. ISSN: 00219797. DOI: [10.1016/j.jcis.2003.08.007](https://doi.org/10.1016/j.jcis.2003.08.007).
- [70] Jülide Hizal and Resat Apak. "Modeling of cadmium(II) adsorption on kaolinite-based clays in the absence and presence of humic acid". en. In: *Applied Clay Science* 32.3-4 (May 2006), pp. 232–244. ISSN: 01691317. DOI: [10.1016/j.clay.2006.02.002](https://doi.org/10.1016/j.clay.2006.02.002).
- [71] Hans-Jürgen Butt, Karlheinz Graf, and Michael Kappl. *Physics and Chemistry of Interfaces*. en. John Wiley & Sons, May 2002, p. 376. ISBN: 978-3-527-60640-5.
- [72] T. Cosgrove. *Colloid Science: Principles, Methods and Applications*. Colloid Science: Principles, Methods and Applications. John Wiley & Sons, 2010. ISBN: 978-1-4443-2019-0.
- [73] Marvin A. Tung. "Rheology of protein dispersions". In: *Journal of Texture Studies* 9.1-2 (June 1978), pp. 3–31. ISSN: 0022-4901. DOI: [10.1111/j.1745-4603.1978.tb01292.x](https://doi.org/10.1111/j.1745-4603.1978.tb01292.x).
- [74] J. W. Goodwin. "The rheology of dispersions". In: *Colloid Science*. Ed. by D. H. Everett. Vol. 2. The Royal Society of Chemistry, 1975, pp. 246–293. ISBN: 978-0-85186-518-8.

- [75] Laurent Bazinet, Maher Trigui, and Denis Ippersiel. "Rheological Behavior of WPI Dispersion as a Function of pH and Protein Concentration". en. In: *Journal of Agricultural and Food Chemistry* 52.17 (Aug. 2004), pp. 5366–5371. ISSN: 0021-8561, 1520-5118. DOI: [10.1021/jf049893v](https://doi.org/10.1021/jf049893v).
- [76] Robert J. Hunter. "The flow behavior of coagulated colloidal dispersions". In: *Advances in Colloid and Interface Science* 17.1 (Aug. 1982), pp. 197–211. ISSN: 00018686. DOI: [10.1016/0001-8686\(82\)80019-5](https://doi.org/10.1016/0001-8686(82)80019-5).
- [77] Peter J. Scales et al. "Shear yield stress of partially flocculated colloidal suspensions". In: *AIChE Journal* 44.3 (1998), 538–544.
- [78] A.A. Kulmyrzaev and H. Schubert. "Influence of KCl on the physicochemical properties of whey protein stabilized emulsions". en. In: *Food Hydrocolloids* 18.1 (Jan. 2004), pp. 13–19. ISSN: 0268005X. DOI: [10.1016/S0268-005X\(03\)00037-7](https://doi.org/10.1016/S0268-005X(03)00037-7).
- [79] Sven Holger Behrens et al. "Charging and Aggregation Properties of Carboxyl Latex Particles: Experiments versus DLVO Theory". en. In: *Langmuir* 16.6 (Mar. 2000), pp. 2566–2575. ISSN: 0743-7463, 1520-5827. DOI: [10.1021/la991154z](https://doi.org/10.1021/la991154z).
- [80] S.B. Hall et al. "An interfacial equilibria model for the electrokinetic properties of a fat emulsion". In: *International Journal of Pharmaceutics* 70.3 (Apr. 1991), pp. 251–260. ISSN: 0378-5173. DOI: [10.1016/0378-5173\(91\)90289-Z](https://doi.org/10.1016/0378-5173(91)90289-Z).
- [81] Ionel Popa et al. "Attractive Electrostatic Forces between Identical Colloidal Particles Induced by Adsorbed Polyelectrolytes". en. In: *The Journal of Physical Chemistry B* 113.25 (June 2009), pp. 8458–8461. ISSN: 1520-6106, 1520-5207. DOI: [10.1021/jp904041k](https://doi.org/10.1021/jp904041k).
- [82] Jacob N. Israelachvili. *Intermolecular and Surface Forces: Revised Third Edition*. en. Academic Press, July 2011, p. 706. ISBN: 978-0-12-391933-5.
- [83] J.H. Masliyah and S. Bhattacharjee. *Electrokinetic and Colloid Transport Phenomena*. Wiley, 2006. ISBN: 978-0-471-79973-3.

- [84] M. Elimelech, J. Gregory, and X. Jia. *Particle Deposition and Aggregation: Measurement, Modelling and Simulation*. en. Butterworth-Heinemann, Oct. 2013, p. 458. ISBN: 978-1-4831-6137-2.
- [85] HC Hamaker. "The London—van der Waals attraction between spherical particles". In: *physica* 4.10 (1937), pp. 1058–1072. ISSN: 0031-8914.
- [86] James W. Murray. *Activity Scales and Activity Corrections*. 2010.
- [87] S.B. Hall et al. "An interfacial equilibria model for the electrokinetic properties of a fat emulsion". In: *International Journal of Pharmaceutics* 70.3 (Apr. 1991), pp. 251–260. ISSN: 0378-5173. DOI: [10.1016/0378-5173\(91\)90289-Z](https://doi.org/10.1016/0378-5173(91)90289-Z).
- [88] Lawrence K Creamer et al. "Heat-Induced Redistribution of Disulfide Bonds in Milk Proteins. 1. Bovine  $\beta$ -Lactoglobulin". In: *Journal of Agricultural and Food Chemistry* 52.25 (2004), pp. 7660–7668. DOI: [10.1021/jf049388y](https://doi.org/10.1021/jf049388y).
- [89] R Miller et al. "Dynamic Surface Tension and Adsorption Kinetics of  $\beta$ -Casein at the Solution/Air Interface". In: *Langmuir* 20.3 (2004), pp. 771–777. DOI: [10.1021/la030332s](https://doi.org/10.1021/la030332s).
- [90] Eric Dickinson and Soon-Taek Hong. "surface Coverage of .beta.-Lactoglobulin at the Oil-Water Interface: Influence of Protein Heat Treatment and Various Emulsifiers". In: *Journal of Agricultural and Food Chemistry* 42.8 (1994), pp. 1602–1606. DOI: [10.1021/jf00044a003](https://doi.org/10.1021/jf00044a003).
- [91] Peter J Atkinson et al. "Neutron reflectivity of adsorbed [small beta]-casein and [small beta]-lactoglobulin at the air/water interface". In: *J. Chem. Soc., Faraday Trans.* 91.17 (1995), pp. 2847–2854. DOI: [10.1039/FT9959102847](https://doi.org/10.1039/FT9959102847).
- [92] Jean-Luc Courthaudon et al. "Influence of Emulsifier on the Competitive Adsorption of Whey Proteins in Emulsions". In: *Food. Struct.* 10.2 (1991), pp. 109–115.
- [93] J. Chen, E. Dickinson, and G. Iveson. "Interfacial interactions, competitive adsorption and emulsion stability". In: *Food structure (USA)* 12.2 (1993), p. 1. ISSN: 1046-705X.

- [94] Leonor Pérez-Fuentes et al. "Adsorption of milk proteins ( $\beta$ -casein and  $\beta$ -lactoglobulin) and BSA onto hydrophobic surfaces". In: *Materials* 10.8 (2017), pp. 1–25. ISSN: 19961944. DOI: [10.3390/ma10080893](https://doi.org/10.3390/ma10080893).
- [95] Gerald S Manning. "Limiting Laws and Counterion Condensation in Polyelectrolyte Solutions I. Colligative Properties". In: *The Journal of Chemical Physics* 51.3 (1969), pp. 924–933. DOI: [10.1063/1.1672157](https://doi.org/10.1063/1.1672157).
- [96] Richard W O'Brien and Lee R White. "Electrophoretic mobility of a spherical colloidal particle". In: *J. Chem. Soc., Faraday Trans. 2* 74.0 (1978), pp. 1607–1626. DOI: [10.1039/F29787401607](https://doi.org/10.1039/F29787401607).
- [97] William Brown et al. *Organic Chemistry, Enhanced Edition*. en. Cengage Learning, Jan. 2010, p. 1253. ISBN: 978-0-538-49675-9.
- [98] Howard A. Barnes. "Rheology of emulsions—a review". In: *Colloids and surfaces A: physicochemical and engineering aspects* 91 (1994), 89–95.
- [99] Tharwat F. Tadros. *Emulsion formation and stability*. John Wiley & Sons, 2013.
- [100] M. Anandha Rao and M. Anandha Rao. "Flow and Functional Models for Rheological Properties of Fluid Foods". In: Boston, MA: Springer US, 2014, pp. 27–61. ISBN: 978-1-4614-9229-0 978-1-4614-9230-6.
- [101] Ronald G. Larson. *The Structure and Rheology of Complex Fluids*. en. OUP USA, Jan. 1999, p. 696. ISBN: 978-0-19-512197-1.
- [102] B.C. Ong, Y.K. Leong, and S.B. Chen. "Yield stress-zeta potential relationship of oxide dispersions with adsorbed polyacrylate — Steric effect and zeta potential at the flocculated-dispersed transition state". en. In: *Powder Technology* 186.2 (Aug. 2008), pp. 176–183. ISSN: 00325910. DOI: [10.1016/j.powtec.2007.11.047](https://doi.org/10.1016/j.powtec.2007.11.047).
- [103] E Dickinson and G Stainsby. *Colloids in food*. English. Barking, Essex: Applied Science Publishers, 1982, xiv + 533pp. ISBN: 0853341532.
- [104] Nissim Garti and Dov Reichman. "Food Structure Hydrocolloids as Food Emulsifiers and Stabilizers". In: *Food Structure* 12.4 (1993), pp. 411–426.

- [105] Robert J Hunter. *Foundations of colloid science / Robert J. Hunter*. Oxford ; New York: Oxford University Press, 2001. ISBN: 0198505027 (alkaline paper).
- [106] Rajendra P. Borwankar, Lloyd A. Lobo, and Darsh T. Wasan. "Emulsion stability - kinetics of flocculation and coalescence". In: *Colloids and Surfaces* 69.2-3 (1992), pp. 135–146. ISSN: 01666622. DOI: [10.1016/0166-6622\(92\)80224-P](https://doi.org/10.1016/0166-6622(92)80224-P).
- [107] M van den Tempel. "Stability of oil-in-water emulsions I: The electrical double layer at the oil-water interface". In: *Recueil des Travaux Chimiques des Pays-Bas* 72.5 (1953), pp. 419–432. DOI: [10.1002/rec1.19530720507](https://doi.org/10.1002/rec1.19530720507).
- [108] S. Ravindran et al. "Understanding how the properties of whey protein stabilized emulsions depend on pH, ionic strength and calcium concentration, by mapping environmental conditions to zeta potential". In: *Food Hydrocolloids* 79 (2018), pp. 572–578. ISSN: 0268005X. DOI: [10.1016/j.foodhyd.2017.12.003](https://doi.org/10.1016/j.foodhyd.2017.12.003).
- [109] Michelle C. McKinley. "The nutrition and health benefits of yoghurt". In: *International journal of dairy technology* 58.1 (2005), 1–12.
- [110] Hilton C Deeth and Michael J Lewis. "Practical consequences of calcium addition to and removal from milk and milk products". en. In: *International Journal of Dairy Technology* 68.1 (Feb. 2015), pp. 1–10. ISSN: 1364727X. DOI: [10.1111/1471-0307.12188](https://doi.org/10.1111/1471-0307.12188).
- [111] A Ye, Y Hemar, and H Singh. "Enhancement of coalescence by xanthan addition to oil-in-water emulsions formed with extensively hydrolysed whey proteins". en. In: *Food Hydrocolloids* 18.5 (Sept. 2004), pp. 737–746. ISSN: 0268005X. DOI: [10.1016/j.foodhyd.2003.11.010](https://doi.org/10.1016/j.foodhyd.2003.11.010).
- [112] Aiqian Ye, Yacine Hemar, and Harjinder Singh. "Influence of polysaccharides on the rate of coalescence in oil-in-water emulsions formed with highly hydrolyzed whey proteins". In: *Journal of Agricultural and Food Chemistry* 52.17 (2004), pp. 5491–5498. ISSN: 00218561. DOI: [10.1021/jf030762o](https://doi.org/10.1021/jf030762o).

- [113] Paul A. Gunning et al. "Gravitational destabilization of emulsions flocculated by non-adsorbed xanthan". In: *Topics in Catalysis* 2.2 (1988), pp. 119–129. ISSN: 0268005x. DOI: [10.1016/S0268-005X\(88\)80010-9](https://doi.org/10.1016/S0268-005X(88)80010-9).
- [114] Changhui Sun, Sundaram Gunasekaran, and Mark P. Richards. "Effect of xanthan gum on physicochemical properties of whey protein isolate stabilized oil-in-water emulsions". In: *Food Hydrocolloids* 21.4 (2007), pp. 555–564. ISSN: 0268005X. DOI: [10.1016/j.foodhyd.2006.06.003](https://doi.org/10.1016/j.foodhyd.2006.06.003).
- [115] Cecil W. Davies. "397. The extent of dissociation of salts in water. Part VIII. An equation for the mean ionic activity coefficient of an electrolyte in water, and a revision of the dissociation constants of some sulphates". In: *Journal of the Chemical Society (Resumed)* (1938), 2093–2098.
- [116] C. Viebke and P. A. Williams. "Determination of molecular mass distribution of  $\kappa$ -carrageenan and xanthan using asymmetrical flow field-flow fractionation". In: *Food Hydrocolloids* 14.3 (2000), pp. 265–270. ISSN: 0268005X. DOI: [10.1016/S0268-005X\(99\)00066-1](https://doi.org/10.1016/S0268-005X(99)00066-1).
- [117] Rajendra P. Borwankar, Lloyd A. Lobo, and Darsh T. Wasan. "Emulsion stability - kinetics of flocculation and coalescence". In: *Colloids and Surfaces* 69.2-3 (1992), pp. 135–146. ISSN: 0166-6622. DOI: [10.1016/0166-6622\(92\)80224-P](https://doi.org/10.1016/0166-6622(92)80224-P).
- [118] G R Wiese and T W Healy. "Effect of particle size on colloid stability". In: *Transactions of the Faraday Society* 66.0 (1970), pp. 490–499. ISSN: 0014-7672. DOI: [10.1039/TF9706600490](https://doi.org/10.1039/TF9706600490).
- [119] M. S. Veshchunov and V. I. Tarasov. "Extension of the smoluchowski theory to transitions from dilute to dense regime of brownian coagulation: Triple collisions". In: *Aerosol Science and Technology* 48.8 (2014), pp. 813–821. ISSN: 15217388. DOI: [10.1080/02786826.2014.931567](https://doi.org/10.1080/02786826.2014.931567).
- [120] Marco Lattuada. "Predictive model for diffusion-limited aggregation kinetics of nanocolloids under high concentration". In: *Journal of Physical Chemistry B* 116.1 (2012), pp. 120–129. ISSN: 15205207. DOI: [10.1021/jp2097839](https://doi.org/10.1021/jp2097839).



- [121] M. C. Heine and S. E. Pratsinis. "Brownian coagulation at high concentration". In: *Langmuir* 23.19 (2007), pp. 9882–9890. ISSN: 07437463. DOI: [10.1021/la7012599](https://doi.org/10.1021/la7012599).
- [122] E. E. Meyer et al. "Origin of the long-range attraction between surfactant-coated surfaces". In: *Proceedings of the National Academy of Sciences* 102.19 (2005), pp. 6839–6842. ISSN: 0027-8424. DOI: [10.1073/pnas.0502110102](https://doi.org/10.1073/pnas.0502110102).
- [123] Ionel Popa et al. "Attractive electrostatic forces between identical colloidal particles induced by adsorbed polyelectrolytes". In: *Journal of Physical Chemistry B* 113.25 (2009), pp. 8458–8461. ISSN: 15206106. DOI: [10.1021/jp904041k](https://doi.org/10.1021/jp904041k).
- [124] Zhiwei Sun et al. "A microscopic approach to studying colloidal stability". In: *The Journal of Chemical Physics* 119.4 (2003), pp. 2399–2405. ISSN: 0021-9606. DOI: [10.1063/1.1585022](https://doi.org/10.1063/1.1585022).
- [125] S C Wang and Gert Ehrlich. "Adatom diffusion on W(211): Re, W, Mo, Ir, and Rh". In: *Surface Science* 206.3 (1988), pp. 451–474. ISSN: 0039-6028. DOI: [https://doi.org/10.1016/0039-6028\(88\)90146-X](https://doi.org/10.1016/0039-6028(88)90146-X).
- [126] F Tanaka and S F Edwards. "Viscoelastic properties of physically crosslinked networks: Part 3. Time-dependent phenomena". In: *Journal of Non-Newtonian Fluid Mechanics* 43.2 (1992), pp. 289–309. ISSN: 0377-0257. DOI: [https://doi.org/10.1016/0377-0257\(92\)80029-W](https://doi.org/10.1016/0377-0257(92)80029-W).
- [127] Eric R. Dufresne et al. "Computer-generated holographic optical tweezer arrays". en. In: *Review of Scientific Instruments* 72.3 (2001), p. 1810. ISSN: 00346748. DOI: [10.1063/1.1344176](https://doi.org/10.1063/1.1344176).
- [128] Arthur Ashkin. "Forces of a single-beam gradient laser trap on a dielectric sphere in the ray optics regime". In: *Biophysical journal* 61.2 (1992), p. 569.
- [129] Keir C. Neuman and Steven M. Block. "Optical trapping". en. In: *Review of Scientific Instruments* 75.9 (2004), p. 2787. ISSN: 00346748. DOI: [10.1063/1.1785844](https://doi.org/10.1063/1.1785844).
- [130] Arthur Ashkin et al. "Observation of a single-beam gradient force optical trap for dielectric particles". In: *Optics letters* 11.5 (1986), pp. 288–290.

- [131] P H Jones, O M Marag, and G Volpe. *Optical Tweezers: Principles and Applications*. Cambridge University Press, 2015. ISBN: 9781107051164.
- [132] Kishan Dholakia, Michael MacDonald, and Gabriel Spalding. “Optical tweezers: the next generation”. In: *Physics World* 15.10 (2002), pp. 31–35. ISSN: 0953-8585. DOI: [10.1088/2058-7058/15/10/37](https://doi.org/10.1088/2058-7058/15/10/37).
- [133] Richard W Bowman and Miles J Padgett. “Optical trapping and binding”. In: *Reports on Progress in Physics* 76.2 (Feb. 2013), p. 026401. ISSN: 0034-4885, 1361-6633. DOI: [10.1088/0034-4885/76/2/026401](https://doi.org/10.1088/0034-4885/76/2/026401).
- [134] Paolo Polimeno et al. “Optical tweezers and their applications”. In: *Journal of Quantitative Spectroscopy and Radiative Transfer* 218 (2018), pp. 131–150. ISSN: 00224073. DOI: [10.1016/j.jqsrt.2018.07.013](https://doi.org/10.1016/j.jqsrt.2018.07.013).
- [135] Eric R. Dufresne et al. “Computer-generated holographic optical tweezer arrays”. In: *Review of Scientific Instruments* 72.3 (2001), pp. 1810–1816. ISSN: 00346748. DOI: [10.1063/1.1344176](https://doi.org/10.1063/1.1344176).
- [136] Jennifer E Curtis, Brian A Koss, and David G Grier. “Dynamic holographic optical tweezers”. In: *Optics Communications* 207.1 (2002), pp. 169–175. ISSN: 0030-4018. DOI: [https://doi.org/10.1016/S0030-4018\(02\)01524-9](https://doi.org/10.1016/S0030-4018(02)01524-9).
- [137] Zheng Kuang et al. “High throughput diffractive multi-beam femtosecond laser processing using a spatial light modulator”. In: *Applied Surface Science* 255.5 PART 1 (2008), pp. 2284–2289. ISSN: 01694332. DOI: [10.1016/j.apsusc.2008.07.091](https://doi.org/10.1016/j.apsusc.2008.07.091).
- [138] Julie Nilsen-Nygaard, Marit Sletmoen, and Kurt Ingar Draget. “Stability and interaction forces of oil-in-water emulsions as observed by optical tweezers – a proof-of-concept study”. en. In: *RSC Adv.* 4.94 (Oct. 2014), pp. 52220–52229. ISSN: 2046-2069. DOI: [10.1039/C4RA07140A](https://doi.org/10.1039/C4RA07140A).
- [139] Marjorie R. Griffiths et al. “Measuring the interaction between a pair of emulsion droplets using dual-trap optical tweezers”. In: *RSC Advances* 6.18 (2016), pp. 14538–14546. ISSN: 20462069. DOI: [10.1039/c5ra25073k](https://doi.org/10.1039/c5ra25073k).

- [140] Alison Yao et al. "Microrheology with optical tweezers". en. In: *Lab on a Chip* 9.17 (2009), p. 2568. ISSN: 1473-0197, 1473-0189. DOI: [10.1039/b907992k](https://doi.org/10.1039/b907992k).
- [141] Zbigniew Adamczyk and Paweł Weroński. "Application of the DLVO theory for particle deposition problems". In: *Advances in Colloid and Interface Science* 83.1 (1999), pp. 137–226. ISSN: 0001-8686. DOI: [https://doi.org/10.1016/S0001-8686\(99\)00009-3](https://doi.org/10.1016/S0001-8686(99)00009-3).
- [142] John Gregory. "Monitoring particle aggregation processes". In: *Advances in Colloid and Interface Science* 147-148.C (2009), pp. 109–123. ISSN: 00018686. DOI: [10.1016/j.cis.2008.09.003](https://doi.org/10.1016/j.cis.2008.09.003).
- [143] N. M. Kovalchuk and V. M. Starov. "Aggregation in colloidal suspensions: Effect of colloidal forces and hydrodynamic interactions". In: *Advances in Colloid and Interface Science* 179-182 (2012), pp. 99–106. ISSN: 00018686. DOI: [10.1016/j.cis.2011.05.009](https://doi.org/10.1016/j.cis.2011.05.009).
- [144] M Y Lin et al. "Universality in colloid aggregation". In: *Nature* 339.6223 (1989), pp. 360–362. ISSN: 1476-4687. DOI: [10.1038/339360a0](https://doi.org/10.1038/339360a0).
- [145] M Y Lin et al. "Universal diffusion-limited colloid aggregation". In: *Journal of Physics: Condensed Matter* 2.13 (1990), pp. 3093–3113. ISSN: 0953-8984. DOI: [10.1088/0953-8984/2/13/019](https://doi.org/10.1088/0953-8984/2/13/019).
- [146] A. Moncho-Jordá et al. "The DLCA-RLCA transition arising in 2D-aggregation: Simulations and mean field theory". In: *European Physical Journal E* 5.4 (2001), pp. 471–480. ISSN: 12928941. DOI: [10.1007/s101890170054](https://doi.org/10.1007/s101890170054).
- [147] Peter J. Lu and David A. Weitz. "Colloidal Particles: Crystals, Glasses, and Gels". In: *Annual Review of Condensed Matter Physics* 4.1 (2013), pp. 217–233. ISSN: 1947-5454. DOI: [10.1146/annurev-conmatphys-030212-184213](https://doi.org/10.1146/annurev-conmatphys-030212-184213).
- [148] Denis N. L. McGown and Geoffrey D. Parfitt. "Improved theoretical calculation of the stability ratio for colloidal systems". In: *The Journal of Physical Chemistry* 71.2 (1967), pp. 449–450. ISSN: 0022-3654. DOI: [10.1021/j100861a041](https://doi.org/10.1021/j100861a041).

- [149] Shenghua Xu and Zhiwei Sun. "Computer simulation on the collision-sticking dynamics of two colloidal particles in an optical trap". In: *Journal of Chemical Physics* 126.14 (2007). ISSN: 00219606. DOI: [10.1063/1.2712183](https://doi.org/10.1063/1.2712183).
- [150] Keir C Neuman and Attila Nagy. "Single-molecule force spectroscopy: optical tweezers, magnetic tweezers and atomic force microscopy". In: *Nature Methods* 5 (May 2008), p. 491.
- [151] Zhiwei Sun et al. "A microscopic approach to studying colloidal stability". In: *The Journal of Chemical Physics* 119.4 (2003), pp. 2399–2405. DOI: [10.1063/1.1585022](https://doi.org/10.1063/1.1585022).
- [152] Max Bender. "The electric charge on macroscopic glass surface". In: *Journal of Colloid Science* 9.5 (Oct. 1954), pp. 400–408. ISSN: 0095-8522. DOI: [10.1016/0095-8522\(54\)90028-8](https://doi.org/10.1016/0095-8522(54)90028-8).
- [153] Sven Holger Behrens et al. "Charging and Aggregation Properties of Carboxyl Latex Particles: Experiments versus DLVO Theory". en. In: *Langmuir* 16.6 (Mar. 2000), pp. 2566–2575. ISSN: 0743-7463, 1520-5827. DOI: [10.1021/1a991154z](https://doi.org/10.1021/1a991154z).
- [154] Keith J. Laidler. "The development of the Arrhenius equation". In: *Journal of Chemical Education* 61.6 (1984), p. 494. ISSN: 0021-9584. DOI: [10.1021/ed061p494](https://doi.org/10.1021/ed061p494).
- [155] Shenghua Xu and Zhiwei Sun. "Progress in coagulation rate measurements of colloidal dispersions". In: *Soft Matter* 7.24 (2011), pp. 11298–11308. ISSN: 1744683X. DOI: [10.1039/c1sm06237a](https://doi.org/10.1039/c1sm06237a).
- [156] B.C. Ong, Y.K. Leong, and S.B. Chen. "Yield stress-zeta potential relationship of oxide dispersions with adsorbed polyacrylate — Steric effect and zeta potential at the flocculated-dispersed transition state". en. In: *Powder Technology* 186.2 (Aug. 2008), pp. 176–183. ISSN: 00325910. DOI: [10.1016/j.powtec.2007.11.047](https://doi.org/10.1016/j.powtec.2007.11.047).
- [157] Mats Larsson, John Duffy, and Adrian Hill. "Suspension stability : Why particle size , zeta potential and rheology are important". In: *Annual Transactions of the Nordic Rheology Society* 20 (2012), pp. 209–214.

- [158] Cheng S. Lee et al. "Factors Affecting Direct Control of Electroosmosis Using an External Electric Field in Capillary Electrophoresis". In: *Analytical Chemistry* 63.15 (1991), pp. 1519–1523. ISSN: 15206882. DOI: [10.1021/ac00015a005](https://doi.org/10.1021/ac00015a005).
- [159] Ali Reza Nazmi et al. "Effect of protein charge manipulation on alpha-caseinate self-assembly monitored by analytical ultracentrifugation". In: *to be published* ().
- [160] Jim C. Chen and Albert S. Kim. "Brownian Dynamics, Molecular Dynamics, and Monte Carlo modeling of colloidal systems". en. In: *Advances in Colloid and Interface Science* 112.1-3 (Dec. 2004), pp. 159–173. ISSN: 00018686. DOI: [10.1016/j.cis.2004.10.001](https://doi.org/10.1016/j.cis.2004.10.001).
- [161] Alessandro Patti and Alejandro Cuetos. "Brownian dynamics and dynamic Monte Carlo simulations of isotropic and liquid crystal phases of anisotropic colloidal particles: A comparative study". en. In: *Physical Review E* 86.1 (July 2012). ISSN: 1539-3755, 1550-2376. DOI: [10.1103/PhysRevE.86.011403](https://doi.org/10.1103/PhysRevE.86.011403).
- [162] SH[Ubar]ICHI Nosé. "A molecular dynamics method for simulations in the canonical ensemble". en. In: *Molecular Physics* 100.1 (Jan. 2002), pp. 191–198. ISSN: 0026-8976, 1362-3028.
- [163] David E. Potter. *Computational physics*. en. J. Wiley, 1973. ISBN: 978-0-471-69555-4.
- [164] M. P. Allen and D. J. Tildesley. *Computer Simulation of Liquids*. en. Clarendon Press, 1989. ISBN: 978-0-19-855645-9.
- [165] P. H. S. Santos, O. H. Campanella, and M. A. Carignano. "Brownian Dynamics Study of Gel-Forming Colloidal Particles". en. In: *The Journal of Physical Chemistry B* 114.41 (Oct. 2010), pp. 13052–13058. ISSN: 1520-6106, 1520-5207. DOI: [10.1021/jp105711y](https://doi.org/10.1021/jp105711y).
- [166] A Elaissari. *Colloidal Polymers: Synthesis and Characterization*. Surfactant Science. CRC Press, 2003. ISBN: 9780203911488.
- [167] Eric Dickinson and Soon-Taek Hong. "surface Coverage of. beta.-Lactoglobulin at the Oil-Water Interface: Influence of Protein Heat Treatment and Various Emulsifiers". In: *Journal of Agricultural and Food Chemistry* 42.8 (1994), 1602–1606.

- 
- [168] Svetlana R. Derkach. *HOOMD-blue - Home*. en. Oct. 2009. DOI: [10.1016/j.cis.2009.07.001](https://doi.org/10.1016/j.cis.2009.07.001).
- [169] Sumedh R. Risbud and James W. Swan. "Dynamic self-assembly of colloids through periodic variation of inter-particle potentials". en. In: *Soft Matter* 11.16 (2015), pp. 3232–3240. ISSN: 1744-683X, 1744-6848. DOI: [10.1039/C5SM00185D](https://doi.org/10.1039/C5SM00185D).
- [170] Zsigmond Varga, Gang Wang, and James Swan. "The hydrodynamics of colloidal gelation". en. In: *Soft Matter* 11.46 (2015), pp. 9009–9019. ISSN: 1744-683X, 1744-6848. DOI: [10.1039/C5SM01414J](https://doi.org/10.1039/C5SM01414J).